

THE FLUIDIZED BED REDUCTION OF ZINC CALCINE

by

William James Middleton

ABSTRACT

An experimental study has shown that it is possible to produce zinc metal by hydrogen reduction of roasted zinc sulphide concentrates in a fluidized bed at temperatures in the range of 800-900°C.

Increases in temperature and increases in hydrogen flowrate in the range of space velocities from 3.77 to 7.54 cm. sec⁻¹ have a marked beneficial effect on zinc reduction rates. The reduction process is apparently controlled by gas phase mass transport.

Calculations based on an industrial scale integrated roaster bed-reduction bed combination indicates that under ideal conditions (operation at 1000°C) a) the process is autogenous when oxygen enriched air (37%O₂) is used for roasting and b) the maximum attainable hydrogen reducing efficiency is 20%.

A suggestion for a possible industrial design is presented and industrial projections for the use of hydrogen and methane as gaseous reducing agents are made.

Name: William James Middleton.

Title of Thesis: The Fluidized Bed Reduction of Zinc Calcine.

Department: Metallurgical Engineering.

Degree: Master of Engineering.

**THE FLUIDIZED BED REDUCTION
OF ZINC CALCINE**

by

William James Middleton

**A thesis submitted to the Faculty of Graduate Studies
and Research in partial fulfilment of the
requirements for the degree of
Master of Engineering**

**Department of Metallurgical Engineering
McGill University
Montreal, Canada.**

March, 1971.

© William James Middleton 1971

TABLE OF CONTENTS

<u>Chapter</u>		<u>Page</u>
One	INTRODUCTION	1
	1.0 Purpose of the Present Investigation	1
	1.1 Objectives of the Present Work.	2
	1.2 Thesis Arrangement	3
Two	CURRENT INDUSTRIAL USES OF FLUIDIZED BEDS	5
	2.0 Definition	5
	2.1 Survey of Industrial Applications in the Chemical Industry	5
	2.2 Survey of Fluidized Bed Processes in Metallurgy	7
Three	ZINC TECHNOLOGY	12
	3.0 Current Zinc Production Figures	12
	3.1 The Uniqueness of Zinc Smelting	12
	3.2 Retort Smelting	13
	3.2-1 Chemistry of Retort Smelting-Reduction of Zinc Oxide by Carbon	13
	3.2-2 Horizontal Retort Smelting	14
	3.2-3 Continuous Vertical Retort Smelting.	16
	3.2-4 The Electrothermic Zinc Smelting Process	18
	3.3 Blast Furnace Smelting	21
	3.4 Experimental Studies on Zinc Production	25
	3.5 Rate Studies on the Gaseous Reduction of Zinc Oxide	28
	3.6 Summary	30

<u>Chapter</u>		<u>Page</u>
Four	OTHER EXPERIMENTAL WORK INVOLVING THE REDUCTION OF METAL OXIDES IN FLUIDIZED BEDS	31
	4.0 Fluidized Bed Reduction of Iron Oxides	31
	4.1 Summary and Comments	35
Five	THEORETICAL CONSIDERATIONS OF FLUIDIZATION	36
	5.0 The Behaviour of Gas Fluidized Beds	36
	5.1 The Minimum Fluidizing Velocity	37
	5.2 The Terminal Velocity	48
	5.3 Summary	48
Six	ROASTING OF ZINC CONCENTRATES	49
	6.0 The Physical Chemistry of Zinc Concentrate Roasting	49
	6.1 The Fe-S-O System	57
	6.2 The Zn-Fe-S-O System	61
	6.3 Analysis of Roasting Zinc Concentrates to Retard Zinc Ferrite Formation	64
	6.3-1 Effect of Temperature on Zinc Oxide Recovery .	64
	6.3-2 Effect of Gas Composition on Zinc Oxide Recovery	65
	6.4 Summary of Zinc Concentrate Roasting for the Recovery of Free Zinc Oxide	66
Seven	THE ZINC OXIDE - HYDROGEN SYSTEM AT ELEVATED TEMPERATURES	67
	7.0 Reduction of Zinc Oxide by Hydrogen	68
	7.1 Reactions with Other Components of the Zinc Calcine	70
	7.2 The Choice of Hydrogen as a Fluidizing and Reducing Gas	71

<u>Chapter</u>		<u>Page</u>
Eight	APPARATUS AND EXPERIMENTAL TECHNIQUE	72
	8.0 General Approach to the Experimental Technique	72
	8.1 Apparatus	72
	8.2 Raw Material — Zinc Calcine	84
	8.3 Preliminary Tests	85
	8.4 Experimental Procedure	86
	8.5 Chemical Analysis	88
	8.5-1 Determination of Zinc	88
	8.5-2 Determination of Iron	89
Nine	RESULTS	91
	9.0 Results and Experimental Observations — General	91
	9.1 Caking and Clinkering	91
	9.2 Reaction Kinetics and Zinc Elimination	97
	9.2-1 The Effect of Temperature on Zinc Elimina- tion and the Apparent Reaction Rate	97
	9.2-2 The Effect of the Hydrogen Flowrate on Zinc Elimination and the Apparent Reaction Rate	100
	9.3 Hydrogen Efficiency	106
Ten	DISCUSSION	111
	10.0 Feasibility Considerations — Clinkering and Particle Agglomerations	111
	10.1 Feasibility Considerations — Hydrogen Effici- ency	117
	10.2 Reaction Kinetics	120
	10.2-1 Variation of the Reaction Rate with Tempera- ture	120
	10.2-2 Variation of the Reaction Rate with Gas Flow- rate	122

<u>Chapter</u>	<u>Page</u>
10.3 Variation of the Reaction Rate with Time.	123
10.4 Postulation of Reaction Mechanisms	127
10.4-1 Reaction Rate as a Function of Time	127
10.4-2 Interpretation of the Reaction Rate	127
10.4-3A Particle Size and Interfacial Area	129
10.4-3B The Product K_A as a Function of Temperature and Flowrate	132
10.4-4 Variation of K_A with Gas Flowrate.	132
10.4-5 Reaction Mechanism.	135
10.5 Predictions for Full Scale Reactors	139
10.5-1 Basis of the Design Calculations.	142
10.5-2 Calculation of the Plan Area Requirements for ZnO Reduction.	144
10.5-3 Heat Calculations Based on a Roast-Reduction Integrated Process for the Production of Zinc	145
10.6 Summary and Critique of the Present Work.	155
10.7 Suggestions for Future Work.	160
10.8 Conclusions.	162
 APPENDIX I	 164
 ACKNOWLEDGEMENTS	 167
 LIST OF SYMBOLS	 168
 LIST OF TABLES	 171
 LIST OF FIGURES	 173
 REFERENCES	 176

CHAPTER ONE

INTRODUCTION

1.0 Purpose of the Present Investigation

With present day technology, the only viable pyrometallurgical methods of producing zinc from roasted zinc concentrates are either 1) the heating of a mixture of zinc oxide and carbonaceous reducing agent in sealed retorts using an external source of heat or 2) the reduction of zinc oxide by carbon monoxide in a blast furnace. The retort method suffers from a very slow rate of zinc production while the blast furnace technique must employ expensive coke as the principal reducing agent.

The purpose of this work, therefore, has been to explore the technical feasibility of producing zinc by the gaseous reduction of roasted zinc concentrates in a fluidized bed. Many existing zinc producing plants are increasingly turning to the use of fluidized beds for the roasting of zinc sulphide concentrates to zinc oxide and hence this investigation is but a part of an overall zinc production scheme whereby roasted zinc concentrates from a fluidized bed roasting step would subsequently be reduced in a fluidized bed. The resulting zinc vapours from the reduction would be condensed in a lead or zinc splash condenser.

It is only since World War Two that solids fluidization has come to be exploited as a reduction technique. Selected examples of the industrial uses of fluidized beds are described in Chapter 2.

Heat and mass transfer rates are usually significantly greater in fluidized beds than in conventional contacting processes, the high rates being largely due to the fact that the reacting particles are surrounded by agitated gas. Fluidized beds, therefore, are generally well suited for reactions which require or evolve large quantities of heat. The agitated motion of the particles and gas results in high transfer rates particularly at the bed-wall surfaces. Heat is, therefore, quickly moved from the surfaces to the interior of the bed. High rates between the particles and the fluid also account for the near isothermal conditions observed in fluidized beds. Hence localized hot and cold spots, observed frequently in fixed bed processes, are minimized in fluidized beds.

The many advantages of a fluidized bed reactor suggested, therefore, the potential usefulness of an investigation into the gaseous reduction of zinc oxide in a fluidized bed. It would seem to be particularly useful to determine if the observed superiority of fluidized beds for other reactors can be used to advantage for the production of zinc.

1.1 Objectives of the Present Work

The behaviour and reaction kinetics of the fluidized bed roasting of zinc concentrates have been established through industrial experience with the process^(3 - 6) and through experimental studies⁽⁷⁾. The bulk of the future work will have to be concerned with the fluidized bed reduction process.

The main objectives of this study were:

- 1) to determine if it is technically possible to produce zinc

metal in a fluidized bed by the gaseous reduction of zinc calcine.

- 2) to study the effect of temperature and gas flowrate on the rates of zinc calcine reduction in a fluidized bed.

It was hoped that if promising results were obtained, the experimental data would be sufficient to lead to a larger scale investigation, perhaps on a pilot plant scale.

A concluding section of this thesis suggests some ideas which might form the basis for future work.

1.2 Thesis Arrangement

The arrangement of this thesis has been planned with the underlying theme of ultimately suggesting a new method of producing zinc metal. A brief explanation of the progression of the thesis follows.

Chapter 2 surveys the current industrial uses of fluidized beds in an attempt to demonstrate their versatility and as a partial justification for considering fluidized beds as a logical step in any new attempt to produce zinc.

Chapter 3 gives a detailed account of the existing state of zinc technology and, in particular, discusses the problems of zinc smelting. The current high temperature solutions to these problems are discussed as well as previous experimental investigations aimed at studying new methods of zinc production. A section on rate studies is also included in this chapter.

Chapter 4 deals with experimental studies directed at the use of fluidized beds to reduce other metal oxides, in particular, iron oxide. These results show that the idea of metal oxide reduction in fluidized beds is not new but that the notion to attempt zinc oxide reduction in fluidized beds is novel to the field of zinc technology.

Chapter 5 discusses the overall behaviour of gas-solid fluidized beds and elucidates some of the nomenclature used in fluidization technology. Calculations of some of the variables important in the experimental fluidization studies of this work are also discussed.

Chapter 6 discusses methods which may be employed during the roasting of iron bearing zinc concentrates to produce an optimum feed material for a subsequent fluidized bed reduction step, i.e., methods which will lead to a maximum amount of free zinc oxide in the roast product.

Chapter 7 deals with the thermodynamic equilibria for the reduction of zinc oxide with hydrogen. Reasons for the use of hydrogen in this investigation are cited.

Chapters 8, 9, and 10 describe the experimental part of the investigation. Chapter 8 describes the experimental procedure. Chapter 9 comments on the experimental results with some emphasis on the features of the reduction results which are potential drawbacks to an industrial process, namely charge agglomeration and caking. The results of the rate studies are also given. Chapter 10 concludes the work with a discussion on the experimental results, a proposal for reaction mechanisms, some industrial design calculations and suggestions for future work.

CHAPTER TWO

CURRENT INDUSTRIAL USES OF FLUIDIZED BEDS

2.0 Definition

The term "fluidization" refers to the method of contacting solids with fluids whereby finely divided solids are transformed into a fluidlike state by passing an upward stream of gas or liquid through the particles. Fluid-solid contact is excellent in fluidized beds and hence mass transfer and heat transfer rates are very high. In addition, because of the excellent heat transfer characteristics, localized temperature variations are minimal in fluidized beds. Table 2.0-1 shows a comparison between different types of gas-solid contacting systems.

2.1 Survey of Industrial Applications in the Chemical Industry

Although applications of fluidization techniques can be traced back to the sixteenth century, it has only been within recent years that solids fluidization has received widespread attention as a chemical and metallurgical engineering tool. The chief application to date has been in the catalytic cracking of petroleum, using fluidized catalyst particles, which was developed due to a heightened demand for large quantities of high octane aviation fuel during World War Two. The success of these catalytic cracking units has led to a large number of basic and applied studies in the field.

The bulk of the quantitative experimental work on fluidization has been concerned with the mechanics of fluidization, i. e., correlations between the pressure drops across fluidized beds and the fluid and solid properties of the bed. Considerable study of the heat and mass transfer characteristics and mixing characteristics in fluidized beds (8-19) has also been carried out.

TABLE 2.0-1

Comparison of Types of Contacting for Reacting Gas-Solid Systems, Illustrated by Metallurgical Examples

Mode of Gas-Solid Contact	Efficiency of Gas-Solid Contact	Temperature Distribution	Required Particle Size Distribution
Fixed Bed (e.g. Upper Shaft of Blast Furnace)	Particles are stationary leading to much channelling and short circuiting of gas. Conversion of solid is poor.	Poor. Localized temperature gradients are frequently encountered	Uniform particle size required. Small particles are frequently blown out.
Moving Bed (e.g. Sintering Machines)	Same as for Fixed Beds	Large temperature gradients are obtained in the direction of the gas flow due to localized zones of reaction.	Uniform pellet size is usually required for even gas flow and consistent sinter quality.
Wedge Roasters (e.g. Herreshoff type)	Incomplete gas-solid contact. However, better than fixed beds due to rabbling of solids by mechanical rakes.	Poor for roaster as a whole but relatively uniform on each hearth.	Wide range acceptable because of low gas flowrates.
Rotary Kilns	As for Wedge Roasters	Uniform. Heating is gentle and slow. Low production rates.	Fines tend to cake and agglomerate on the surface of the kiln.
Flash Roasters (e.g. Cominco Roaster)	Good Contact.	Poor temp. distribution because of short contact times during fall through roaster.	Narrow range of small particles required because of short contact times.
Fluidized Bed	Good contact.	Excellent temp. distribution because of violent solids agitation and contact.	Wide range acceptable although restricted by particle terminal velocity.

These investigations have been instrumental in furthering applied studies on fluidization techniques. In addition to the cracking of hydrocarbons, higher order hydrocarbons are now produced in fluid bed reactors as are ethylene glycol, alkyl chloride, phthalic anhydride, acrylonitrile, and vinyl acetate.

The use of fluidized beds for the calcination of limestone, dolomite, and phosphate rock as well as for the clinkering of cement has been extensively evaluated. These processes have now obtained commercial acceptance with considerable cost savings over conventional kiln processes.

2.2 Survey of Fluidized Bed Processes in Metallurgy

In 1947, the Dorr-Oliver Company built the first Fluo-Solids roaster for the roasting of arsenopyrite (FeAsS). Although this plant proved to be unsuccessful, owing to an arsenic handling problem, it led to the use of fluid bed roasters for the roasting of most other types of sulphide ores. Some of these are shown in Table 2.2-1. In addition to the main purposes cited in the tabulation, it was found that continuous fluidized bed operation led to average sulphur dioxide concentrations in the product gases of 10-15%. Conventional roasting processes using hearth or flash-type roasters obtain average sulphur dioxide concentrations in the product gases of 5-10%.

TABLE 2.2-1
Survey of Metal Sulphide Roasting

Process	Main Purpose	Advantages
Nickel Sulphide Roasting (20)	The production of coarse, granular nickel oxide from the fine sulphide concentrate obtained from the conventional separation of Bessemerized matte.	Eliminates difficult mechanical problems encountered in the conventional sintering process and results in a more reactive product for subsequent reduction.
Zinc Sulphide Roasting (3, 4, 5, 6)	To produce a calcine suitable for acid leaching. The subsequent leach liquor is used as an electrolyte for the electrowinning of zinc.	Using fluid bed roasters a full 2-3% increase in the yield of leachable zinc over conventional suspension and hearth roasting has been realized, principally due to a reduction in the sulphide sulphur content. (5)
Copper Sulphide Roasting (21)	To increase the recovery of smelter sulphur and to increase the throughput of copper concentrates.	The recovery of sulphur has been increased by 20-25%. Smelter throughputs increased by up to 40%. In addition, finer control of reverberatory matte grades has been obtained.
Sulphation Roasting of Refractory Ores. (22)	To open orebodies of refractory ores to exploitation by selective sulphation roasting with SO ₂ gas to produce water leachable metal sulphates.	The stability of metal sulphates is acutely temperature sensitive. The near isothermal temperature conditions achieved in fluid bed reactors eliminates local "hot" spots and affords greater control over sulphating temperatures.

Although the bulk of the commercial applications of fluid bed processes in the metallurgical industry are concerned with the roasting of metal sulphides, significant contributions have been made from other sectors of the industry, notably from the iron and steel industry. The purpose has been threefold: (1) to attempt to find an acceptable alternative for the iron blast furnace, (2) to produce iron and steel from the fines of high grade ores, and (3) to employ the lower grade ores and available fuels (non-coking bituminous coals, anthracite, lignite, etc.) to produce iron and steel. These so-called direct reduction processes are summarized in Table 2.2-2. The INCO process for reducing nickel oxide is also included in this table.

Except for a few restricted cases, improvements in blast furnace operation, initiated during the development stages of these new processes, gave the blast furnace a decided cost advantage and further work on direct reduction processes was largely suspended. Only the H-IRON and the Direct Fuel Injection processes (Table 2.2-2) are in commercial production today, the former as a supplier of iron powder for powder metallurgical purposes. The latter operation is presently used by the Montecatini Edison works in Follonica, Italy to produce high grade iron concentrate by converting hematite to magnetite which is removed from the gangue materials by magnetic separation. This method reduces transportation costs and lowers blast furnace operating costs by providing a partially reduced ore to the charge.

TABLE 2.2-2
Survey of Direct Reduction Processes and
INCO Nickel Oxide Reduction Process

Process	Author	Notes
Nu-Iron	United States Steel Co. (2, 23, 24)	Continuous two stage fluidized bed. The reductant gas is hydrogen obtained from the combustion of natural gas, fuel oil or powdered coal. Feed to the first stage is Fe_2O_3 and to the second stage is FeO . Reducing gas entering at 1500°F (30 psig) converts FeO to Fe in the second stage. Off-gas from the second stage reduces Fe_2O_3 to FeO at 1300°F . Final Fe is cooled and briquetted for melting.
H-Iron	Hydrocarbon Research and Bethlehem Steel Corp. (2, 23, 25)	Three stage batch fluidized bed reduction process. The reducing gas is hydrogen obtained from the partial oxidation of coke-oven gas. The fluidized beds are operated at 1000°F and 500 psig. The feed material (high grade Fe_3O_4) is 47% reduced after the first stage, 87% after the second and 97-98% reduced at discharge.
FIOR	ESSO Research and Engineering Co. (2)	Continuous fluidized bed using partially combusted natural gas — 21% CO , 41% H_2 , 38% N_2 as the reducing gas. The process is operated at atmospheric pressure and 1500 - 1600°F . The product is a free-flowing powder containing 89-93% metallic iron which is agglomerated or briquetted.
Stelling	P.O. Stelling (2, 23)	Continuous fluidized bed utilizing carbon monoxide as the reducing gas. The feed material is hematite or magnetite. The process is operated at atmospheric pressure and 1100 - 1300°F . The product is mainly high carbon iron, some FeO , and traces of metallic iron.

TABLE 2.2-3 (Cont'd)

Process	Author	Notes
Direct Fuel Injection	G. Tomasicchio (26)	Employs a Dorr-Oliver FluoSolids Reactor. The reducing gas is partially oxidized fuel oil plus air and the feed material is hematite. The operating temperatures vary between 650 and 900°C depending on the type of ore to be processed. The product is magnetite.
NiO Fluidized Bed Reduction Process	International Nickel Co., Canada, Ltd. (27)	Roasted nickel oxide (0.01% S) is chlorinated in a fluidized bed to lower the copper content to 0.25%. The resulting calcine is reduced to 90% Ni in a fluidized bed using hydrogen obtained from the decomposition of ammonia. The hydrogen enters the bed at 960-1000°F and flows through the bed with a space velocity of 7 fps. The bed, itself, is maintained at a temperature of 900°F. The retention time of the solids in the bed is approximately 4 hours. 70-75% of the hydrogen is recycled.

CHAPTER THREE

ZINC TECHNOLOGY

3.0 Current Zinc Production Figures

Table 3.0-1 shows the contribution of the various zinc producing processes to the total world zinc production for 1965 and 1967 (excluding Warsaw Pact Countries).

TABLE 3.0-1
Current Zinc Production Figures

	1965		1967	
	Metric Tons	% World Output	Metric Tons	% World Output
Horizontal Retort	400,000	11.5	925,000	22
Vertical Retort	440,000	12.5	500,000	12
Imperial Smelting Process	230,000	6.5	500,000	12
Electrolytic	1,890,000	54.0	1,975,000	47
Other	540,000	15.5	300,000	7
TOTAL:	3,500,000	100.0	4,200,000	100

3.1 The Uniqueness of Zinc Smelting

Whereas the majority of the world's major metals (iron, copper, lead) are being produced in large blast furnaces or reverberatory furnaces, zinc is still being produced in furnaces of relatively small size. This fact may be attributed to two characteristics of zinc smelting, namely that zinc oxide is reducible only with difficulty and that zinc metal boils at 907°C. This latter characteristic has prevented the direct tapping of liquid zinc from furnaces.

3.2 Retort Smelting

3.2-1 Chemistry of Retort Smelting—Reduction of Zinc Oxide by Carbon

The physical chemistry of retort smelting is characterized by the overall reaction



which is believed to proceed in two stages according to the following reactions:



Reaction (3.2-1) is then the sum of two endothermic reactions (3.2-2) and (3.2-3).

Except for the Electrothermic Process where heat for these reactions is supplied through the electrical resistance of the charge, both horizontal and vertical retort processes supply this heat by conduction through the container walls from gas or coal fired furnaces. As a result the amount of zinc smelted per unit area is small.

The main features of the retort smelting reactions is that no oxygen is introduced into the system. It is on this point that the retort reaction differs from that of the blast furnace production of zinc which is described later in this chapter.

Calculations based on the retort reactions show that the equilibrium products of reactions (3.2-2) and (3.2-3) are such that at temperatures above 1000°C the retort gases contain approximately equimolar amounts of carbon monoxide and zinc vapour (less than 1% carbon dioxide).

Unhindered condensation of gaseous zinc is usually made difficult due to the reversibility of the smelting reactions. With retort gases containing the components Zn, CO, and CO₂, both CO and CO₂ can reoxidize zinc vapour to zinc oxide according to:



Fortunately, reaction (3.2-4) is slow due to the difficulty of graphite nucleation. ⁽²⁸⁾ Since the retort gases contain less than 1% CO₂ the formation of zinc oxide by slow cooling due to reaction (3.2-5) will account for a maximum reoxidation of 1.2% of the total zinc in the gas stream. ⁽²⁸⁾ In retort smelting, therefore, condensation of the zinc vapour poses no major problems.

3.2-2 Horizontal Retort Smelting

Figure 3.2-2 shows a cross section of a zinc distilling furnace using horizontal retorts. The retorts are slightly inclined from the horizontal and are shaped something like large test tubes. They are about 5 feet long and 8 or 9 inches in inside diameter. They may have circular or oval cross sections. Horizontal retorts are generally constructed from fireclay and are manufactured at the smelter in most cases. The retorts are placed in the furnace as shown in Figure 3.2-2 and are heated by the flame gases which envelop them; the furnace itself is usually a gas fired regenerative furnace.

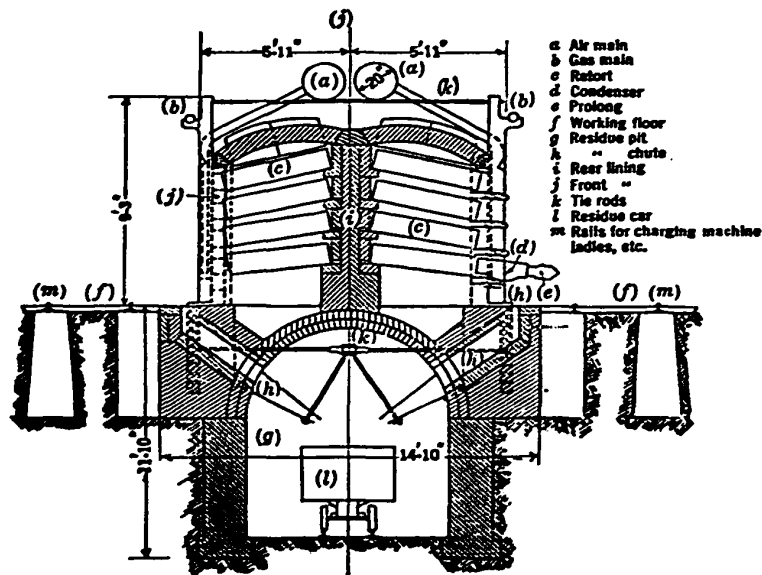


Figure 3.2-2. Zinc Distillation Furnace. (29)

Zinc calcine is mixed with the proper amount of reducing agent (anthracite coal, noncoking bituminous coal, or coke breeze) and is charged into the retort in batches of 100 to 150 pounds per retort. When the retort is filled, a rod is run through the charge at the top to provide an escape channel for the vapour, the condensers are placed in position and sealed in place with clay, and a small amount of coal is placed in the mouth. The retorts are brought up to temperature and distillation proceeds until all the zinc has been removed. After reduction is complete, the residue is removed, the retort recharged with fresh calcine and the procedure is repeated. A complete cycle usually requires 24-48 hours. The residue remains as a solid and there is no slag formation.

It should be noted that each retort is provided with its own condenser which protrudes outside the furnace walls. The zinc condenses to liquid zinc and the CO gas passes through and burns at the condenser mouth. Molten zinc is emptied from the condenser by scraping the zinc into a suspended kettle usually three times during a charge cycle.

The main features to note concerning the use of horizontal retorts is that they are simple to operate and the charge does not require elaborate preparation. However, the units are small and the operation is intermittent, so that considerable labour is required and the use of automatic controls is not feasible.

Production from an individual horizontal retort is less than 25 pounds of zinc per day.

3.2-3 Continuous Vertical Retort Smelting

A continuous vertical retort was developed by the New Jersey Zinc Company⁽³¹⁾ which is built in the shape of a vertical channel of rectangular cross section. The internal cross section is 6 feet by 1 foot and the heated portion has a height of about 25 feet. Above the heated portion is a refractory extension into which the charge is fed through a double bell type hopper system. Below the heated portion is an iron extension which terminates in a water seal. The retort is heated externally in the same manner as the horizontal retorts, and the side walls of the heated portion are made of silicon carbide tiles.

The calcine is mixed with reducing carbon and a binder, pressed into briquets, dried, and then heated to a coking temperature. These

briquets are continuously hot charged to the upper extension of the retort. The spent briquets, after passing through the heated zone, are discharged through the water seal at the bottom of the retort.

As the briquets pass through the heated zone the zinc oxide is reduced and the zinc vapour and CO gas pass out through a side opening near the top of the heated zone. Charge preparation is extremely important in this operation as each briquet acts as a self contained miniature retort. As the briquet is brought up to temperature, the components react and the zinc and CO gases are expelled. The zinc is condensed by passing the effluent $\text{CO} + \text{Zn}_{(g)}$ gases through a chamber in which droplets of zinc are being splashed from a cooled bath of liquid zinc.

The coking process is sufficient to prevent disintegration of the briquets and there is no slagging or fusion. The spent briquets which are discharged are in fact skeletons of the original briquets.

Because externally heated vertical retorts are operated continuously, they are particularly suited to automatic controls. However, the charge requires elaborate preparation in order to assure proper discharge. Although vertical retorts are much bigger than horizontal retorts, they are still small units since the internal thickness is only about 1 foot. This point exemplifies an inherent weakness of all externally heated retorts. They must be small in order to assure that heat penetrates to the centre of the charge.

Production from a vertical retort is in the order of 5 to 8 tons of zinc per day.

3.2-4 The Electrothermic Zinc Smelting Process

Figure 3.2-3 is a cross section of the furnace and auxiliary equipment developed by the St. Joseph Lead Company⁽³²⁾ and Figure 3.2-4 is a detailed view of the furnace. These furnaces are essentially vertical retorts which are heated internally. They are cylindrical in shape having internal diameters of 5 to 12 feet and are about 40 feet high. Heat is introduced electrically, utilizing the charge itself as the resistance which develops the heat. Carbon electrodes inserted near the top of the furnace are connected to similar carbon electrodes at the bottom of the furnace by a column of solid charge. The charge is prepared in the same manner as used in the vertical retorts and the reactions are identical.

The Electrothermic Process condenses zinc by drawing (under partial vacuum) bubbles of the effluent CO plus $Zn_{(g)}$ through a cooled bath of liquid zinc.

Since heat in the Electrothermic Process is generated within the charge, there is no limitation to the size of these furnaces. They have all the advantages of the vertical retorts but, however, they make use of a relatively expensive method of heating.

Production from an 8 foot diameter electrothermic furnace is approximately 50 tons of zinc per day.

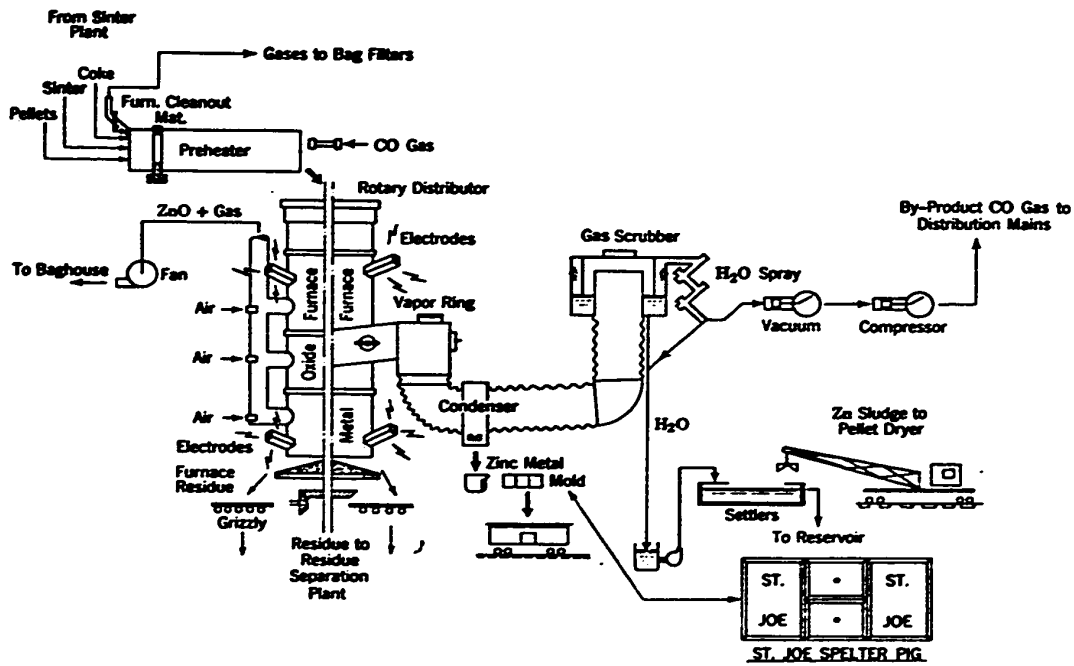


Figure 3.2-3 St. Joseph Electrothermic Furnace (From Weaton et al.⁽³²⁾).

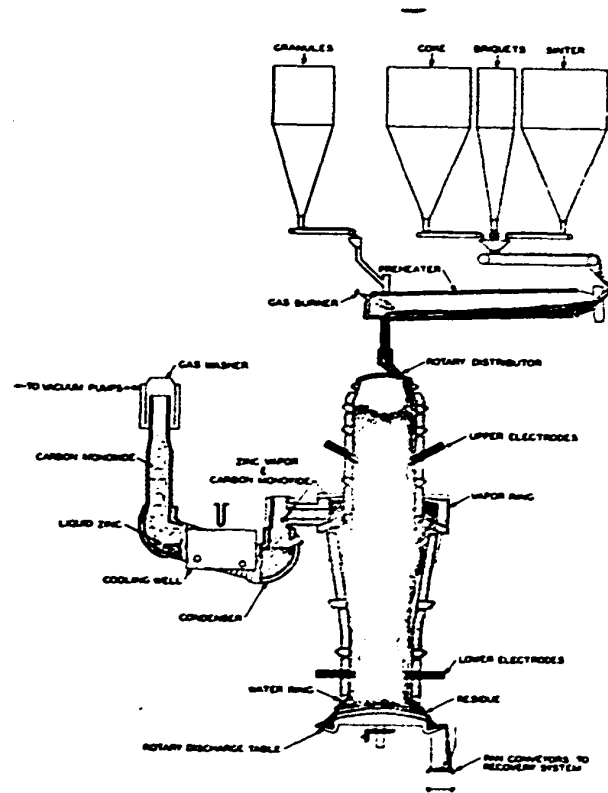


Fig. 3.2-4 Electrothermic Zinc Metal Furnace⁽³³⁾.

3.3 Blast Furnace Smelting

The conception and implementation of the Imperial Smelting Process deserves special attention since it represents a major breakthrough in zinc smelting technology. For the first time, zinc can now be produced in quantity, continuously, in a single unit. In 1967 the largest Imperial Smelting Furnace produced 56,000 long tons of zinc as compared with 15,000 for the largest retort.

The Imperial Smelting Furnace (Figure 3.3-1) is a blast furnace essentially modelled after the lead blast furnace.

The charge is a mixture of sintered (oxidized) lead-zinc concentrate, flux and coke. The blast is preheated air or oxygen enriched air. Zinc vapour is drawn off near the top of the furnace while lead and a copper matte phase is collected in the hearth. A supernatant layer of iron-lime silicate slag is also collected in the hearth.

Volatilized zinc vapour is separated from the other components of the gas stream (CO , CO_2 , N_2 , 1000°C) by condensation in a lead splash condenser (inlet lead temperature $\sim 450^\circ\text{C}$, outlet temperature $\sim 570^\circ\text{C}$).

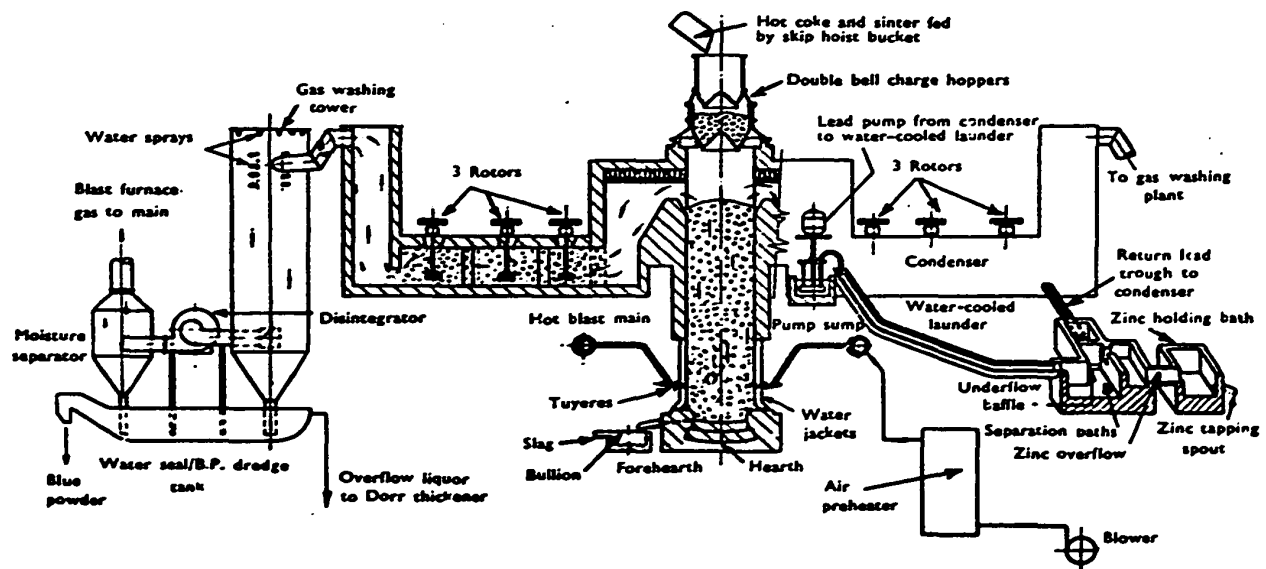


Figure 3.3-1 Imperial Smelting Furnace (36).

In the blast furnace, reduction of the metal oxides according to reaction (3.2-1), (p. 13) is extremely unlikely. Rather, gaseous reduction will predominate. The reducing gas mixture is generated in the tuyère zone where solid carbon is oxidized by the air blast according to:



Above the tuyères, in the metal reduction zone, the three principal reactions are:



It can be seen, therefore, that the essential difference between the retort processes and the blast furnace or Imperial Smelting Process is that oxygen is introduced through the tuyères to generate a) CO reducing gas from the charged coke and b) heat. The introduction of oxygen through the tuyères results, however, in a high CO_2 concentration in the off gas. Thus the blast furnace is faced with a condensation problem which is largely absent in the retort processes, i.e., by reaction (3.2-5), $\text{CO}_2 + \text{Zn}_{(g)} \longrightarrow \text{CO} + \text{ZnO}$. Typical off gas compositions run: 5-7% Zn, 12% CO_2 , 18% CO, and the remainder N_2 .

Consideration of the above reactions largely explains the following unique features of the Imperial Smelting Process:

- (a) The charge is preheated to approximately 800°C before entering the furnace to prevent the condensation of zinc vapour in the furnace on the cold charge.
- (b) The air blast is preheated to between 600°C and 1000°C to ensure that sufficient heat is supplied to the metal reduction zone and to ensure a hot, fluid slag.
- (c) The condenser is unique, using liquid lead splashes (450°C) to rapidly cool or quench the furnace gases to minimize the

amount of reoxidation of zinc vapour.

- (d) The addition of top air (frequently 10% of the blast volume) is unique and is employed to raise the temperature of the exit gases (to 1000°C) by burning zinc vapour to zinc oxide and CO to CO₂. The resultant increased temperature minimizes the reversal of reaction (3.2-2) in the upper part of the furnace and in the flues leading to the condenser.
- (e) Zinc and lead leaving the condenser are separated by liquation by virtue of the immiscibility gap in the Pb-Zn system above 420°C. Figure 3.3-2 shows the Pb-Zn phase diagram and the condenser operating temperatures.

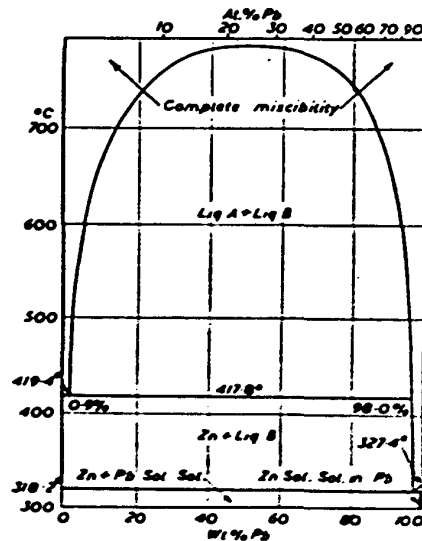


Figure 3.3-2 Lead-Zinc Phase Diagram (from Smithells)⁽³⁷⁾

3.4 Experimental Studies on Zinc Production

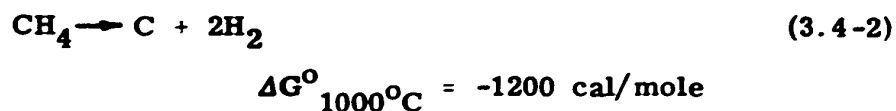
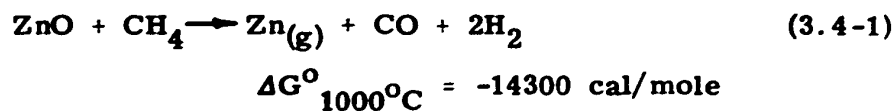
Although no experimental investigations with specific reference to the fluidized bed reduction of zinc oxide or calcined zinc concentrates have been reported in the literature, several investigations have dealt with the feasibility of producing zinc by:

- 1) the gaseous reduction of the oxide using hydrocarbon gases;
- 2) the direct reduction of zinc concentrates using metallic reductants.

In addition, a number of papers have been published dealing specifically with the mechanisms and reaction kinetics of zinc oxide and zinc calcine reduction by different gases.

As shown in Section 3.0 (Table 3.0-1) the retort processes for the production of zinc still account for a major portion of the world's zinc output. Developed by experience over a long period of time, the state of the art had, by the 1930's, been perfected to such a degree that no major improvements could be implemented without a radical change in method.

Maier⁽³⁸⁾, in a thermodynamic study of zinc smelting, showed that the limits of the reduction of zinc oxide by methane could be predicted by the following reactions:





$$\Delta G^{\circ}_{1000^{\circ}\text{C}} = +10500 \text{ cal/mole}$$



$$\Delta G^{\circ}_{1000^{\circ}\text{C}} = +9600 \text{ cal/mole}$$

Doerner⁽³⁹⁾ confirmed Maier's predictions by reducing calcined zinc concentrates with methane and natural gas in electrothermally heated vertical retorts. Above 900°C, reaction (3.4-1) was shown to proceed rapidly and almost to completion. In addition, an increase in temperature above 900°C yielded an increase in the production rate of zinc.

Thermal decomposition of methane by reaction (3.4-2) proved troublesome on heating to the reaction temperature, 900-1000°C, but this effect diminished above 900°C except where there were local deficiencies of zinc oxide.

Reoxidation of zinc, due to the reversibility of reactions (3.4-3) and (3.4-4), was found to be an important hindrance to zinc condensation. The product of this reoxidation was yellow, crystalline zinc oxide which deposited in those areas of the retort where the temperature fell below 850°C. Although the effect of reactions (3.4-3) and (3.4-4) were not studied in detail in the Doerner investigation, the net contribution of these reactions is indicated by the CO₂ and H₂O content of the gaseous products. During all phases of the investigation the CO₂ content varied between 0.4% (at 925°C ; low gas velocity) and 1.3% (1000°C; high gas velocity). No water vapour was detected in any of the tests. The maximum amount of reoxidation would, therefore, be quite small.

The direct reduction of zinc concentrates has been the subject of a number of experimental and pilot plant scale investigations. The governing equation is of the form



where X is a suitable reducing agent. Copper and iron have been the most extensively employed reducing agents. Imbert⁽⁴⁰⁾ patented a process whereby either of the above reducing agents could be used to reduce zinc sulphide at atmospheric pressure. At the high temperatures required, the system was molten and this resulted in the formation of copper matte. The reactants dissolved in the copper matte and thus their activities were reduced.

Peterson⁽⁴¹⁾ extended the experimental work in both small and large scale tests. Although promising results were obtained on a small scale, scaling-up of the tests resulted in excessive "blue powder" formation. "Blue powder" is condensed zinc which has not coalesced because of a coating of zinc oxide on the surface.

By the use of vacuum, Gross and Warrington⁽⁴²⁾ were able to reduce zinc sulphide with iron at temperatures as low as 900°C. Their results indicated that the rate of reaction was unaffected by the constitution of the ore (a synthetic zinc sulphide containing 97.7% Zn and an ore containing 79.5% Zn were used). In addition, the results indicated that the ratio of ZnS to Zn in the vapour phase was very small (10^{-3} to 10^{-6} at 900°C and 1000°C respectively). This result was supported by the results of a later study by McCabe⁽⁴³⁾ who measured the equilibrium pressure above ZnS in the range 680°C to 825°C.

It is doubtful if zinc reduction using metallic reducing agents will ever attain economic success.

3.5 Rate Studies on the Gaseous Reduction of Zinc Oxide

Truesdale and Waring⁽⁴⁴⁾ conducted a study of the relative rates of the reactions involved in the reduction of zinc ores. The method employed was to measure the weight loss against time of specially prepared briquets heated in a tube furnace in a stream of reducing gas. Studies of the systems ZnO-CO and ZnO-H₂ showed that hydrogen was a more effective reductant than carbon monoxide. For the case of roasted zinc sulphide concentrates and willemite (ZnO·SiO₂) ore, the reaction rate was seemingly controlled by the diffusion of gas through pores in the particles. Increases in the temperature and the gas flow-rate both resulted in significant increases in the reduction rate.

Imoto et al⁽⁴⁵⁾ have studied the reduction of zinc oxide by hydrogen at reduced pressure (10-85mm Hg and 617-762°C) in static gas and a moving gas stream. These workers theorized that the zinc oxide decomposed to zinc vapour and oxygen and that the hydrogen reacted with oxygen in the vapour phase. That is, the reaction could be represented by the following set of equations:



They suggested that the rate determining step is the reaction between hydrogen and oxygen to form water vapour.

The reactions mainly responsible for the production of zinc in the zinc blast furnace are:



as was shown by Bodenstein⁽⁴⁶⁾ some forty years ago. Since each of these reactions is dependent on the other for its supply of CO and CO₂, the overall rate of production of zinc vapour is determined by the slower of the two reactions.

Maier⁽³⁸⁾ concluded that while the zinc reduction reaction (3.5-3) is more rapid than reaction (3.5-4) at lower temperatures ($\sim 1100^{\circ}\text{C}$), the difference diminishes with rising temperature, although at 1300°C reaction (3.5-3) is still faster.

Truesdale and Waring⁽⁴⁴⁾ suggested on the basis of their experimental results that reaction (3.5-4) could be accelerated by careful selection of the type of carbon used. Charcoal, coke, and graphite were shown to be progressively less reactive forms of carbon.

Shkuridin⁽⁴⁷⁾ has undertaken a comprehensive study of the kinetics of zinc oxide reduction by pure carbon monoxide. The investigation indicated that the process is a complex one influenced by temperature, the CO partial pressure in the gas stream, and the coarseness of the material. The dependence of the reaction rate constant on the CO partial pressure was given by:

$$K = A P_{\text{CO}}^n \quad (3.5-5)$$

where K is the reaction rate constant. "A" is a constant related to the equilibrium constant for reaction (3.5-3), and P_{CO} is the CO partial pressure. "n" is an empirical constant for each experimental calcine.

Jones and Davis⁽⁴⁸⁾ successfully accelerated reaction (3.5-3) by incorporating in the reduction system the nonreducible oxide, SrO. The

modified reduction equation becomes:



Using this technique, reduction rates an order of magnitude greater than for the unmodified reaction were realized.

Langenberg⁽⁴⁹⁾ obtained similar results using lithium cations to alter the reduction mechanism, while Doerner⁽³⁹⁾ used nickel as a catalyst in some of his reduction tests with methane and natural gas.

3.6 Summary

New and fresh ideas in the field of zinc production metallurgy have had a slow and rather unsuccessful emergence. After abandoning further work on the improvement of the old retort processes, recent attention has been aimed at gaseous and direct reduction processes, with only partial success in each. Invariably the ultimate failure of the design concept can, in each case, be attributed to a) excessive reoxidation of the distilled zinc (i.e., condensation problems), or b) production rates which were too slow to be economically attractive (i.e., the direct reduction processes).

Of all the processes investigated in these feasibility studies, only one, the Imperial Smelting Process, discussed earlier in this chapter, has emerged as an alternative to the retort processes. Still, this process suffers from some unattractive features, particularly low purity of product and a high quantity of zinc recycling as drosses and "blue powder" which threaten its further adoption in North America.

Clearly, further study is required in the area of zinc production metallurgy. Little or no reported work has considered the possibility of producing zinc by the reduction of zinc calcine in a fluidized bed.

CHAPTER FOUR

OTHER EXPERIMENTAL WORK INVOLVING THE REDUCTION OF METAL OXIDES IN FLUIDIZED BEDS

4.0 Fluidized Bed Reduction of Iron Oxides

Chapter Two has cited five specific instances where the fluidized bed reduction technique for iron oxides has proved successful enough to warrant the construction of semi-industrial scale pilot plants and fully fledged production plants. The intent has been to find a replacement for the iron blast furnace.

Recent experimental investigations have centered upon the use of fluidized beds to reduce iron bearing materials which are not suitable for charging to the blast furnace. The most notable of these materials is mill scale which is, because of its high purity, an exceptionally good starting material for the production of high purity iron powders.

Brant and Marshall⁽⁵⁰⁾ conducted an extensive survey of the reducibility of a wide range of iron ores with hydrogen and mixtures of H_2 , CO , and N_2 in a fluidized bed at $1400^{\circ}F$. Fine particle sizes were used (usually -20 + 100 mesh) and it was noted that large variations in the reduction rates resulted. Table 4.0-1 shows the chemical analyses of the ores studied and Table 4.0-2 shows the observed times required, under identical conditions, to achieve 80% metallization of the iron. These authors concluded that it was necessary to select ores that reduce rapidly for use in low temperature reduction processes.

It is on this latter point that the iron blast furnace demonstrates its versatility since it will make liquid iron from any material which contains iron. If the lower temperatures in the upper shaft are insuf-

TABLE 4.0-1
Chemical Analysis of the Ores Treated by Brant and Marshall

Name of Ore	Percent by Weight (Dry)				
	Fe	O	SiO ₂	Al ₂ O ₃	Magnetic (%)
Labrador	60.8	25.6	7.9	1.7	0.0
Brazilian	66.4	28.7	0.6	0.7	1.6
Marcona	62.8	26.3	6.7	0.0	19.8
Chilean	64.7	26.4	5.4	1.1	77.8
Mexican	64.0	28.1	1.6	1.1	32.3
Rusk Ore	38.8	14.6	15.5	6.5	0.0
Rusk Conc	42.4	15.4	16.3	7.2	0.0
Siderite	40.5	14.1	10.9	4.2	0.0
Liberian	65.1	26.7	3.5	1.2	72.8

TABLE 4.0-2
Effect of the Iron Ore on the Time Required to Achieve 80%
Metallization as Observed by Brant and Marshall

Name of Ore	Reducing Gas	Temperature °F	Time to Achieve 80% Metallization Minutes
Labrador	Hydrogen	1400 (760°C)	33
Brazilian	Hydrogen	1400	37
Marcona	Hydrogen	1400	37
Chilean	Hydrogen	1400	100
Mexican	Hydrogen	1400	37
Rusk Ore	Hydrogen	1400	22
Rusk Conc	Hydrogen	1400	20
Siderite	Hydrogen	1400	19
Liberian	Hydrogen	1400	Did not reach 80%

ficient to give rapid reduction of the ore, the higher temperatures in the hearth will be more than adequate.

Masonov and co-workers⁽⁵¹⁾ studied the reduction of iron ore 68.3% Fe (0.22% FeO, 97.2% Fe₂O₃) and rolling mill scale 71% Fe (39.1% FeO, 1.2% metallic Fe, and 56.3% Fe₂O₃) with hydrogen at elevated pressures in a single stage fluidized bed. Batch type operation was carried out at temperatures between 490 and 650°C. The results showed that the use of elevated pressures (up to 30 atm.) increased the reduction rate of these materials for the range of variables studied (temperature, particle size, hydrogen flowrate, and pressure). The following table (Table 4.0-3) shows the effect of hydrogen pressure on the reduction of the iron ore at a temperature of 490°C and a hydrogen flowrate of 2.5 liters/sec.

TABLE 4.0-3*

Effect of Hydrogen Pressure on Iron Oxide Reduction

Time mins.	Temp. °C	% Reduction			
		3 atm	4 atm	5 atm	6 atm
5	490	21.9	31.2	35.1	38.5
10	490	47.4	58.6	64.0	70.8
15	490	70.8	81.5	85.6	92.5
20	490	84.9	89.0	93.0	95.9
25	490	93.0	89.8	94.3	96.0

* Charge weight in each case was 300g.

These authors attributed the increase in the reduction rate with increasing hydrogen pressure to the greater concentration of reducing gas per unit area of reacting surface. In addition the use of high pressures had

the added advantage of allowing the use of higher hydrogen flowrates without increasing dust losses.

Okura and Lu⁽⁵²⁾ were successful in further improving the efficiency of utilization of reducing gas in the fluidized bed reduction of hematite (-35 + 100 mesh) with hydrogen and H₂-N₂ mixtures at 500-700°C by using a cyclic gas flow technique. The technique involved interrupting the gas flow (to zero flow) 2 or 4 times per second. These authors claim that improvements in the gas efficiency of the order of 20% resulted from an inducement towards particulate fluidization (absence of bubbles, channels, and slugs) by preventing or curbing these abnormalities. It was also found that the active solids circulation, an indication of a well fluidized bed of fine particles, was maintained even during the off-cycle.

The effect of the cyclic operation was most pronounced for cases in which poor fluidization was obtained under steady flow conditions. The beneficial effect of cyclic operation diminished with improved fluidization quality but at no time was it worse than experienced under steady gas flow conditions.

4.1 Summary and Comments

Understandably, of the few metal oxides which have been reduced in a fluidized bed apparatus, by far the most time and effort has been consumed in studying the possibility of reducing iron ores. As stated in Chapter Two, the initial challenge was to find an acceptable alternative to the iron blast furnace.

Since that time, however, blast furnace operators have succeeded in improving the efficiency of the blast furnace to such an extent that fluidized bed reduction schemes are only useful for special applications such as the reduction of iron bearing minerals unsuitable for charging to the blast furnace and for the production of high purity iron powders from essentially pure iron oxide.

It can be seen that the potential use of fluidized beds for metal oxide reduction purposes has been well recognized and that the process has been studied in detail for several systems. It is clear, however, that commercial installations of fluidized beds for the reduction of oxides are still restricted to rather special cases of feed materials and products.

CHAPTER FIVE

THEORETICAL CONSIDERATIONS OF FLUIDIZATION

5.0 The Behaviour of Gas Fluidized Beds

When a fluid is passed through a bed of fine solids at a low rate, it emerges at the upper bed surface by routing itself around the stationary particles. Such a situation is termed a fixed bed and is best illustrated metallurgically by the upper shaft conditions in blast furnace processes.

As the flow rate increases, there is no apparent change in the outward appearance of the bed until a flowrate is reached at which the pressure drop across the bed equals the buoyant weight of the particles per unit area of the bed. Observation of the bed at this flowrate will indicate a few vibrating particles which move about in restricted areas. This state of particle motion is regarded as an expanded bed. In both liquid and gas fluidized beds, an expanded bed constitutes a homogeneous system (i. e. , the solids and fluid form a continuous phase).

With progressively higher flowrates, the bed continues to expand. In gas fluidized beds, however, there is a limit to this expansion, in direct contrast to liquid fluidized beds. In both cases, a flowrate is reached where the particles are all just suspended in the upward fluid flow. The frictional force between the particle and the fluid counterbalances the weight of the particle. The bed is considered to be just fluidized and this situation is referred to as an incipiently fluidized bed or a bed at minimum fluidization.

In liquid fluidized beds an increase in the flowrate above minimum fluidization results in a progressive, smooth expansion of the bed. Except in very unusual cases, the bed remains homogeneous and is described as a particulate fluidized bed.

In contrast, the behaviour of gas fluidized beds above minimum fluidization is markedly different. The bed becomes unstable due to the formation of a bubble phase which is relatively solids-free. Gas in excess of that required to provide incipient fluidization short circuits through the bed via the bubbles. Such a condition has been defined as two phase fluidization, aggregative fluidization, heterogeneous fluidization, or bubble fluidization. The two phases which are present in a dense phase bubbling bed are: 1) the bubble phase, virtually free of solids and 2) the particulate phase which, evidence shows, virtually retains minimum fluidization conditions irrespective of how far above the minimum fluidization conditions the bed is.

5.1 The Minimum Fluidizing Velocity

Undoubtedly one of the most important design variables for fluidized beds is the minimum fluidizing velocity. Much of fluidization theory (i. e., predictions of heat and mass transfer rates, solids mixing characteristics, bubble motion, etc.) involves a knowledge of this variable. The minimum fluidizing velocity sets a lower limit on the gas input rate to a fluidized bed. The upper limit on the gas input rate is governed by the velocity which will carry the solids from the bed.

Several methods have been proposed to determine the minimum fluidizing velocity (U_{mf}) or minimum mass velocity (G_{mf}). These include:

- 1) observing the gas input rate at which bubbles first appear in the bed;
- 2) observing the change in the heat transfer coefficient with increasing gas flow;
- 3) measuring the pressure drop through the solids in the fixed bed state.

The pressure drop method (3) is the most popular and the most reliable technique and it has been used throughout this investigation. Figure 5.1-1 (p. 39) shows, for example, a typical experimental graph of the pressure drop across a bed of zinc calcine (average particle size 73 microns) plotted as a function of the mass gas flowrate of hydrogen (inlet temperature, 23.5°C; average gas pressure in the bed, 1 atmosphere). This experimental curve was obtained by fluidizing zinc calcines in a clear acrylic plastic bed (2 inch i. d.). These experiments were performed to determine a suitable distributor plate for the high temperature zinc reduction studies. The distributor, in this case, is porous fireclay insulating brick. A detailed description of the experiments is presented in Appendix I.

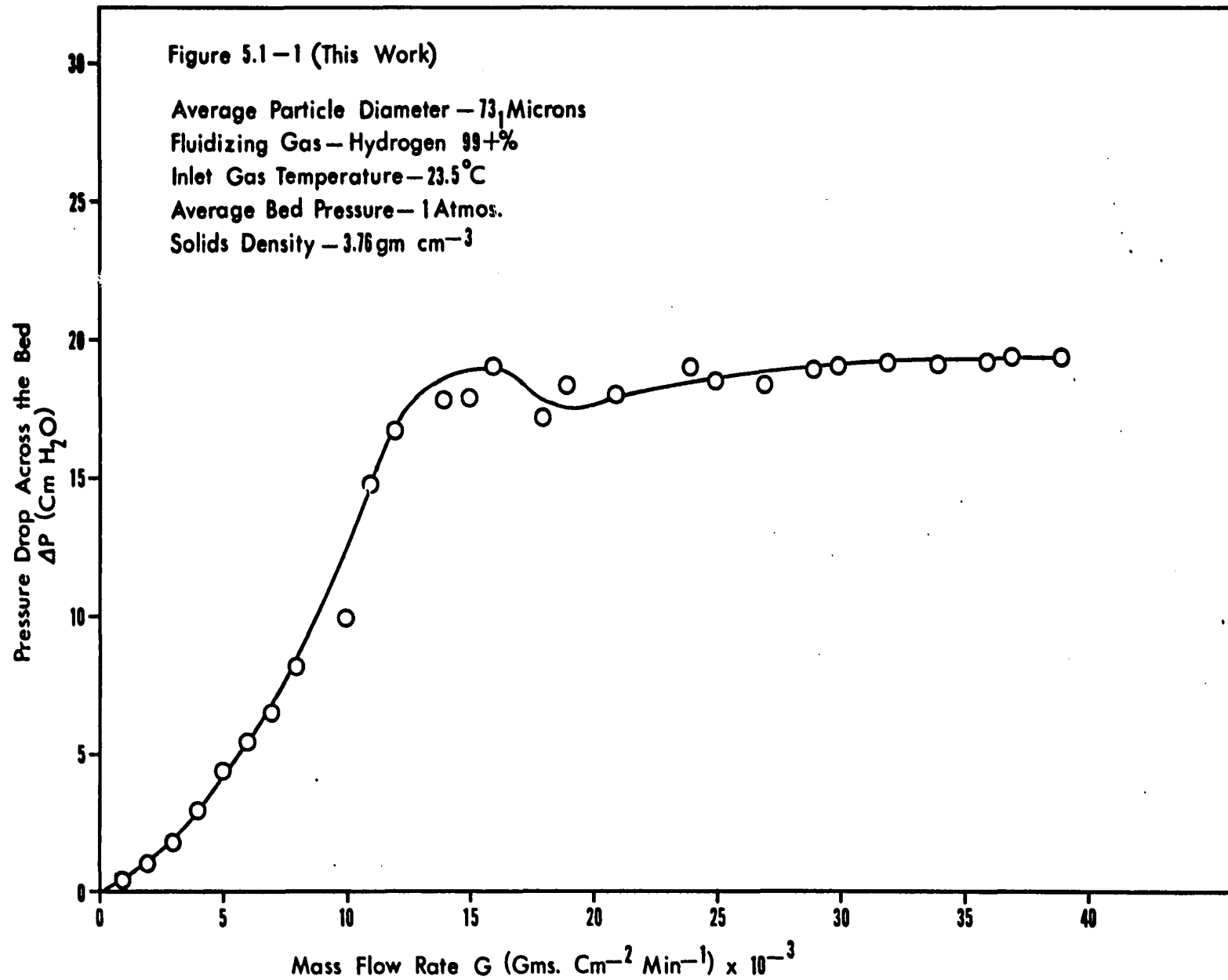


Figure 5.1-1 indicates that as a gas flows upwards through a bed of finely divided particles, there is a definite pressure drop across the bed. In the fixed bed state, this pressure drop is a direct function of the gas flowrate and is approximately linear. Theoretically, the bed will fluidize when the pressure drop across the bed equals the bed weight per unit area. In practice, however, a slightly higher pressure drop is required to overcome inertial forces.

At flowrates higher than those required for minimum fluidization there is a relaxation in the pressure drop followed immediately by a recovery. Under ideal conditions the pressure drop will recover and level off to a constant value equal to the bed weight per unit area. The pressure drop then becomes independent of the gas flowrate.

Many investigators have attempted to predict the minimum fluidizing velocity. Kunii and Levenspiel⁽²⁾ related the pressure drop through a fixed bed to the weight per unit area of the bed at minimum fluidization and derived the following relationship:

$$G_{mf} = \frac{(\phi_s \cdot D_p)^2 \cdot \rho_f \cdot (\rho_s - \rho_f) \cdot g \cdot \epsilon_{mf}^3}{150 \cdot \mu \cdot (1 - \epsilon_{mf})} \quad (5.1-1)$$

where G_{mf} is the minimum fluidizing gas mass velocity in $\text{gms cm}^{-2}\text{sec}^{-1}$

ϕ_s is the particle sphericity, a factor to account for the fact that the particles are not perfect spheres.

D_p is the particle diameter in cm

ρ_f, ρ_s are the fluid and particle densities in g cm^{-3}

ϵ_{mf} is the fraction of the bed at minimum fluidization occupied by the particles, known as the minimum voidage fraction

μ is the gas viscosity, $\text{g cm}^{-1}\text{sec}^{-1}$

Since the particle shape and the minimum voidage fraction are generally not known for design purposes, a great deal of work has been done to develop expressions omitting these terms. The generalized expression most commonly used⁽⁵³⁾ has been of the form:

$$G_{mf} = \frac{k \cdot D_p^a \cdot (\rho_s - \rho_f)^b \cdot \rho_f^c}{\mu^d} \quad (5.1-2)$$

Figure 5.1-2 (p. 42) is a plot of equation 5.1-2 and several other theoretical expressions developed by a number of investigators. The example shown in Figure 5.1-2 is for the fluidization of zinc calcines by hydrogen at 800°C . The expressions are given in Table 5.1-2.

Figure 5.1-2 demonstrates the vast disagreement between investigators.

Where a mixture of particle sizes is to be fluidized, D_p is substituted by the average particle size of the mixture which can be obtained from the expression

$$\bar{D}_p = \frac{1}{\sum \frac{X_i}{D_{pi}}} \quad (5.1-3)$$

where \bar{D}_p is the average particle diameter

X_i is the weight fraction of the i^{th} particle size

D_{pi} is the particle diameter of the i^{th} weight fraction

Figure 5.1-2 Plot of Minimum Velocity vs Particle Diameter

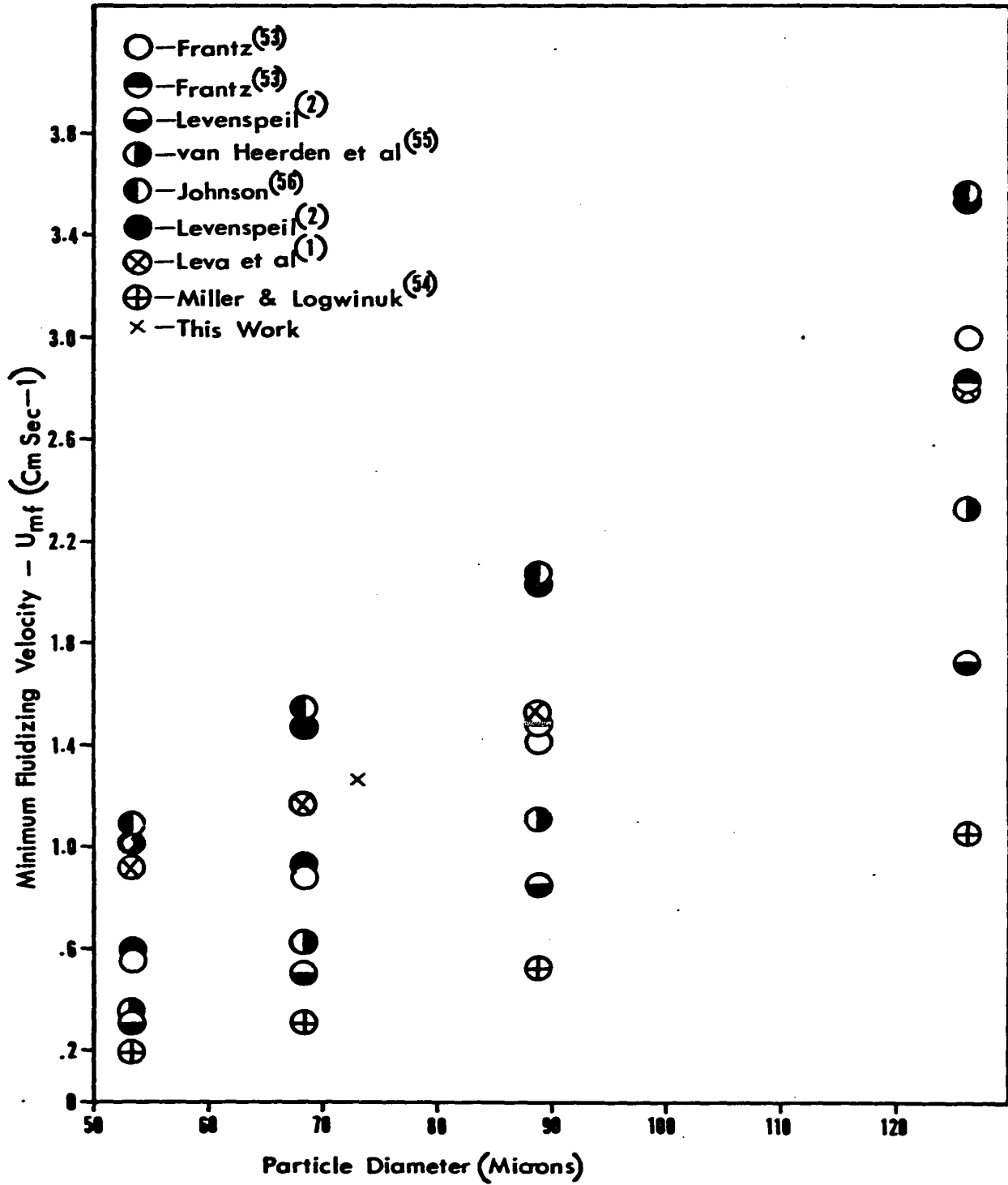


TABLE 5.1-2
Some Empirical and Theoretical Expressions used to
Predict the Minimum Fluidization Gas Velocity

Investigator	Correlation	Units of G_{mf}
Levenspiel (2)	$G_{mf} = \frac{(\phi_s D_p)^2 \rho_f (\rho_s - \rho_f) g \epsilon_{mf}^3}{150 \mu (1 - \epsilon_{mf})}$	$g \text{ cm}^{-2} \text{ sec}^{-1}$
Frantz (53)	$G_{mf} = \frac{4.45 \times 10^{+5} D_p^2 \rho_f (\rho_s - \rho_f)}{\mu}$	$\text{lb ft}^{-2} \text{ hr}^{-1}$
"	$G_{mf} = \frac{1.40 \times 10^5 D_p^{1.8235} \rho_f (\rho_s - \rho_f)^{.9412}}{\mu^{.88235}}$	"
"	$G_{mf} = \frac{1.69 D_p^{1.207} \rho_f^{1.018} (\rho_s - \rho_f)^{1.430}}{\mu^{.729} D_t^{.182}}$	"
Leva (1)	$G_{mf} = \frac{688 D_p^{1.82} \rho_f (\rho_s - \rho_f)^{.94}}{\mu^{.88}}$	"
Miller & Logwinuk (54)	$G_{mf} = \frac{1.25 \times 10^{-3} D_p^2 (\rho_s - \rho_f)^{0.9} \rho_f^{1.1} g_c}{\mu}$	"
Van Heerden, Nobel & Van Krevelen (55)	$G_{mf} = \frac{1.23 \times 10^{-3} D_p^2 \rho_b \rho_f g_c}{B \mu}$	"
Johnson (56)	$G_{mf} = \frac{D_p^2 \phi_s^2 g_c (\rho_s - \rho_f) \rho_f \epsilon^5}{18 [1 + 0.5(1 - \epsilon)]}$	"

Similarly, for cases in which mixtures of gases are to be used, the appropriate weighted average values of the gas viscosity and density must be employed. These are given by

$$\mu_{\text{mix}} = \frac{\rho_{\text{mix}}}{\sum \frac{y_i \rho_i}{\mu_i}} \quad (5.1-4)$$

$$\text{and} \quad \rho_{\text{mix}} = \sum V_i \rho_i \quad (5.1-5)$$

where y_i , ρ_i , μ_i , V_i are the weight fraction, density, viscosity and volume fraction of each gas in the mixture.

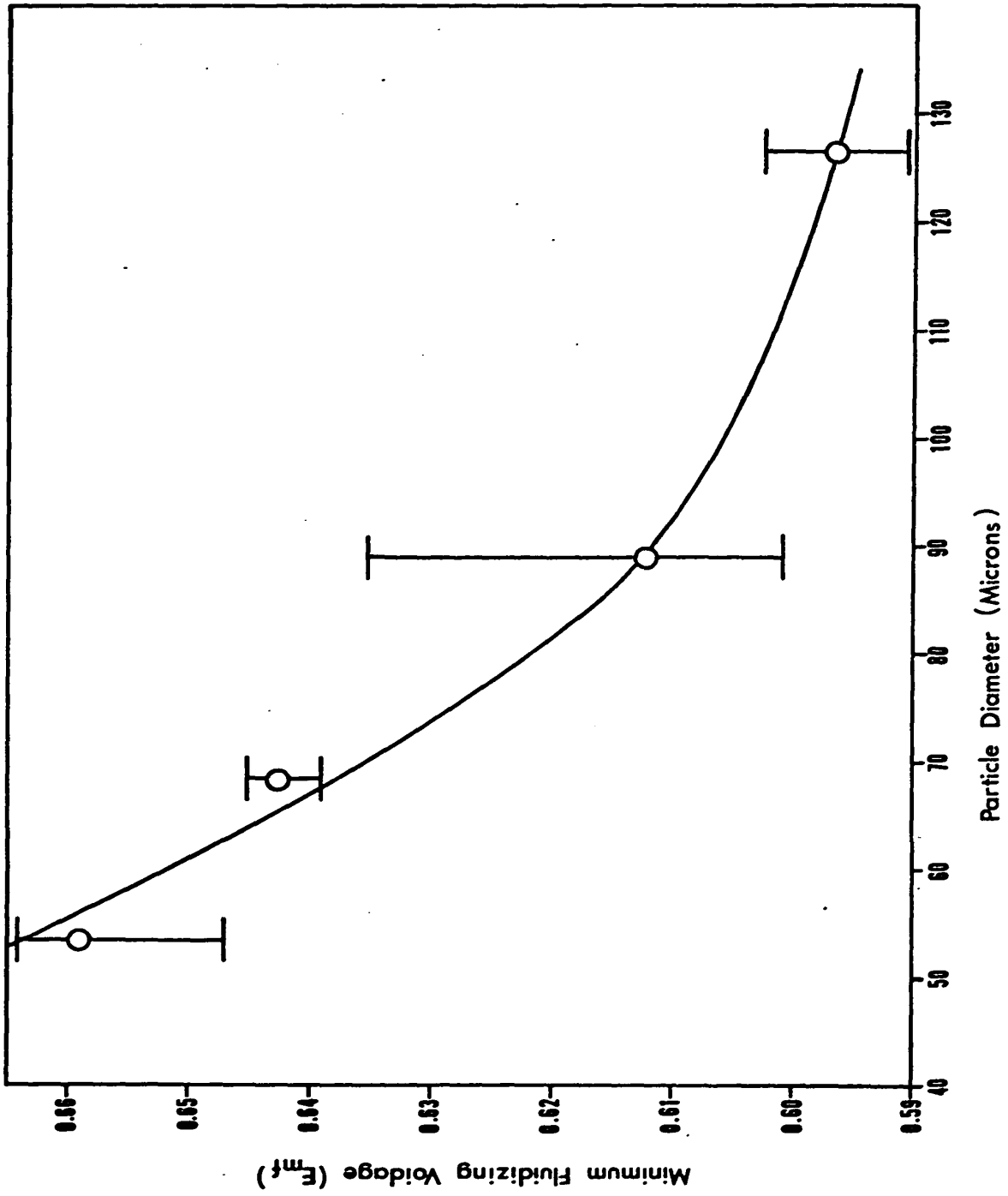
The disagreement between the results of the theoretical equations has made it necessary to use, in the high temperature experiments of this work, the average of these equations to represent the minimum fluidizing gas velocity at elevated temperatures.

The results in Figure 5.1-2 based upon the theoretical expressions have assumed that the particle sphericity was 0.6 (i.e., the ratio of the volume of the particle at diameter d to the volume of a sphere of equivalent diameter d was 0.6).

The minimum fluidization bed voidage fraction (ϵ_{mf}) was based on the values obtained for the packed bed case as described below.

ϵ_{mf} is shown as a function of particle diameter in Figure 5.1-3 (p. 45).

Figure 5.1 — 3 Minimum Fluidizing Voidage vs Particle Diameter



The particle fractions were obtained by screening a portion of the calcine into four size fractions — -100+150 mesh, -150+200 mesh, -200+270 mesh, and -270+325 mesh material using Tyler series screens. The particle size corresponding to each size fraction was assumed to be the simple average of the two limiting mesh sizes, expressed in microns.

The fixed bed voidage was determined by pouring each size fraction into a container of known volume and by weighing. The bed voidage was calculated as

$$\epsilon = 1 - \frac{w}{V \rho_s} \quad (5.1-6)$$

where w is the solids weight occupying the container

V is the volume of the container

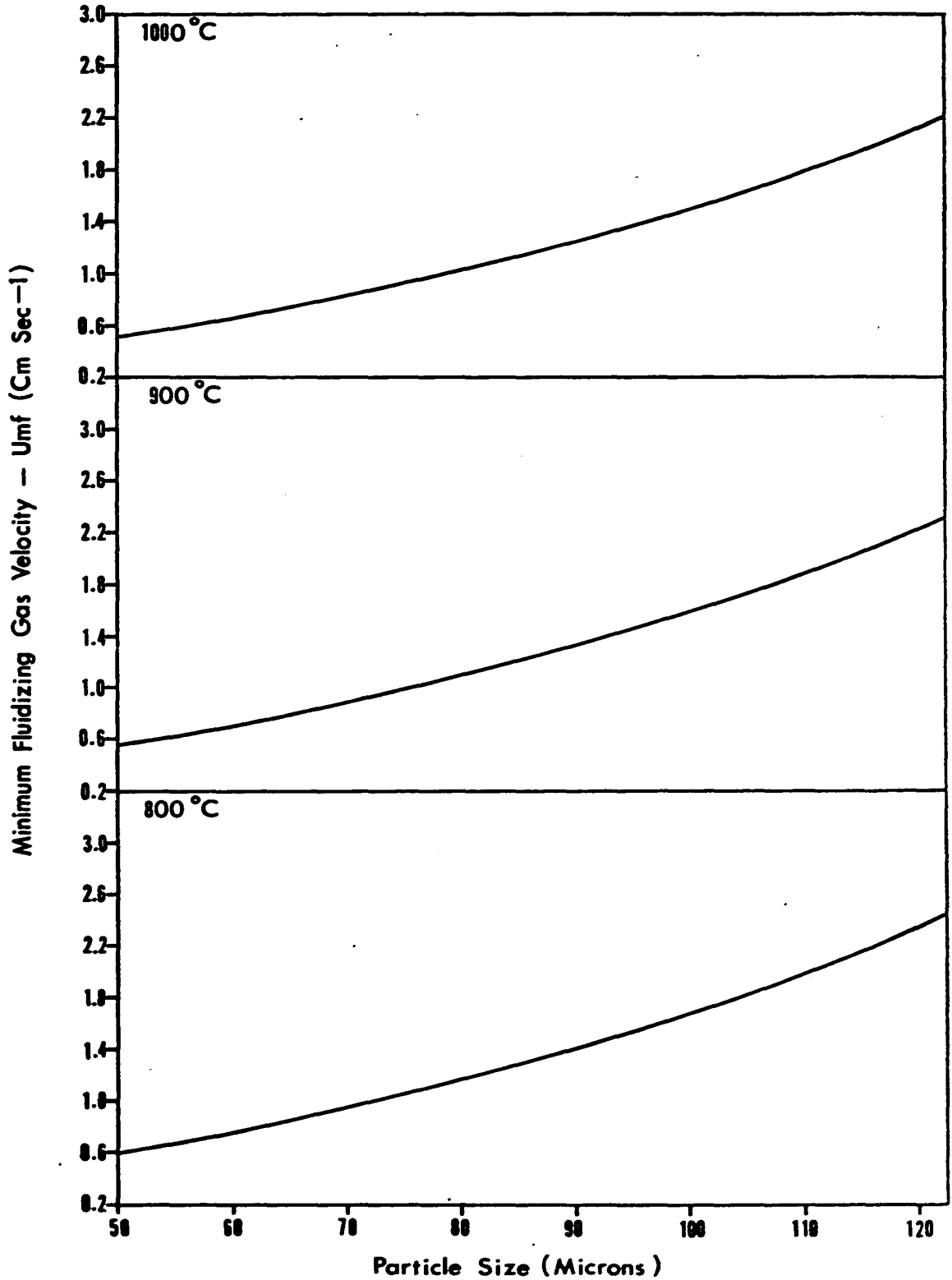
ρ_s is the solids density

The solids density of the zinc calcine was determined by means of a pycnometer using Shell Canada Limited 911 Pella Oil as a liquid displacant and was found to be 3.76 g cm^{-3} .

The procedure for finding the fixed bed voidage fraction was repeated four times for each size fraction and an average value was obtained. Figure 5.1-3 indicates the spread in values obtained. Although Johnson⁽⁵⁶⁾ suggests that in the calculation of the minimum fluidization velocity, the minimum fluidized bed voidage fraction should be considered as 8-10% larger than the fixed bed voidage, this was not adhered to in the present investigation and fixed bed voidage was substituted directly into the theoretical expressions.

In this investigation, the minimum fluidizing velocity will refer to the values given by Figure 5.1-4 for the appropriate operating conditions.

Figure 5.1-4 Plot of Minimum Fluidizing Gas Velocity vs Particle Size



5.2 The Terminal Velocity

As mentioned in Section 5.1 (p. 37), the upper allowable limit on the gas velocity through a fluidized bed is the velocity which will transport the particles from the bed. For particle Reynolds numbers less than 0.4, Levenspiel et al⁽²⁾ show that the terminal velocity, U_t (cm sec⁻¹), can be expressed as

$$U_t = \frac{g(\rho_s - \rho_f) D_p^2}{18 \mu} \quad (5.2-1)$$

Experimentally it has been found that the terminal velocity is 50-90 times the minimum fluidizing velocity. Extremely turbulent conditions are experienced in most gas fluidized beds at gas velocities as low as 6-11 times U_{mf} ⁽²⁾. The terminal velocity is, therefore, very rarely a critical variable except in those cases where a mixture of solid particles contains a wide range of particle sizes.

5.3 Summary

This chapter has presented a description of the behaviour of fluidized beds particularly in terms of the minimum fluidization velocity. A review of methods for calculating the minimum fluidization velocity has been presented and the difficulties encountered with the calculations have been discussed.

In addition, the minimum fluidizing velocity for the zinc calcine-hydrogen system being studied in this investigation has been predicted on the basis of experimental and present knowledge.

CHAPTER SIX

ROASTING OF ZINC CONCENTRATES

6.0 The Physical Chemistry of Zinc Concentrate Roasting

The increasingly important position of the electrolytic process for the production of high purity primary refined zinc has been noted (Table 3.0-1, p. 12). The general practice followed to produce electrolyte is to leach roasted zinc concentrates in dilute spent electrolyte. However, a serious obstacle encountered in the electrolytic process is the formation of the compound zinc ferrite, $\text{ZnO} \cdot \text{Fe}_2\text{O}_3$, which is only sparingly soluble during the normal leaching of roasted zinc concentrates containing iron. Its formation constitutes a zinc loss in the residue which is proportional to the iron content of the ore.

In addition, although the principal product of the roasting process is zinc oxide, the formation of the normal form of zinc sulphate, $\text{ZnSO}_4 (\alpha)$ or a basic zinc sulphate, $\text{ZnO} \cdot 2\text{ZnSO}_4$, is unavoidable. During normal roasting the conditions of temperature and air admission are controlled in an attempt to produce just sufficient zinc sulphate to overcome losses in the electrolysis circuit.

There are very few thermodynamic data available on the formation of zinc ferrite and as a result its behaviour under conditions of gaseous reduction in a fluidized bed reactor is not predictable. Zinc ferrite formation apparently poses no problems in retort and blast furnace smelting where reduction is carried out at relatively high temperatures (1100-1300°C). Fluidized bed reduction units would normally be run at 800-1000°C to prevent any fusion of calcine components and at these temperatures the characteristics of zinc ferrite formation may be considerably different.

In the absence of reliable information on the formation and reduction of zinc ferrite, it is useful to examine the roasting process with particular emphasis on optimizing conditions to retard the formation of zinc ferrite.

The approach considered is that demonstrated by Benner and Kenworthy⁽⁵⁷⁾. Because of the complexity of the problem, these authors first calculated the thermodynamic data for the ternary systems Zn-S-O and Fe-S-O. They then superimposed the two ternaries to obtain the quaternary system Zn-Fe-S-O. The reactions of the individual systems were assumed not to be altered by the super-

imposition. The resulting diagrams for the Zn-Fe-S-O system were divided into fields in which iron and zinc compounds could co-exist in stable configurations, i. e., at unit activity.

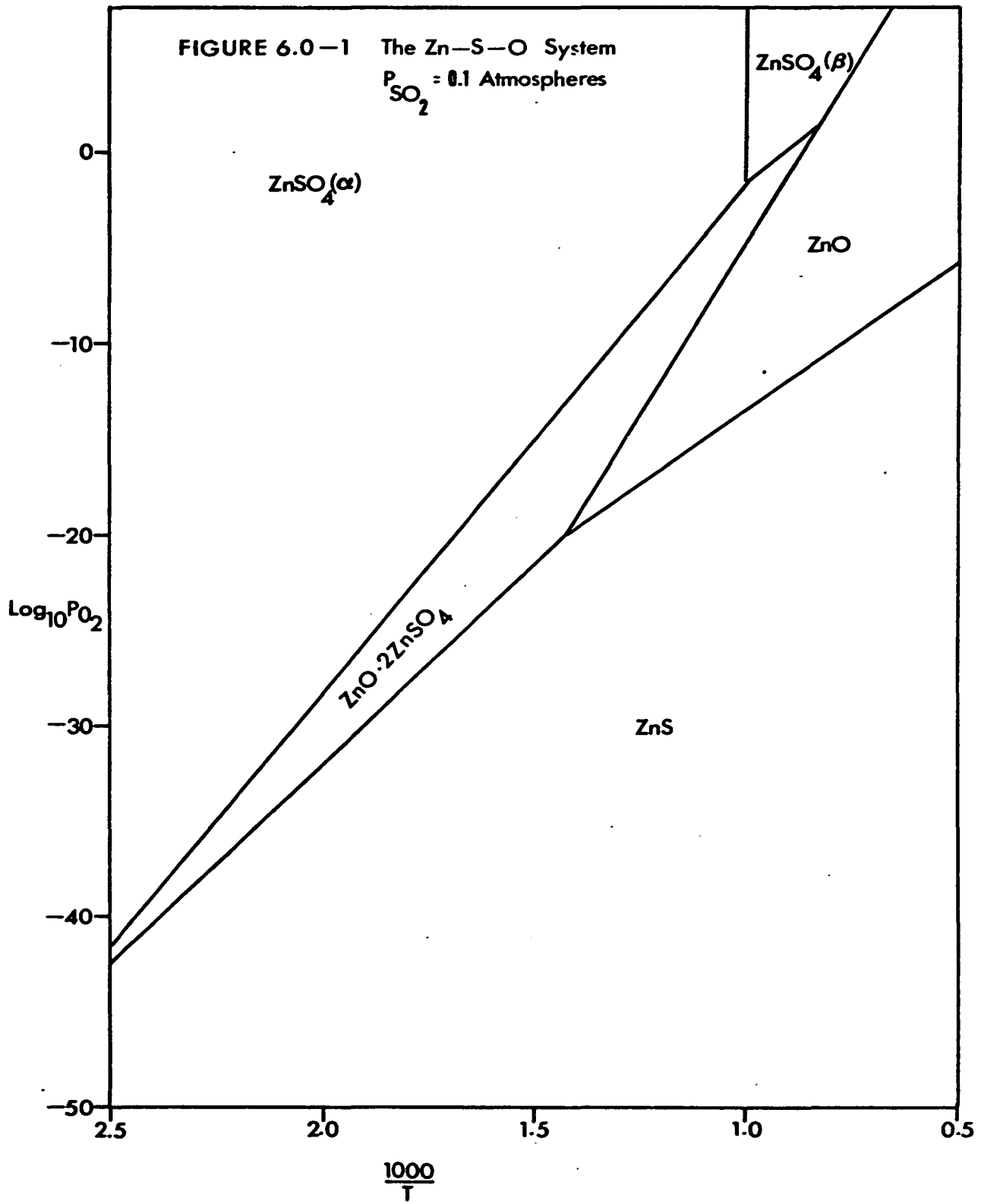
In this chapter the approach has been modified to include the existence of a basic zinc sulphate as reported by Ingraham and Kellogg⁽⁵⁸⁾. The effect of roasting temperature, and the partial pressures of O₂ and SO₂ on the formation and stability of co-existing compounds is examined.

The equations examined and the associated equilibrium constants for the Zn-S-O system are given in Table 6.0-1. The data used are that of Ingraham and Kellogg⁽⁵⁸⁾. The fixing of a constant value of the sulphur dioxide partial pressure, P_{SO_2} , of 0.1 atmospheres permits plotting of the fields of stability of the various possible compounds in the Zn-S-O system as a function of the oxygen partial pressure and roasting temperature. A sulphur dioxide partial pressure of 0.1 was chosen because it represents the sulphur dioxide levels experienced industrially (Canadian Electrolytic Zinc Co. Ltd., Valleyfield, Quebec). This plot is shown in Figure 6.0-1.

TABLE 6.0-1

Equilibrium Constants for Reactions in the Zn-S-O System Reaction

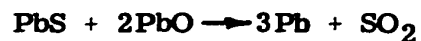
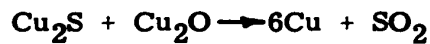
Reaction	Log ₁₀ K				
	900 ^o K	1000 ^o K	1100 ^o K	1200 ^o K	1300 ^o K
(1) $3\text{ZnSO}_4 (\alpha) \rightarrow \text{ZnO} \cdot 2\text{ZnSO}_4 + \text{SO}_2 + 1/2\text{O}_2$	-3.978	-2.119	—	—	—
(2) $3\text{ZnSO}_4 (\beta) \rightarrow \text{ZnO} \cdot 2\text{ZnSO}_4 + \text{SO}_2 + 1/2\text{O}_2$	—	—	-0.869	+0.151	+1.008
(3) $1/2(\text{ZnO} \cdot 2\text{ZnSO}_4) \rightarrow 3/2\text{ZnO} + \text{SO}_2 + 1/2\text{O}_2$	-5.260	-3.394	-1.880	-0.627	+0.424
(4) $3\text{ZnS} + 11/2\text{O}_2 \rightarrow \text{ZnO} \cdot 2\text{ZnSO}_4 + \text{SO}_2$	75.843	64.354	54.973	47.170	40.627
(5) $\text{ZnS} + 3/2\text{O}_2 \rightarrow \text{ZnO} + \text{SO}_2$	21.774	19.189	17.071	15.305	13.825
(6) $\text{Zn}(1, \text{g}) + 1/2\text{S}_2 \rightarrow \text{ZnS}$	10.344	8.778	7.501	6.354	5.060
(7) $\text{Zn}(1, \text{g}) + 1/2\text{O}_2 \rightarrow \text{ZnO}$	14.922	12.872	11.196	9.716	8.154
(8) $1/2\text{S}_2 + \text{O}_2 \rightarrow \text{SO}_2$	17.196	15.094	13.376	11.943	10.731
(9) $1/2\text{O}_2 + \text{SO}_2 \rightarrow \text{SO}_3$	0.810	0.257	-0.190	-0.559	-0.866



These data can be plotted as a function of the $\text{Log}_{10} P_{\text{SO}_2}$ vs $\text{Log}_{10} P_{\text{O}_2}$ at constant temperature as presented in Figure 6.0-2 for three values of the roasting temperature (1100, 1200, 1300°K). The fields in Figure 6.0-2 represent fields of unit activity. For example, the field marked $\text{ZnSO}_4(\alpha)$ shows the temperature and P_{SO_2} and P_{O_2} conditions under which pure $\text{ZnSO}_4(\alpha)$ can exist.

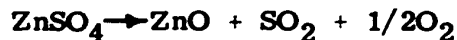
Examination of these equilibrium diagrams illustrates several significant facts about the Zn-S-O system.

- 1) The field of stability of zinc metal is bounded by extremely low values of P_{O_2} and P_{SO_2} and hence roast-reduction type reactions, common in copper and lead metallurgy, i. e., reactions of the form



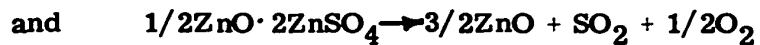
are not attainable in zinc metallurgy.

- 2) Whereas the equilibrium decomposition has long been held to follow the reaction:



this reaction is, in fact, impossible under normal roasting conditions, i. e., the diagrams indicate that the decomposition must proceed in two stages represented

by the reactions



The requirement of the two reaction steps is indicated by the fact that the ZnO and ZnSO₄ areas are in no case adjacent to each other at temperatures up to 1300°K.

- 3) Since most roasters are operated under conditions to produce only a small amount of sulphate in the calcine, the basic zinc sulphate (ZnO·2ZnSO₄) and not the normal zinc sulphate (ZnSO₄) should report.
- 4) For roasters operated at close to equilibrium conditions, Figure 6.0-2 can be utilized to predict the type of calcine which should result from the roasting of sphalerite. For example, Figure 6.0-2 shows a roaster operated with a roaster gas composition 6% O₂ and 10% SO₂ (Canadian Electrolytic Zinc Co. Ltd. practice). At the lower temperature, the roaster will produce a calcine of basic sulphate. To obtain a calcine of zinc oxide, higher roasting temperatures are required or a gas leaner in O₂ and SO₂.

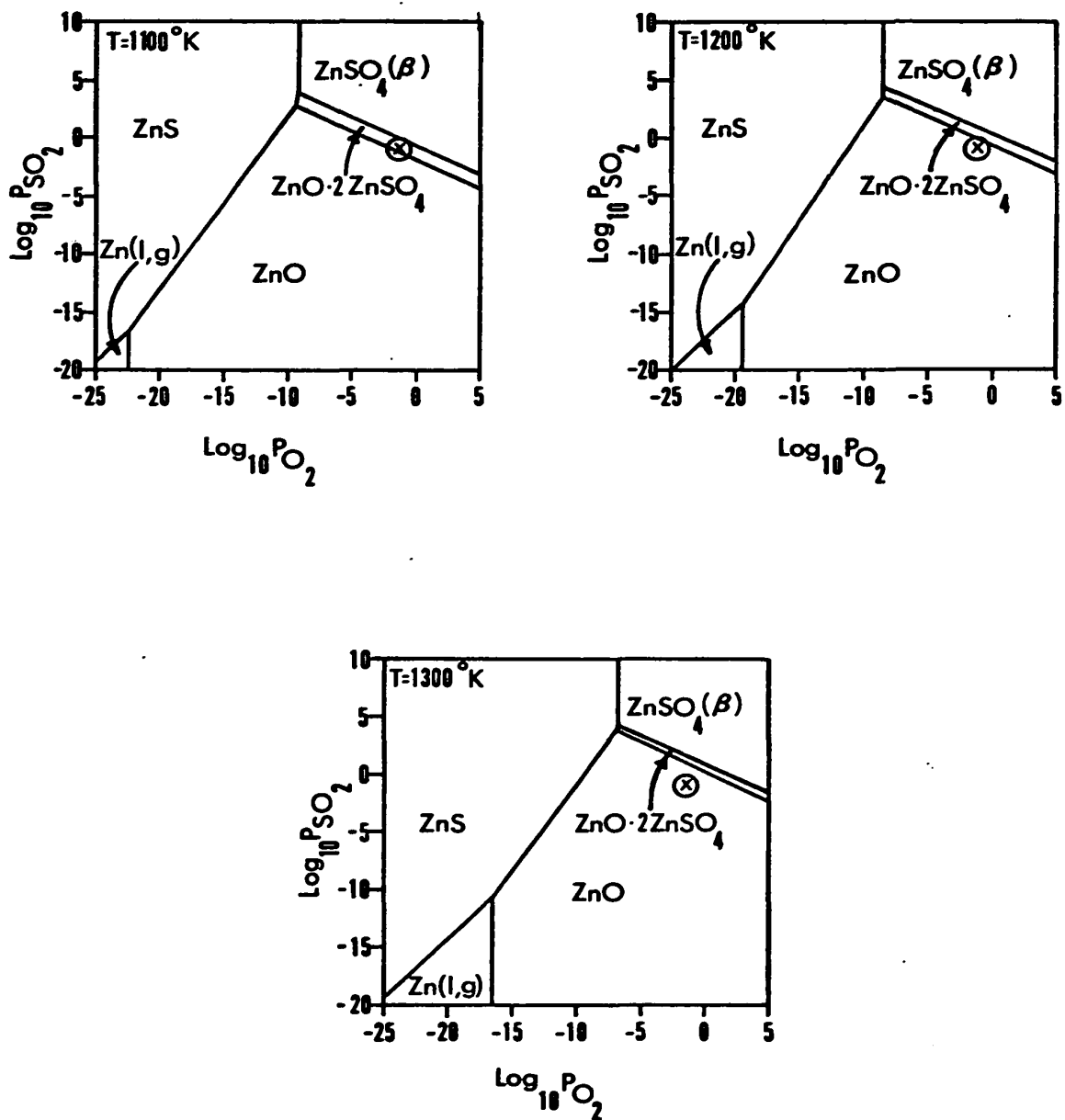


Figure 6.8-2 Stable Equilibria in the Zn-S-O System. Areas are Regions of Stability of one Condensed Phase as Marked.

6.1 The Fe-S-O System

Since there has been less interest in the roasting of FeS than ZnS, there are fewer published thermodynamic data on the Fe-S-O system than on the Zn-S-O system. Within the system the components FeS₂, FeS, FeO, Fe₃O₄, Fe₂O₃, and Fe₂(SO₄)₃ are known to exist and thermodynamic data have been published for these compounds. In addition there is likely to be a number of basic sulphates and other complex compounds associated with the system. No thermodynamic data have been published for these compounds and hence potential reactions between the known compounds only are included in this study. The Fe-S-O system has been studied in the same manner employed for the Zn-S-O system. The reactions considered and the equilibrium constants are given in Table 6.1-1.

TABLE 6.1-1
Equilibrium Constants for Reactions in the Fe-S-O System

Reaction	Log ₁₀ K						
	400	900	1000	1100	1200	1300	1500
1) Fe ₂ O ₃ + 3/2O ₂ + 3SO ₂ → Fe ₂ (SO ₄) ₃	69.2	7.1	2.2	-1.7	-5.0	-7.9	-12.5
2) 4Fe ₃ O ₄ + O ₂ → 6Fe ₂ O ₃	-46.9	-13.1	-10.4	-8.2	-6.3	-4.8	-2.3
3) 3FeS + 5O ₂ → Fe ₃ O ₄ + 3SO ₂	208.0	81.5	71.4	63.2	56.4	50.6	41.4
4) 2FeS + 7/2O ₂ → Fe ₂ O ₃ + 2SO ₂	199.7	78.9	69.4	61.5	55.0	49.5	40.6
5) 2FeS + 5O ₂ + SO ₂ → Fe ₂ (SO ₄) ₃	214.8	63.6	51.5	41.6	33.4	26.4	15.2
6) FeS + 3/2O ₂ → FeO + SO ₂	57.7	23.2	20.4	18.2	16.6	14.7	12.1
7) 3FeO + 1/2O ₂ → Fe ₃ O ₄	34.9	11.9	10.2	8.8	7.6	6.6	5.0

The equilibrium constants for the reactions in Table 6.1-1 were calculated from the thermodynamic data provided by Benner and Kenworthy⁽⁵⁷⁾. Table 6.1-1 does not show data for the reactions involving FeS_2 because it readily decomposes at low temperature to FeS and $\text{S}_2(\text{g})$. Equations 1 to 7 provide the boundary lines for Figure 6.1-1 and it can readily be seen that only reactions 1 to 5 can form stable compounds at the temperature and atmospheric conditions ($P_{\text{SO}_2} = 0.1$ atmospheres) of this figure. The two invariant points shown in Figure 6.1-1 can be represented by the equations

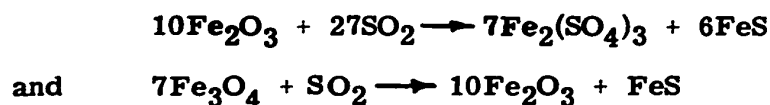
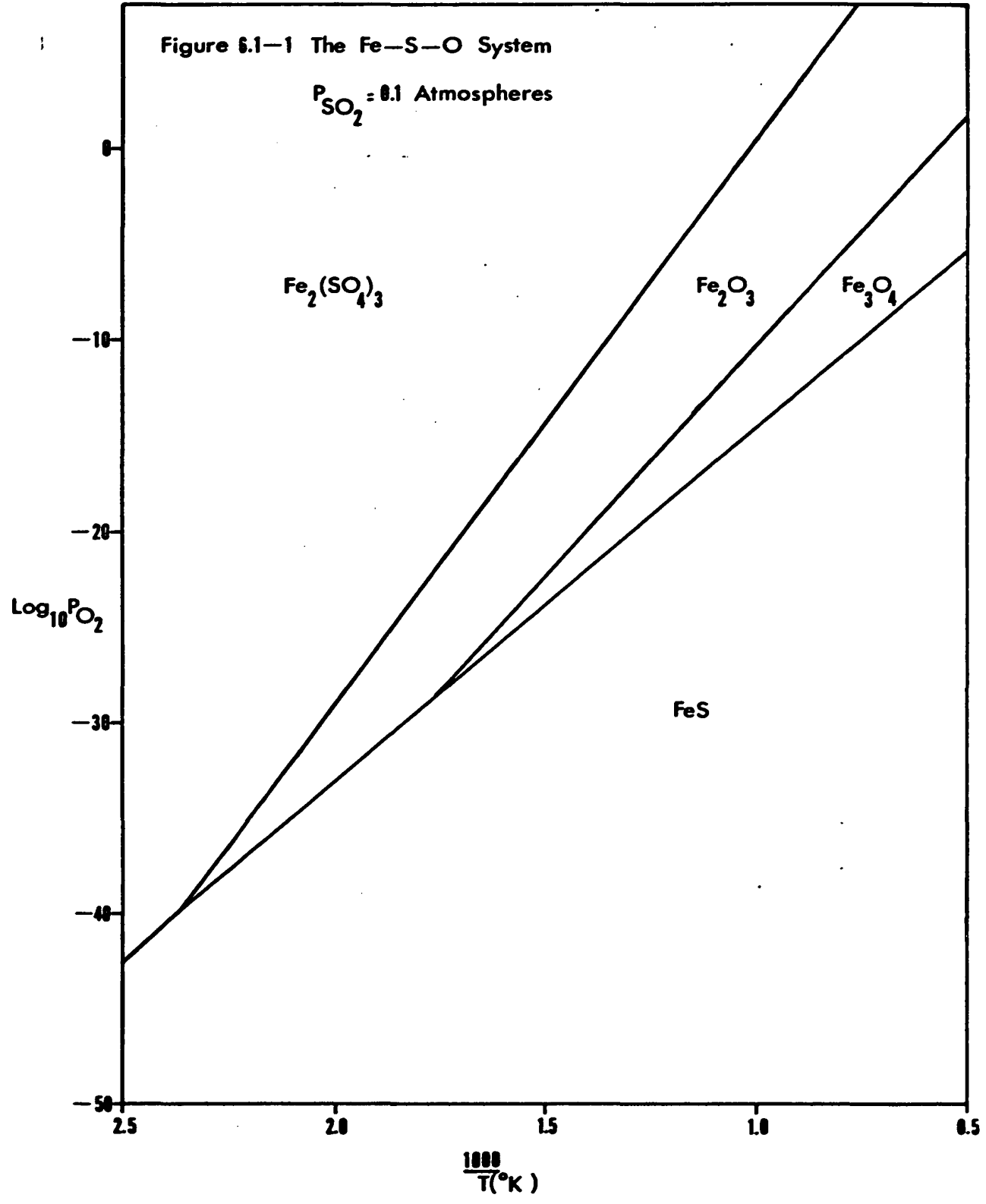


Figure 6.1-2 is a plot of the equations found in Table 6.1-1 as a function of the oxygen and sulphur dioxide partial pressures. The temperatures correspond to those used in the development of the corresponding plots in the Zn-S-O system. Under a normal roasting atmosphere ($\text{Log}_{10}P_{\text{O}_2}$ and $\text{Log}_{10}P_{\text{SO}_2}$ between -1 and -2), Figure 6.1-2 indicates that hematite (Fe_2O_3) should be the stable form of iron oxide. As with the Zn-S-O system the stability of liquid or solid iron is bounded by extremely low partial pressures of oxygen and sulphur dioxide.

Figure 6.1-1 The Fe-S-O System

$P_{SO_2} = 0.1$ Atmospheres



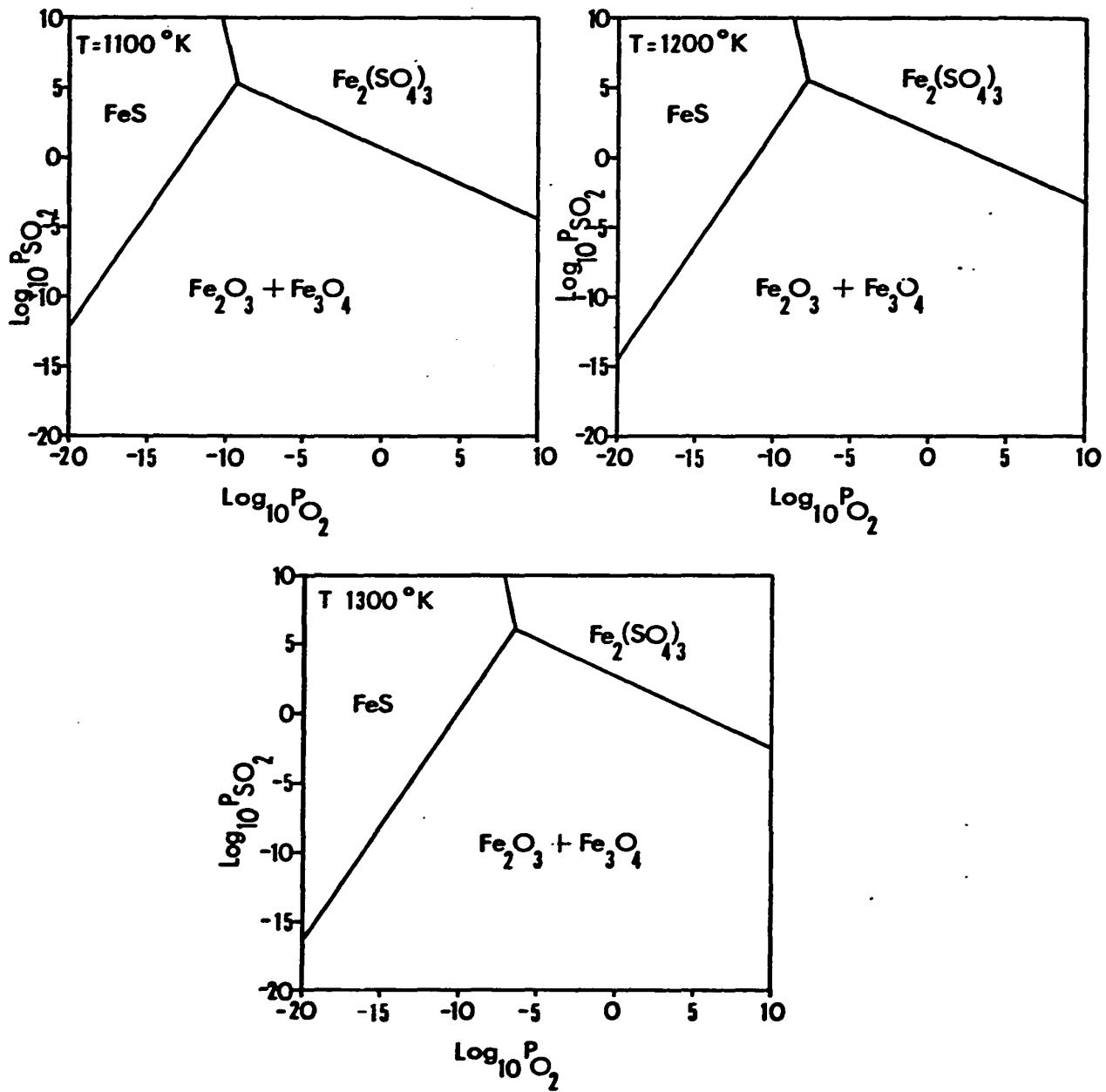
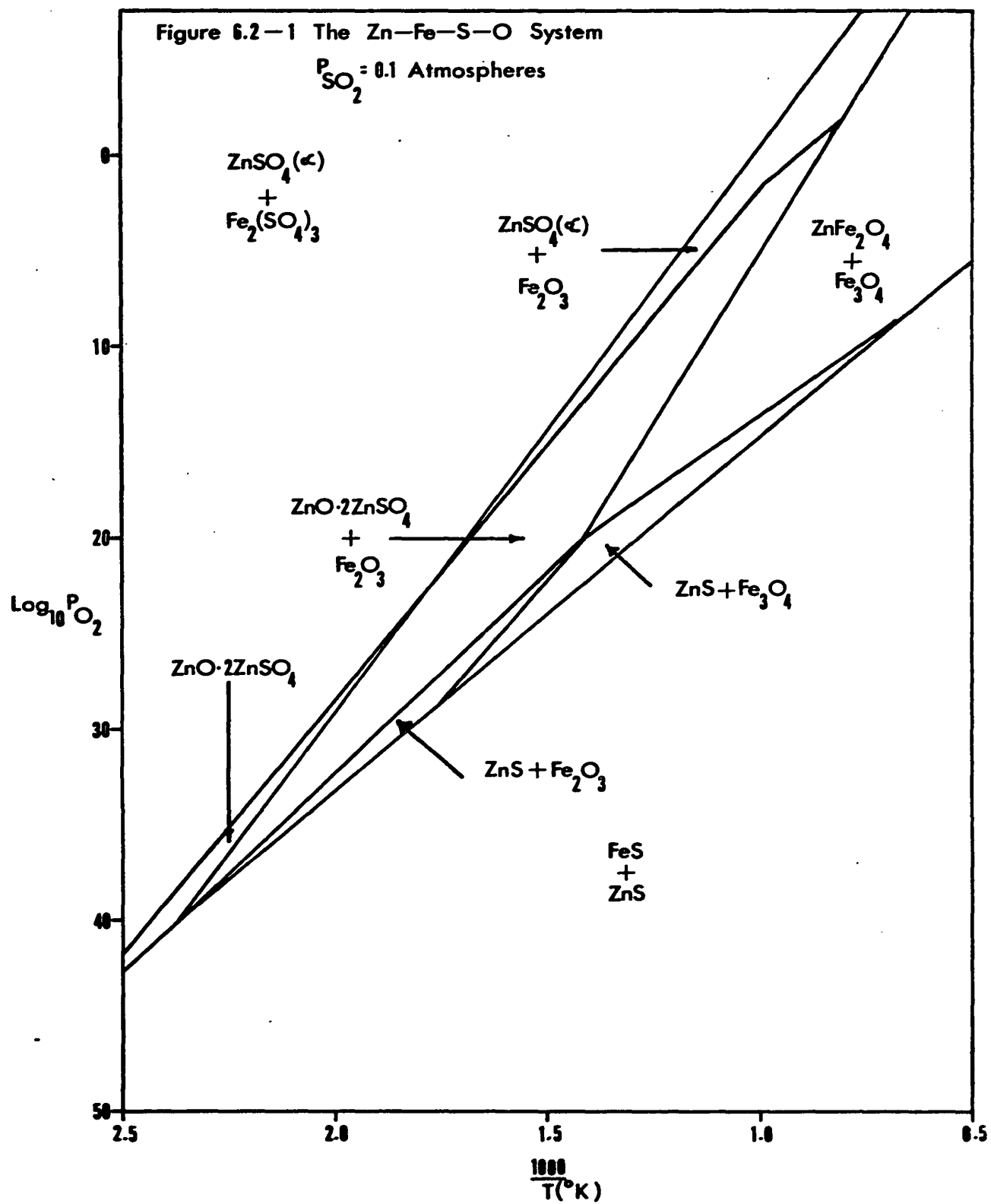


Figure 6.1-2 Stable Equilibria in the Fe-S-O System.
 Areas are Regions of Stability of One
 Condensed Phase as Marked.

6.2 The Zn-Fe-S-O System

Benner and Kenworthy⁽⁵⁷⁾ found that by superimposing the Zn-S-O system on the Fe-S-O system, a good qualitative representation of the Zn-Fe-S-O system could be achieved which agreed within reasonable limits with experimental observation. Figures 6.2-1 and 6.2-2 are the results of the superimposition.



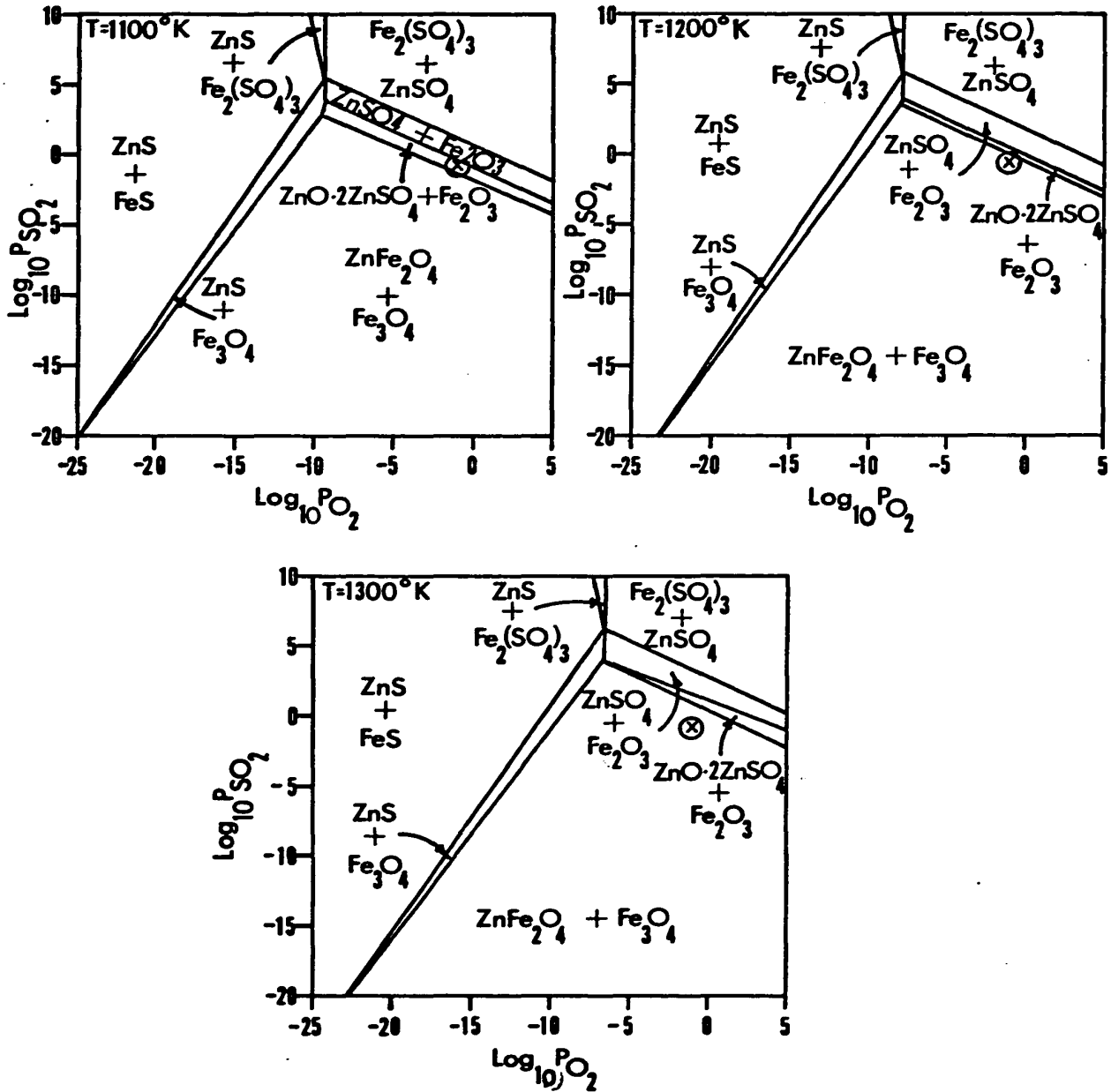


Figure 6.2-2 Stable Equilibria in the Zn-Fe-S-O System. Areas are Regions of Stability of Two Condensed Phases as Marked.

6.3 Analysis of Roasting Zinc Concentrates to Retard Zinc Ferrite Formation

Figures 6.2-1 and 6.2-2 offer a simple thermodynamic picture explaining why the existence of zinc ferrite is more prevalent at higher roasting temperatures. It is only at these elevated temperatures that ZnO and Fe₂O₃ can coexist with oxygen and sulphur dioxide in the atmosphere and consequently it is the only condition under which they can combine to form zinc ferrite. Note, for example, point X in Figures 6.2-1 and 6.2-2 which represents the typical (Canadian Electrolytic Zinc Co. Ltd.) effluent gas of 6% O₂ and 10% SO₂, remainder N₂ of an industrial roaster. It can be seen that at temperatures above 1100°K this gas is in the ZnFe₂O₄ field while at temperatures below 1100°K basic zinc sulphate formation is favoured.

Hopkins⁽⁵⁹⁾ and Kato and Takei⁽⁶⁰⁾ have also reported experimental evidence to show that the kinetics of zinc ferrite formation become extremely rapid at normal roasting temperatures (800-1100°C). Roggero⁽⁴⁾ confirmed that any iron associated with zinc concentrates reported as zinc ferrite in the roasted product.

By considering the roasting process in terms of Figures 6.2-1 and 6.2-2, one can make a number of proposals with regard to the effects of temperature, the oxygen partial pressure, and the sulphur dioxide partial pressure on potential zinc ferrite elimination.

6.3-1 Effect of Temperature on Zinc Oxide Recovery

Figure 6.2-1 shows that as the temperature of roasting is lowered point X will move closer to the ZnO·2ZnSO₄ + Fe₂O₃ region and ultimately into the ZnSO₄(α) + Fe₂O₃ or the ZnSO₄(α) + Fe₂(SO₄)₃ fields. In all cases the formation of ZnFe₂O₄ will no longer be favoured.

Unfortunately the lowering of temperature will also reduce the rate of the roasting reaction and some ZnS will not be completely oxidized.

Benner and Kenworthy⁽⁵⁷⁾ suggest that at very high temperatures (1500-2000^oK) the zinc ferrite contains less than the stoichiometric amount of zinc and hence more free ZnO will be produced during roasting. No industrial confirmation of this suggestion has been obtained and a lowering of temperature still seems to be the best way to avoid zinc ferrite formation.

6.3-2 Effect of Gas Composition on Zinc Oxide Recovery

The oxygen pressure in a fluidized bed roasting operation can be controlled to some extent by varying the amount of excess oxygen (above the stoichiometric quantity) fed into the bed. An increase in oxygen pressure by an increase in excess oxygen will tend to move point X in Figures 6.2-1 and 6.2-2 into the $\text{ZnO} \cdot 2\text{ZnSO}_4 + \text{Fe}_2\text{O}_3$ or the $\text{ZnSO}_4(\alpha) + \text{Fe}_2\text{O}_3$ region thus reducing the possibility of ZnFe_2O_4 formation.

Figure 6.2-2 shows, however, that at 1100^oK even a slight increase in the sulphur dioxide partial pressure will render the formation of ZnFe_2O_4 thermodynamically unfavourable. Snurnikov et al⁽⁶¹⁾, on the other hand, have shown experimentally that increasing the sulphur dioxide partial pressure is ineffective in decomposing zinc ferrite. They found, rather, that sulphatization of free zinc oxide resulted with no appreciable reduction in the ferrite content because free ZnO sulphatizes more actively than that combined in ferrite.

6.4 Summary of Zinc Concentrate Roasting for the Recovery of Free Zinc Oxide

The compound stability diagrams, constructed from the available thermodynamic data, have been useful in a) predicting the compounds present in roasted zinc concentrate under various roasting conditions and b) predicting under what conditions to operate a roasting operation in order to recover a maximum yield of free zinc oxide.

It has been shown that the most important variable in maximizing free zinc oxide formation (minimizing zinc ferrite formation) is temperature. Control of the oxygen and sulphur dioxide partial pressures can also contribute to the maximizing of free zinc oxide production.

CHAPTER SEVEN

THE ZINC OXIDE-HYDROGEN SYSTEM
AT ELEVATED TEMPERATURES7.0 Reduction of Zinc Oxide by Hydrogen

The principal reaction involved in the hydrogen reduction of zinc oxide is



for which extensive thermodynamic data are available⁽⁶²⁾. The reduction of zinc oxide to metallic zinc differs from the reduction of other base metals in two ways. In the first instance zinc oxide exhibits a relatively high degree of stability. Secondly, the metal is highly volatile. The boiling point of zinc is relatively low (907°C) and zinc has an appreciable vapour pressure at lower temperatures. The first step in studying zinc oxide reduction has been to formulate a thermodynamic model of the system, particularly from the point of view of the equilibrium conditions that the system tends to approach.

In the thermodynamic presentation, the problem is studied by considering a bed of finely divided zinc oxide particles fluidized by the reducing gas, hydrogen. The hydrogen is assumed to reach an equilibrium state with the zinc oxide and consequently the equilibrium gas composition of the effluent gas mixture can be calculated. The extent of the reaction and the zinc content of the effluent gas stream will ultimately depend upon kinetic factors (reaction rate, rate of gas flow, the surface area of gas-solid contact) but under the most favourable conditions equilibrium will be attained and the zinc content in the gas will

be a maximum. At equilibrium, the partial pressures of Zn, H₂, and H₂O will satisfy the relationship

$$K_{eq} = \frac{(P_{Zn})(P_{H_2O})}{P_{H_2}} \quad (7.0-2)$$

The stoichiometry of the process shows that one mole of water vapour is produced for each mole of zinc. Therefore, in the effluent gas,

$$P_{Zn} = P_{H_2O} \quad (7.0-3)$$

Since the total pressure in the bed is very nearly atmospheric and since the total pressure is equivalent to the sum of the partial pressures of the three gas constituents:

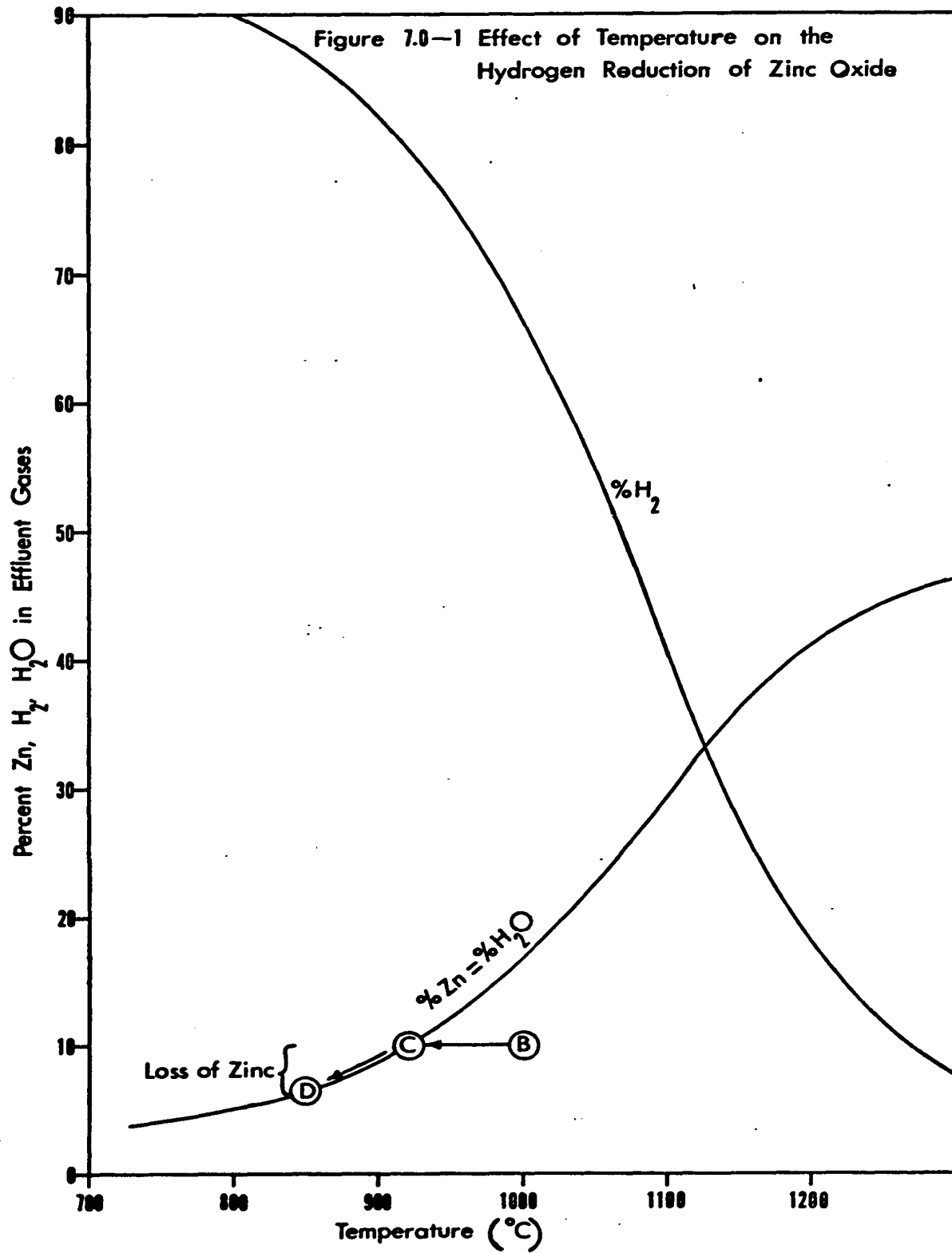
$$P_{Zn} + P_{H_2} + P_{H_2O} = 1 \quad (7.0-4)$$

The partial pressure of oxygen has not been included in the total pressure relationship because, in the system, it is of the order of 10⁻¹⁹ atmospheres and is so small in comparison to the other components of the gas stream that it can be neglected in the calculations.

Simultaneous solution of these equations for a total pressure of 1 atmosphere yields

$$P_{Zn} = P_{H_2O} = \sqrt{K_{eq}(1 + K_{eq})} - K_{eq} \quad (7.0-5)$$

From the free energy relationship for equation 7.0-1, the value of K_{eq} can be calculated for any temperature. The results are shown in Figure 7.0-1.



It must be remembered that the equilibrium zinc content in the effluent gas represents a maximum and that with unfavourable kinetics the maximum may not be realized. Examination of Figure 7.0-1 yields instructive information on the possible use of hydrogen as a reducing agent for zinc oxide with regard to the reoxidation and condensation of gaseous zinc.

Point B on Figure 7.0-1 represents an effluent gas with less zinc and H_2O than the equilibrium amount, i. e., the reaction has not been able to proceed to equilibrium. The cooling of a gas of this composition in order to condense the zinc is represented by the line BC. Where BC intersects the equilibrium curve, the gaseous mixture will just be at equilibrium with solid ZnO. To the left of the curve, the ratio $(P_{H_2O})(P_{Zn})/P_{H_2}$ will be greater than the equilibrium constant for the gaseous reduction reaction 7.0-1 and the water vapour will oxidize the zinc vapour to precipitate ZnO. As the gas is cooled further, ever increasing amounts of ZnO will be deposited as the gas composition readjusts to follow the equilibrium curve (point D).

To attain a maximum yield of condensed zinc, the effluent gases must be maintained as near as possible to the reaction temperature prior to condensing the zinc and any cooling must be very rapid, i. e., the vapour must be shock cooled to condense liquid zinc.

7.1 Reactions With Other Components of the Zinc Calcine

The zinc calcine employed in this investigation is composed almost entirely of zinc in the form of zinc oxide, basic zinc sulphate,

and zinc ferrite.

While the activity of the zinc oxide can be taken as unity, the activity of the zinc oxide associated with the sulphate and zinc ferrite will be lower. It is unlikely, therefore, that either of these compounds will be reduced until virtually all of the pure zinc oxide has been reduced.

The reduction of the zinc calcine, then, can be regarded essentially as a process involving the reduction of pure zinc oxide.

7.2 The Choice of Hydrogen as a Fluidizing and Reducing Gas

Fluidization and reduction of the zinc calcine in this study was accomplished using hydrogen. Although economically a poor choice, hydrogen was employed because:

- (1) hydrogen exhibits a high thermal conductivity for a gas which would aid carrying heat into the bed;
- (2) hydrogen has a high diffusivity leading to high rates of mass transfer;
- (3) the chemical interaction of hydrogen with zinc oxide provides only one mechanism for the reoxidation of zinc, i. e., reversal of the zinc producing reaction, 7.0-1. The H_2/H_2O system was, therefore, the simplest for the fluidized bed investigation.

CHAPTER EIGHT

APPARATUS AND EXPERIMENTAL TECHNIQUE

8.0 General Approach to the Experimental Technique

In simple terms, the reduction experiments of this investigation consisted of heating roasted zinc concentrates to the reduction temperature while fluidizing with nitrogen, followed by reduction with hydrogen for a predetermined period of time.

The progress of the reduction was followed by calculating the amount of zinc removed from the bed based on the analysis of the partially reduced calcine.

The reduction rate was studied by determining the effect of the hydrogen flowrate and the reduction temperature on the progress of reduction with time.

8.1 Apparatus

Figure 8.1-1 shows the schematic presentation of the essential parts of the experimental apparatus. Identification of the components appears in Table 8.1-1. A detailed drawing of the fluidized bed is shown in Figure 8.1-2. Table 8.1-2 identifies the component parts. Figure 8.1-3 shows two photographs of the experimental apparatus.

TABLE 8.1-1

Identification of the Components of Figure 8.1-1

- (1) — Fluidized Bed
- (2) — Marshall Split Furnace, model 2234
- (3) — Gas Preheater
- (4) — Gas Flowmeters
- (5) — Gas Cylinders
- (6) — Off-Gas Transport Line
- (7) — Thermocouples - Pt/Pt 13% Rh type
- (8) — Automatic (ON-OFF) Temperature Controllers
- (9) — Variable Power Transformers
- (10) — Condenser Tube
- (11) — Condenser Furnace
- (12) — Heat Exchanger
- (13) — Water Trap
- (14) — Dust Filter
- (15) — Transport Tube Insulation

Figure 8.1-1 The Experimental Apparatus

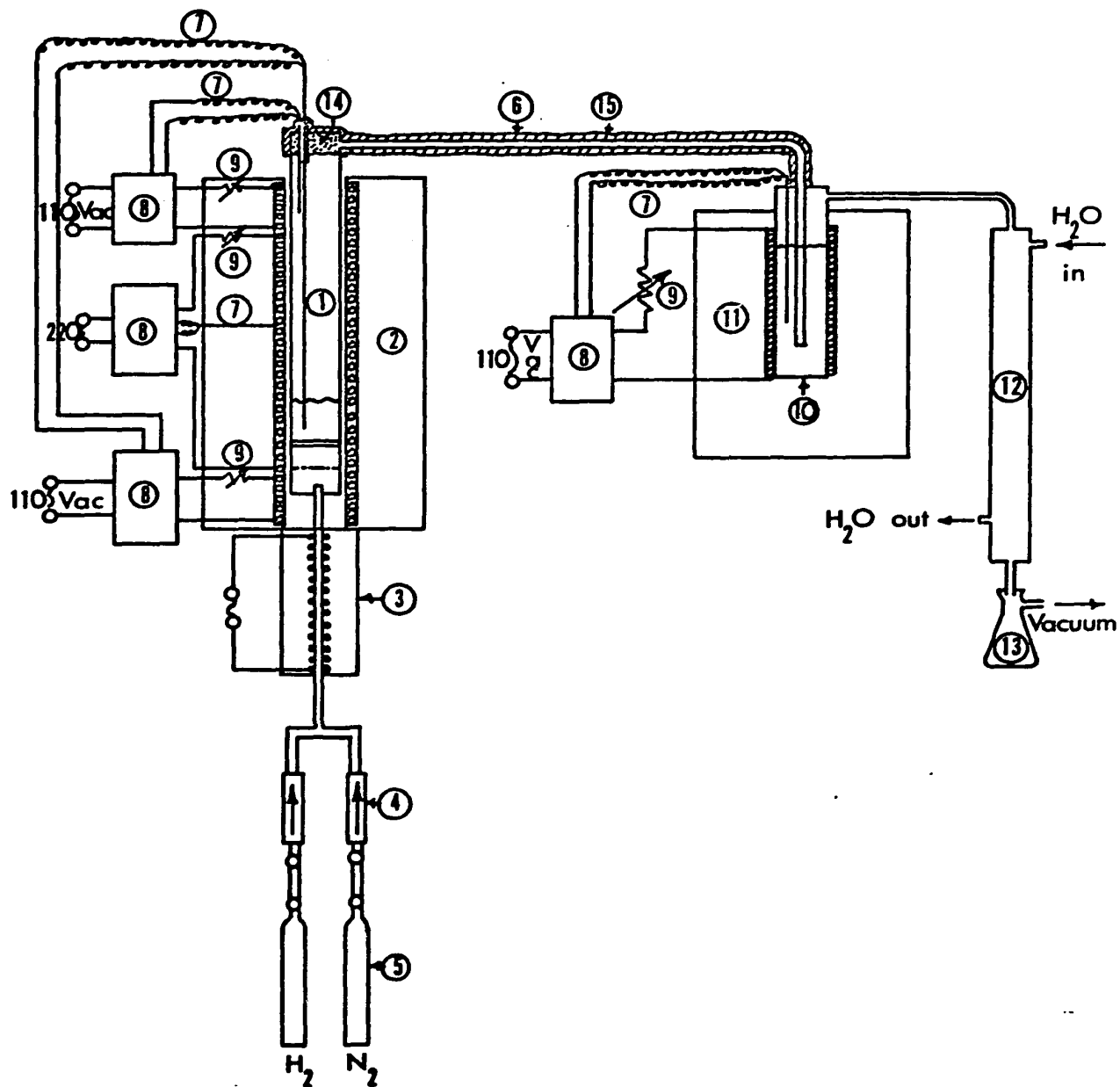


TABLE 8.1-2**Identification of Parts of the Fluidized Bed Reactor**

- (A) — Reactor Shell**
- (B) — Off-Gas Transport Line**
- (C) — "Reactor Hood"**
- (D) — Tube for the Insertion of Thermocouples etc.**
- (E) — Porous Firebrick Distributor Plate**
- (F) — Gas Calming Section**
- (G) — Fluidizing Gas Inlet Tube**
- (H) — Double Flange to Enable Separation of the Hood and
Transport Line From Reactor for Charging etc.**

Figure 8.1-2 Diagram of the Fluidized Bed Reactor

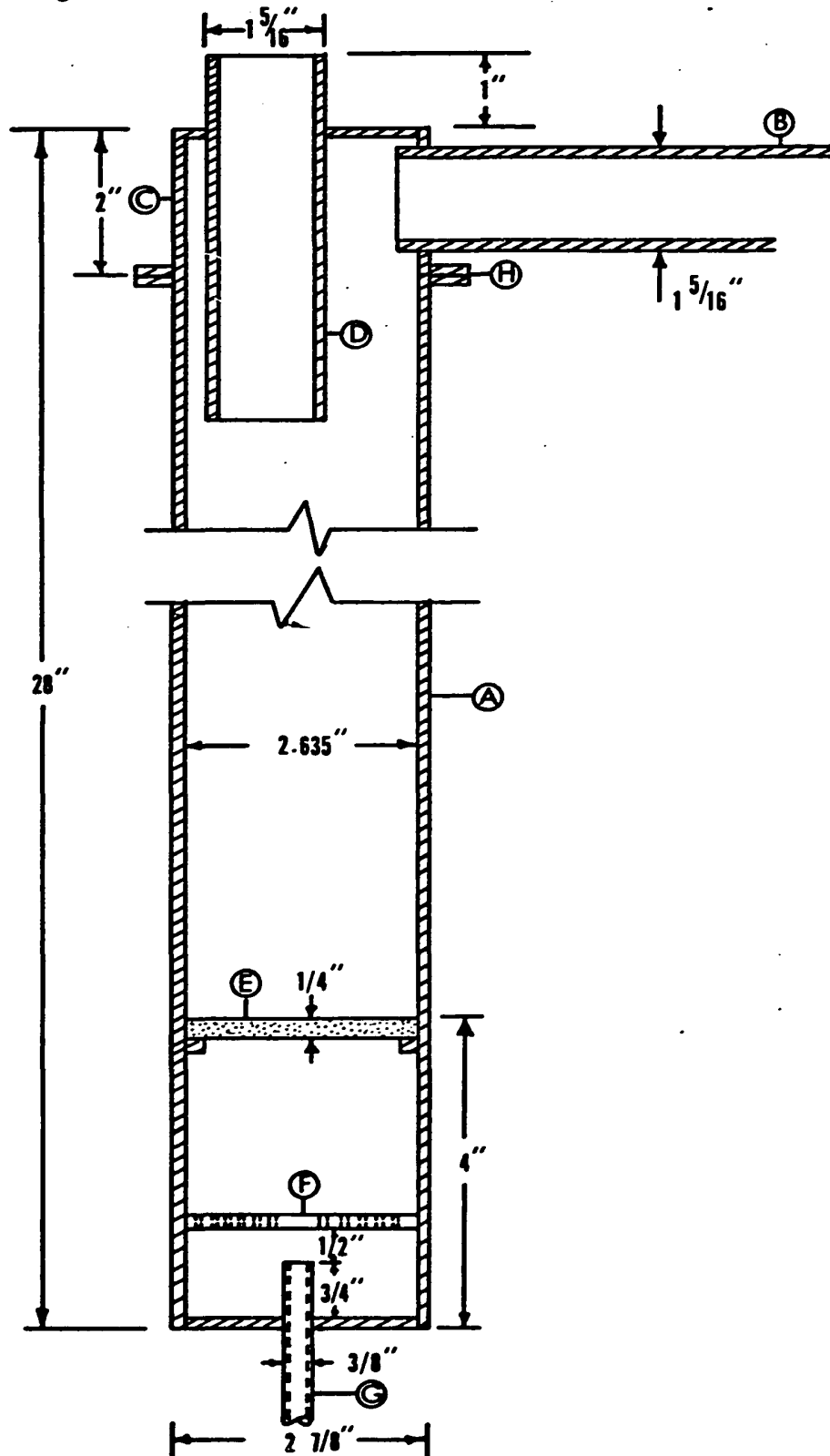


Figure 8.1-3(a)

Photograph of the experimental apparatus. Console on the left of the photograph contains the control circuitry and recording equipment. The "Marshall Split" furnace has been opened to expose the fluidized bed reactor shell (to the immediate right of the control console). The condenser and heat exchanger appear to the right of the fluidized bed reactor.

Figure 8.1-3(b)

Photograph of the experimental apparatus. In this configuration (Marshall Split furnace closed) the apparatus appears as it would during an experimental run.

Figure 8.1-3(a)



Figure 8.1-3(b)

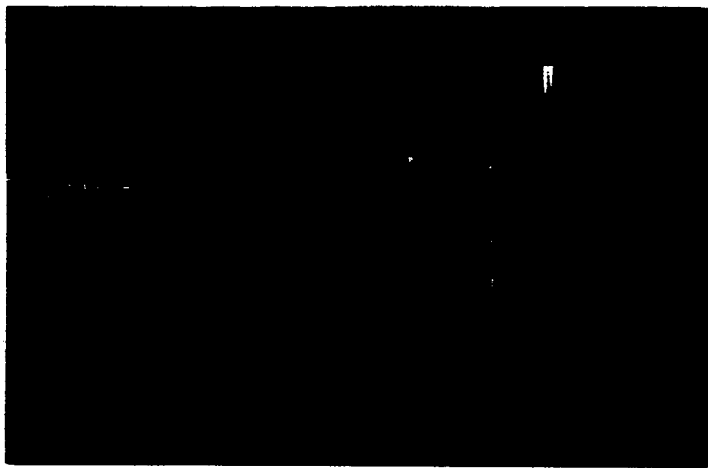


Figure 8.1-3(a)



Figure 8.1-3(b)



The fluidized bed reactor, excluding the distributor plate, the hood and off-gas transport line, and the zinc condenser were constructed of type 304 stainless steel. All parts of the construction which required joining were welded.

Streamlining the gas flow and equalization of the gas pressure across the fluidized bed distributor plate was accomplished by situating a calming vane 1 1/4 inches above the bottom of the reactor. This calming vane consisted of a circular stainless steel disc perforated with 168 one-sixteenth inch diameter holes extending radially every 15 degrees. The centre portion of the disc (1/2 inch diameter) was free of holes and thus the gas jet was deflected laterally, assuring that above the calming vanes there was no disproportionate flow of gas impinging on any one part of the distributor plate.

The distributor plate was made by cutting a 1/4 inch thick disc from insulating firebrick. This type of distributor was selected on the basis of studies conducted on a perspex model as described in Appendix I.

The "reactor hood" (C, Fig. 8.1-2) and off-gas transport line (B, Fig. 8.1-2) to the condenser were welded to form a single unit. Thus the hood could be separated from the reactor to facilitate charging and cleaning. A dust filter, made of Fiberfrax bulk alumina fiber, was packed into the hood. The hood and transport line were insulated against heat losses by packing the exterior of the assembly with approximately 1/2" of Fiberfrax bulk, subsequently bound with

asbestos tape, and finally coated with about 1/4" of asbestos cement. The entire assembly was sealed in place with asbestos cement which set into a hard, non-porous mass.

The condenser was constructed from a piece of 2.635 inch inside diameter (2.875 inch o.d.) type 304 stainless steel tubing, 18 inches long with a welded steel bottom. The upper end of the condenser was closed with a stainless steel disc welded to the reactor off-gas transport line such that when the entire assembly was in place, the transport line extended to within two inches of the bottom of the condenser tube. The condenser was sealed with asbestos cement.

An off-gas line (9/16" o.d., 5/16" i.d.) made of ordinary black iron pipe led from a point one inch from the top of the condenser tube to a water cooled heat exchanger. During operation, the condenser was filled with nine inches of molten lead controlled at a temperature of 500°C. The bath was held under vacuum to afford passage of the reactor off-gases through the lead melt and to minimize back pressure on the fluidized bed.

A 3.0 KVA Marshall Split furnace, Model 2234, 3" diameter core, (Norton Vacuum Equipment Co., Sunnydale, Calif.) was employed to heat the fluidized bed. The furnace was split vertically and could be opened to permit removal of the reactor tube. Power was fed to the furnace through three separate circuits. The bottom of the fluidized bed reactor was suspended three inches above the bottom of the furnace so that the lower heating elements, extending below the bed, could serve as a gas preheater. The length of the heating zone was twenty four inches.

The condenser was heated using spare elements from the Marshall furnace. Application of full line voltage (110 VAC) produced 500 watts of power for condenser heating purposes. The condenser

tube (10, Fig. 8.1-1) was heated over its lower nine inches. The entire condenser assembly was surrounded by a 12" diameter insulating jacket filled with vermiculite insulation.

In all cases, temperatures were recorded using Pt/Pt-13% Rh thermocouples. Three thermocouples were used to control temperatures in the fluidized bed reactor and one in the condenser. The fluidized bed reactor incorporated two internal thermocouples, one extending 12 3/4 inches from the top of the hood to control the off-gas temperature and another extending into the bed itself to control the bed temperature. The third thermocouple was situated in the centre of the middle bank of heating elements of the furnace.

The condenser thermocouple was inserted into the lead bath through the top of the condenser with the tip 4" from the bottom of the condenser tube.

All thermocouples were sheathed in alumina insulators and enclosed in stainless steel tubing (type 304, 0.10" i.d.) sealed at the bead end by Mullite cement.

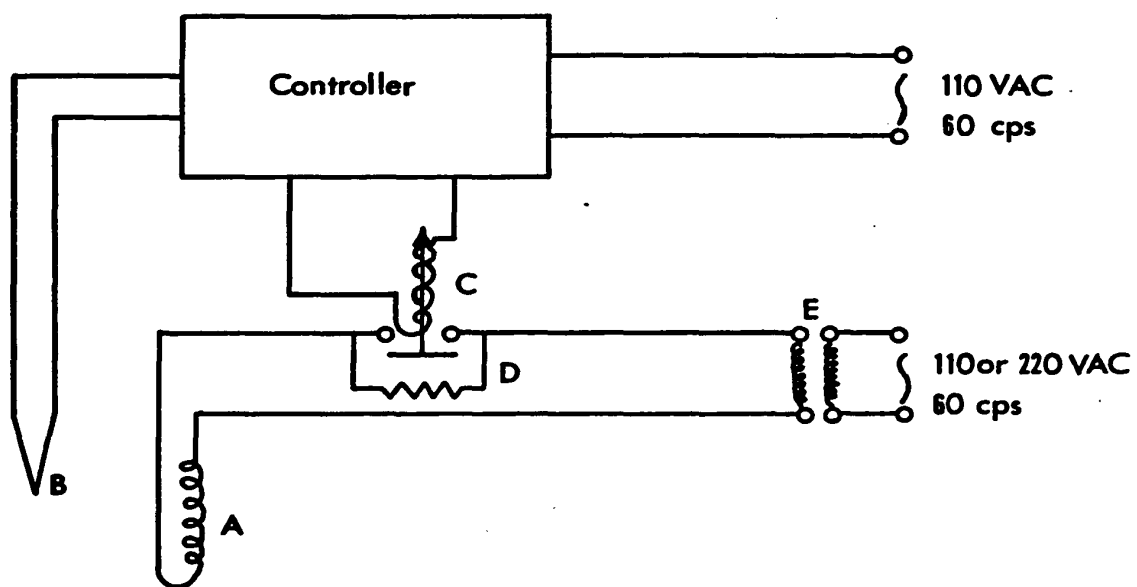
Temperature control was accomplished by means of "Thermovolt" (Model P21HAZR, Thermovolt Instruments, Toronto, Ontario) ON-OFF type controllers which consist of a measuring circuit and a separate solid state control circuit. The controllers activated a mercury relay which was used to interrupt the main current load. Swings of temperature experienced during the ON-OFF cycle were minimized by the parallel connection of an external resistance wire winding, the resistance of which was sufficient to reduce the power to the furnace coils by one-half. A schematic drawing of the control circuit is shown in Figure 8.1-4.

Power to the furnace coils was controlled by a "Powerstat" variable transformer (0-110VAC or 0-220VAC).

TABLE 8.1-4**Identification of the Parts of the Control Circuit**

- (A) — Furnace Coil**
- (B) — Platinum/Platinum 13% Rhodium thermocouple**
- (C) — Mercury Relay**
- (D) — 10 Ω Shunt Resistance Winding**
- (E) — "Powerstat" Variable Auto Transformer (0-110VAC)
or (0-220VAC)**

Figure 8.1-4 Schematic Drawing of the Control Circuit



8.2 Raw Material — Zinc Calcine

The roasted zinc concentrate or zinc calcine used in the course of this investigation was obtained from the fluidized bed roasting circuit at Canadian Electrolytic Zinc, Ltd., Valleyfield, Quebec. The chemical analysis, performed by Canadian Electrolytic Zinc, Ltd. laboratory, is given in Table 8.2-1.

TABLE 8.2-1

Chemical Analysis of Canadian Electrolytic Zinc Calcine

<u>Component</u>	<u>Percentage</u>
Total Zinc	59.9
Copper	0.41
Cadmium	0.11
Lead	0.13
Iron	11.7
Sulphide sulphur	0.50
Sulphate sulphur	1.51
Cobalt	0.023
Nickel	0.0008
Water Soluble Zinc	1.57
Acid Soluble Zinc	54.4

The main feature of this calcine is its low lead content. Oxides of lead are easily reduced and gaseous reduction will yield liquid lead. If the lead content of the calcine is significant, liquid lead would wet the surface of the particles and cause agglomeration, leading, possibly, to poor fluidization or even defluidization of the bed.

8.3 Preliminary Tests

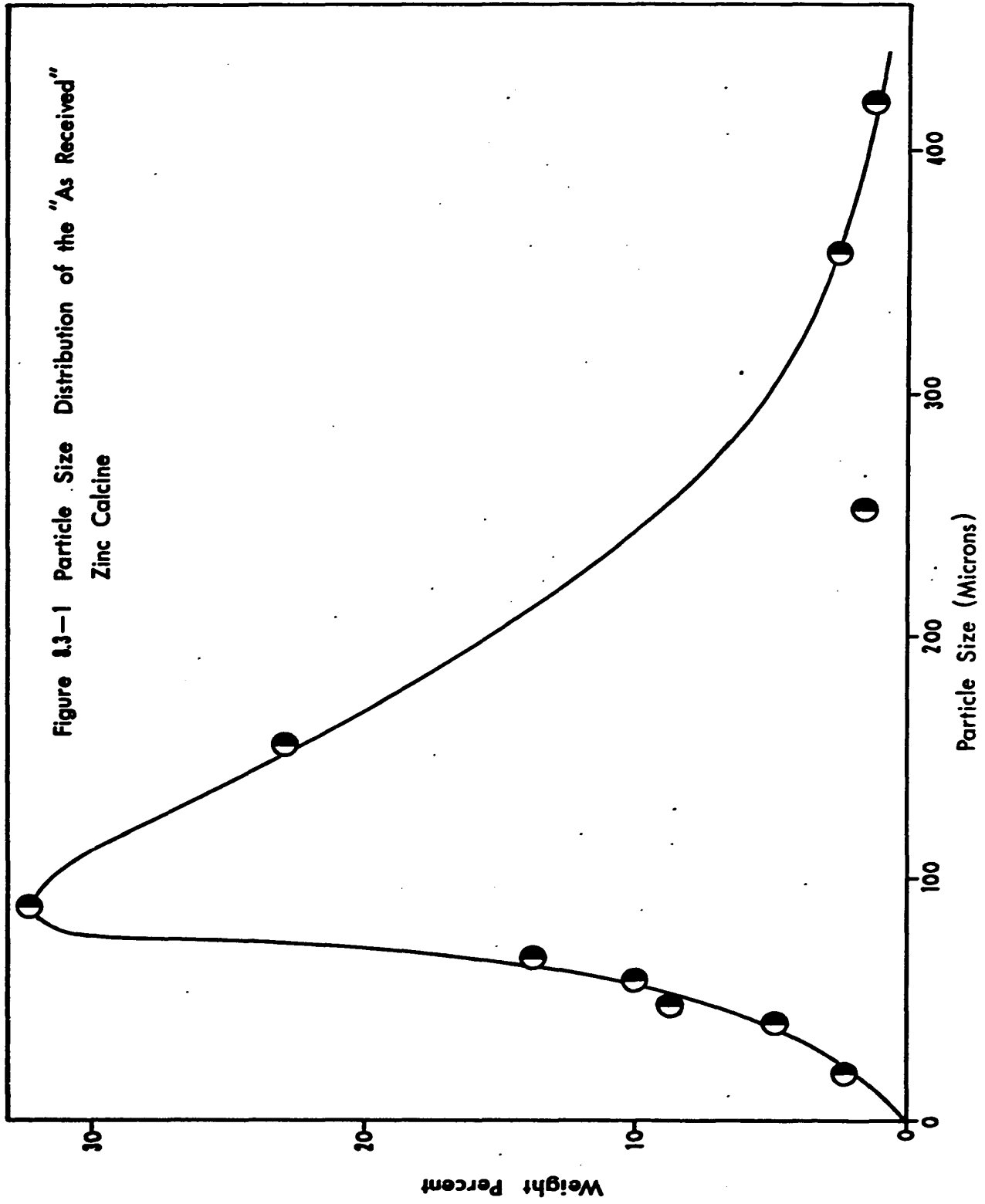
Prior to the start of the reduction experiments, tests were performed to determine:

- (1) the particle size distribution of the calcine
- (2) the density of the calcine

The particle size distribution was obtained by sieving the calcine on Tyler Standard Sieve Series Screens using a mechanical vibrator for agitation. The distribution plotted as weight percent of a particular micron size against the particle diameter is shown in Figure 8.3-1. The material of a particle size which represents the major portion of the mixture (-150+200 mesh, $\bar{D}_p = 89.5 \mu$) was extracted and used in the experimental runs.

The density was determined by the method outlined previously (Chapter Five, p.46) for the calculation of minimum fluidization gas rates.

Figure 1.3-1 Particle Size Distribution of the "As Received"
Zinc Calcine



8.4 Experimental Procedure

735 grams of -150+200 mesh zinc calcine were carefully charged to the fluidized bed reactor avoiding excessive dust losses. The off-gas transport line was sealed in place and all the thermocouple leads were connected. After sufficient time had elapsed to allow for the hardening of the asbestos sealant, cooling water to the heat exchanger (12, Fig. 8.2-1) and the vacuum to the condenser were turned on.

The nitrogen to the fluidized bed was set at a flowrate of $3000 \text{ cm}^3 \text{ min}^{-1}$ and was adjusted periodically during heat up to this value, at temperature. Power to the recording instruments and the furnace coils was turned on and heat up proceeded until the desired operating temperature was reached. 3 to 5 hours were generally required for heat up to operating temperatures in the range of 800 to 900°C .

Prior to switching to hydrogen, the temperature was checked with a Leeds-Northrup potentiometer. Periodic temperature checks were also carried out by potentiometer during the course of the run.

At temperature, the nitrogen flow was stopped and the hydrogen was introduced into the reactor at a predetermined flowrate. The start of the reduction run, i.e., zero time, was taken to be at hydrogen switch-on. The run was allowed to proceed for the predetermined length of time, following which the gas flow was reverted to nitrogen and electrical power to the fluidized bed was shut off.

When the reactor had cooled, the off-gas transport line was disengaged and the reactor was emptied of its contents. A sample of the spent calcine was extracted and analysed by wet chemical techniques for total zinc and total iron.

Initially, attempts were made to extract samples periodically from the bed during the course of an extended run by means of a vacuum tube extending to a point 1" above the expanded bed. Unfortunately this sampling technique had to be abandoned because water vapour condensation in the line inevitably caused blocking.

Each experimental run, therefore, represented one point on the curve of percent zinc eliminated from the bed vs time.

8.5 Chemical Analysis

8.5-1 Determination of Zinc

The analytical technique employed to determine total zinc in the residues was adopted from the current practice used at Cominco Ltd., Trail, B.C. A residue sample weighing between 0.1 and 0.2 grams was accurately weighed and was placed in a 400 ml beaker. After moistening with 10 ml of distilled water, 5 ml of concentrated HNO_3 were added and the mixture was allowed to digest. 5 ml of HCl and a few ml of HF were added and digestion was continued. 3 to 5 ml of 1:1 H_2SO_4 were added and the solution was taken to dryness over a low heat.

After dryness was attained, the beaker and contents were cooled, 5 ml HCl and 15 ml distilled water were added and the contents were heated to take up the soluble salts. The beaker was again cooled and the sides washed with 15 to 20 ml H₂O. 1/2 gram of NH₄Cl and 2 to 3 ml of a 1% solution of H₂O₂ were then added and the iron was precipitated using concentrated NH₄OH (10 ml excess using a litmus indicator). The precipitate was boiled for a few minutes and subsequently filtered into a 400 ml beaker, washing three times with a hot 1% NH₄OH, NH₄Cl wash.

The precipitate was washed back into the original beaker by dissolving it with a 10% HCl wash, and reprecipitated as before with H₂O₂, NH₄OH etc. The precipitate was filtered through the original filter paper and washed three times. The two combined filtrates, containing all the zinc, were neutralized using HCl. 2 to 5 grams of lead shot was added and the solution was boiled for twenty minutes.

The zinc content was determined by titrating with a solution of potassium ferrocyanide (1 ml = 0.010 gm Zn) using ammonium molybdate as an outside indicator until one drop gave a brown colour with the indicator.

8.5-2 Determination of Iron

The iron content of the residues was determined by the Dichromate Method described in the ASTM Standards. The iron precipitate from the zinc determination was dissolved from the filter paper using a hot 10%

HCl solution and the filtrate was collected in a 400 ml beaker. The filter paper was washed with copious amounts of hot distilled H₂O before discarding. The resultant iron solution was boiled slowly for a few minutes and was then reduced with a solution of stannous chloride (50 gpl) until colourless, taking precautions to avoid an excess of stannous chloride.

The assay was diluted to 100 ml with a saturated solution of mercuric chloride. 3 ml of 85% phosphoric acid were added and the assay was titrated with potassium dichromate using 1 ml of 0.2% sodium diphenylaminesulphonic acid as an internal indicator. The endpoint was reached when the assay turned from green to dark purple.

CHAPTER NINE

RESULTS

9.0 Results and Experimental Observations

The results and experimental observations obtained from this experimental investigation will be commented on from an experimental and industrial viewpoint, and in particular the process will be analysed with respect to three general areas of study, namely (1) Caking and clinkering, (2) Reduction kinetics and (3) Efficiency of reducing gas.

9.1 Caking and Clinkering

Visual observations of the partially reduced calcine indicated that clinkers of agglomerated calcine were formed during all tests irrespective of the operating conditions. The word "clinker" is a misnomer, in this case, as the observed agglomerations were essentially a loose mass which, in most cases, crumbled easily on touching. In reduction runs of up to six hours duration, clinker formation had little detrimental effect on zinc elimination. To investigate further the effect of clinker formation on the ultimate performance of the fluidized bed, an extended run (17 hours at 850°C and a hydrogen space velocity of 7.54 cm sec⁻¹) was carried out. The results of this run indicate that even at high zinc elimination clinkering was no worse than in shorter runs.

Over the entire range of temperatures (800-900°C) and hydrogen space velocities (3.77 cm sec⁻¹ to 7.54 cm sec⁻¹) used in the present work, clinkers tied up between 8% and 28% of the initial charge weight.

Taking into account the different operating conditions used, clinkering tied up an average of 19% of the initial charge weight.

While the overall effect of these clinkers on the quality of the fluidization obtained and on the zinc elimination rates cannot be absolutely ascertained, the very porous and crumbly nature of the observed clinkers lead to the assumption that clinkering did not adversely affect the rate of zinc elimination from the charge. It is also felt that the clinkering did not have any appreciably adverse effect on the quality of fluidization obtained.

Qualitative observations show that clinker formation is promoted by temperature increases but that the maximum clinker dimensions seem to be independent of temperature. In addition, the onset of clinker formation did not, in any way, seem to be influenced by any specific degree of reduction. Although only two hydrogen flowrates were employed in this investigation, an increase in the flowrate resulted in a decreased tendency to form clinkers and also helped to reduce the average clinker size formed.

Figure 9.1-1 shows photographs of some of the clinkers and also gives the experimental conditions at which they formed.

Caking, as it is used in this study, refers to the tendency for the spent calcine to stick or cake in hard masses to the walls of the reaction vessel, because of the generally higher temperatures experienced at the walls. Caking was not observed in any of the experiments and no wall scraping was necessary. This would not, therefore, appear to be a problem in an industrial scale reactor.

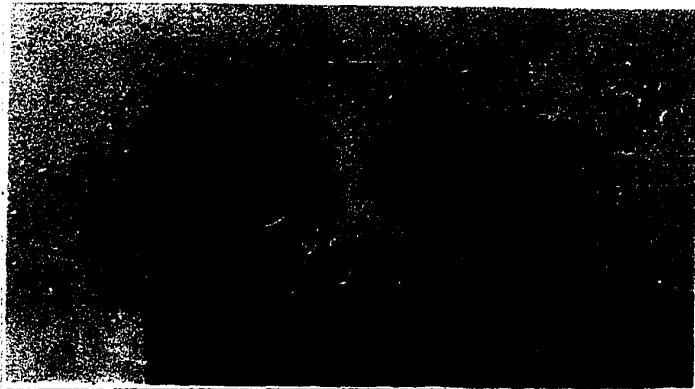
**Figure 9.1-1 Photographs of Some of the Clinkers Obtained During
the Reduction of Zinc Calcine.**

- a) **Clinkers extracted from the fluidized bed reactor after 2 hours reduction at 900°C and a hydrogen flowrate of 8 litres min⁻¹ (3.77 cm sec⁻¹). Approximate % Zinc Elimination = 9%.**
- b) **Clinkers extracted from the fluidized bed reactor after 2 hours reduction at 850°C and a hydrogen flowrate of 8 litres min⁻¹ (3.77 cm sec⁻¹). Approximate % Zinc Elimination = 7.5%.**
- c) **Clinkers extracted from the fluidized bed reactor after 2 hours reduction at 800°C and a hydrogen flowrate of 8 litres min⁻¹ (3.77 cm sec⁻¹). Approximate % Zinc Elimination = 5%.**

a)



b)



c)



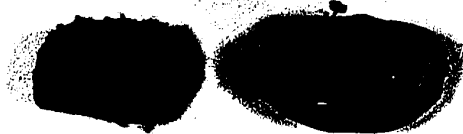
a)



b)



c)



- d) **Clinkers extracted from the fluidized bed reactor after 3 hours reduction at 900°C and a hydrogen flowrate of 8 litres min⁻¹ (3.77 cm sec⁻¹). Approximate % Zinc Elimination = 16%.**
- e) **Clinkers extracted from the fluidized bed reactor after 6 hours reduction at 900°C and a hydrogen flowrate of 8 litres min⁻¹ (3.77 cm sec⁻¹). Approximate % Zinc Elimination = 30.5%.**
- f) **Clinkers extracted from the fluidized bed reactor after 2 hours reduction at 850°C and a hydrogen flowrate of 8 litres min⁻¹ (3.77 cm sec⁻¹). Approximate % Zinc Elimination = 7.5%.**
- g) **Clinkers extracted from the fluidized bed reactor after 2 hours reduction at 850°C and a hydrogen flowrate of 16 litres min⁻¹ (7.54 cm sec⁻¹). Approximate % Zinc Elimination = 12%.**

d)



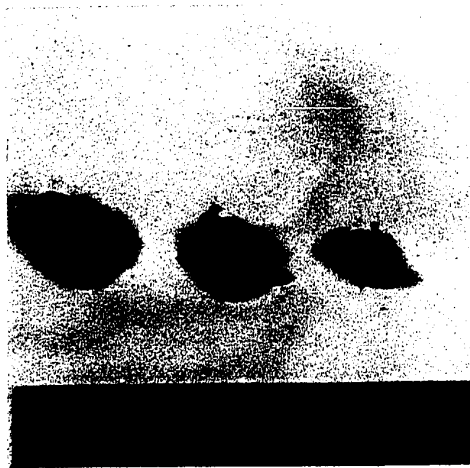
e)



f)



g)



d)



e)



f)



g)



9.2 Reaction Kinetics and Zinc Elimination

One of the most important objects of the study was to determine the effect of temperature and hydrogen flowrate on the reduction kinetics of the fluidized bed system. The experiments were, therefore, carried out at three temperatures, 800°C, 850°C, and 900°C, and two hydrogen flowrates, 8 liters min⁻¹ bed space velocity (3.77 cm sec⁻¹)* and 16 liters min⁻¹ (7.54 cm sec⁻¹), measured at one atmosphere pressure and the reaction temperature. Attempts to reach higher temperatures were unsuccessful because of the power limitations of the furnace and the difficulties encountered in using a gas preheater.

9.2-1 The Effect of Temperature on Zinc Elimination and the Apparent Reaction Rate

Table 9.2-1 lists the experimental conditions for the study of the influence of the reaction temperature on the percentage zinc elimination from the bed and Table 9.2-2 lists the calculated apparent reaction rates. It will be noted that all conditions except temperature were held constant during this series of tests.

Figure 9.2-1 shows a plot of the percentage zinc elimination from the charge against time for the three temperatures studied and a constant hydrogen flowrate of 8 liters min⁻¹ (3.77 cm sec⁻¹). The results show clearly that temperature increases have a beneficial effect on the rate of zinc elimination.

* Gas velocity in an area equivalent to the cross sectional area of the bed.

In this investigation, calculations of the percent zinc elimination, i.e., the weight of zinc expelled from the bed divided by the initial weight of zinc in the bed, were based on the assumption that the weight of iron in the bed remains constant. The percentage zinc elimination, based on the total zinc and iron analyses of the spent calcines, can be expressed as

$$\begin{aligned} \% \text{ Zinc Elim.} &= \frac{(\% \text{ Zn initial})(\text{wt. initial}) - (\% \text{ Zn final})(\text{wt. final})}{(\% \text{ Zn initial})(\text{wt. initial})} \quad (100) \\ &= 1 - \left[\frac{(\% \text{ Zn final})(\text{wt. final})}{(\% \text{ Zn initial})(\text{wt. initial})} \right] \quad (100) \end{aligned}$$

A constant weight of iron in the system gives the equation

$$(\% \text{ Fe initial})(\text{wt. initial}) = (\% \text{ Fe final})(\text{wt. final})$$

or

$$\frac{(\text{wt. final})}{(\text{wt. initial})} = \frac{(\% \text{ Fe initial})}{(\% \text{ Fe final})}$$

which leads to the equation used in the calculations

$$\% \text{ Zinc Elim.} = 1 - \left[\frac{(\% \text{ Zn final})(\% \text{ Fe initial})}{(\% \text{ Zn initial})(\% \text{ Fe final})} \right] \quad (100) \quad (9.2-1)$$

The linearity of the plots in Figure 9.2-1 over the first six hours greatly facilitated the calculation of apparent reaction rates based on a knowledge of the slope of the curves and the initial weights of zinc in the charge. Figure 9.2-2 shows a plot of the apparent reaction rate (gm moles min^{-1}) against the reaction temperature. As expected, the reaction rate increases significantly with increasing temperature.

TABLE 9.2-1
Experimental Conditions for the Study of the Effect of Reaction
Temperature on the Rate of Zinc Elimination From the Fluidized Bed

Reaction Temperature °C	Space Velocity* cm sec ⁻¹	Reaction Time min	Particle Size Fraction	Residue Analysis		Pct. Zinc Elimination
				%Zn	%Fe	
800	3.77	60	-150+200	66.43	13.36	2.88
800	3.77	120	-150+200	65.50	13.47	5.01
800	3.77	240	-150+200	63.07	13.68	9.95
800	3.77	360	-150+200	61.12	14.40	17.11
800	3.77	390	-150+200	60.78	14.66	19.02
850	3.77	60	-150+200	63.98	13.06	4.29
850	3.77	120	-150+200	64.18	13.54	7.42
850	3.77	180	-150+200	64.11	14.17	11.61
850	3.77	240	-150+200	63.75	14.71	15.35
850	3.77	300	-150+200	61.34	14.91	19.64
850	3.77	360	-150+200	60.06	15.20	22.79
900	3.77	60	-150+200	64.75	13.31	5.34
900	3.77	120	-150+200	63.03	13.56	9.21
900	3.77	180	-150+200	61.31	14.28	16.14
900	3.77	240	-150+200	61.31	15.15	20.96
900	3.77	300	-150+200	60.84	15.14	21.51
900	3.77	360	-150+200	59.99	16.89	30.65

* Gas velocity in the empty bed.

TABLE 9.2-2
Calculated Apparent Reaction Rates for the Reduction of
Zinc Calcines by Hydrogen in a Fluidized Bed

Reaction Temperature °C	Space Velocity cm min ⁻¹	Calculated Slope From Expt'l Curves % Zn Elim hr ⁻¹	* Calculated Apparent Reaction Rate (moles min ⁻¹)
800	3.77	2.85	3.199 x 10 ⁻³
850	3.77	3.87	4.343 x 10 ⁻³
900	3.77	5.20	5.836 x 10 ⁻³

*Constant charged bed weight of 735 grams

9.2-2 Effect of the Hydrogen Flowrate on Zinc Elimination and the
Apparent Reaction Rate

Table 9.2-3 shows the experimental conditions employed in studying the effect of hydrogen flowrate on the rate of zinc elimination from the charge. This aspect of the investigation was studied at constant conditions but for flowrate (temperature 850°C). The percentage of zinc eliminated from the bed is plotted (Fig. 9.2-4 and Fig. 9.2-5) against the reaction time as before.

These experimental results indicate that increases in the hydrogen flowrate result in increases in the rate of zinc elimination and in the apparent overall reaction rate. This study has been limited to two relatively low flowrates and any future work should encompass a wider range of flowrates for a detailed study of the effect of this variable.

Figure 9.2-1 Effect of Temperature on the % Zinc Elimination
Hydrogen Flowrate = 1000 cc min^{-1} (3.77 cm sec^{-1})
Charge = 735 gms

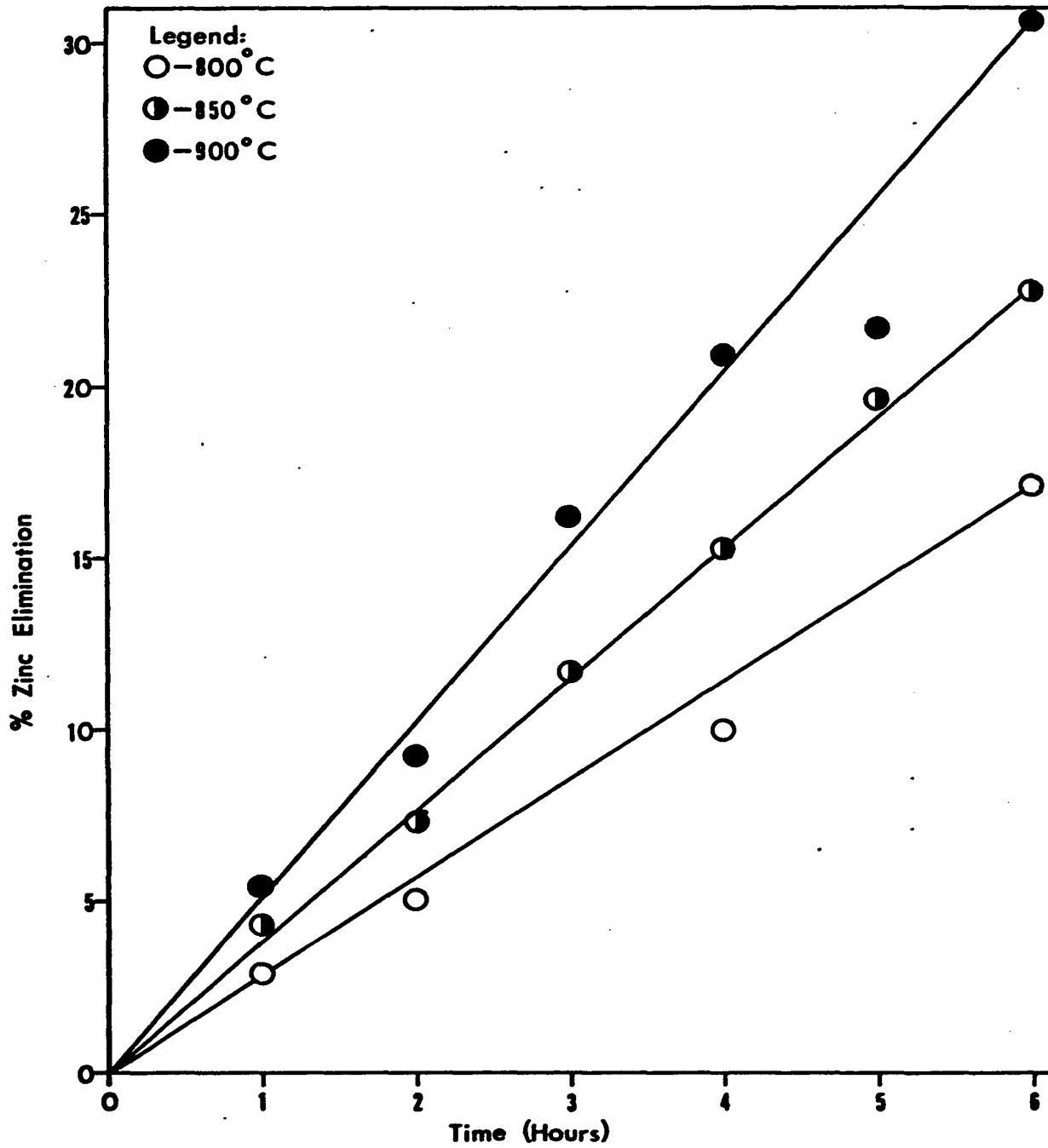


Figure 9.2-2 Variation of the Apparent Reaction Rate with Temperature

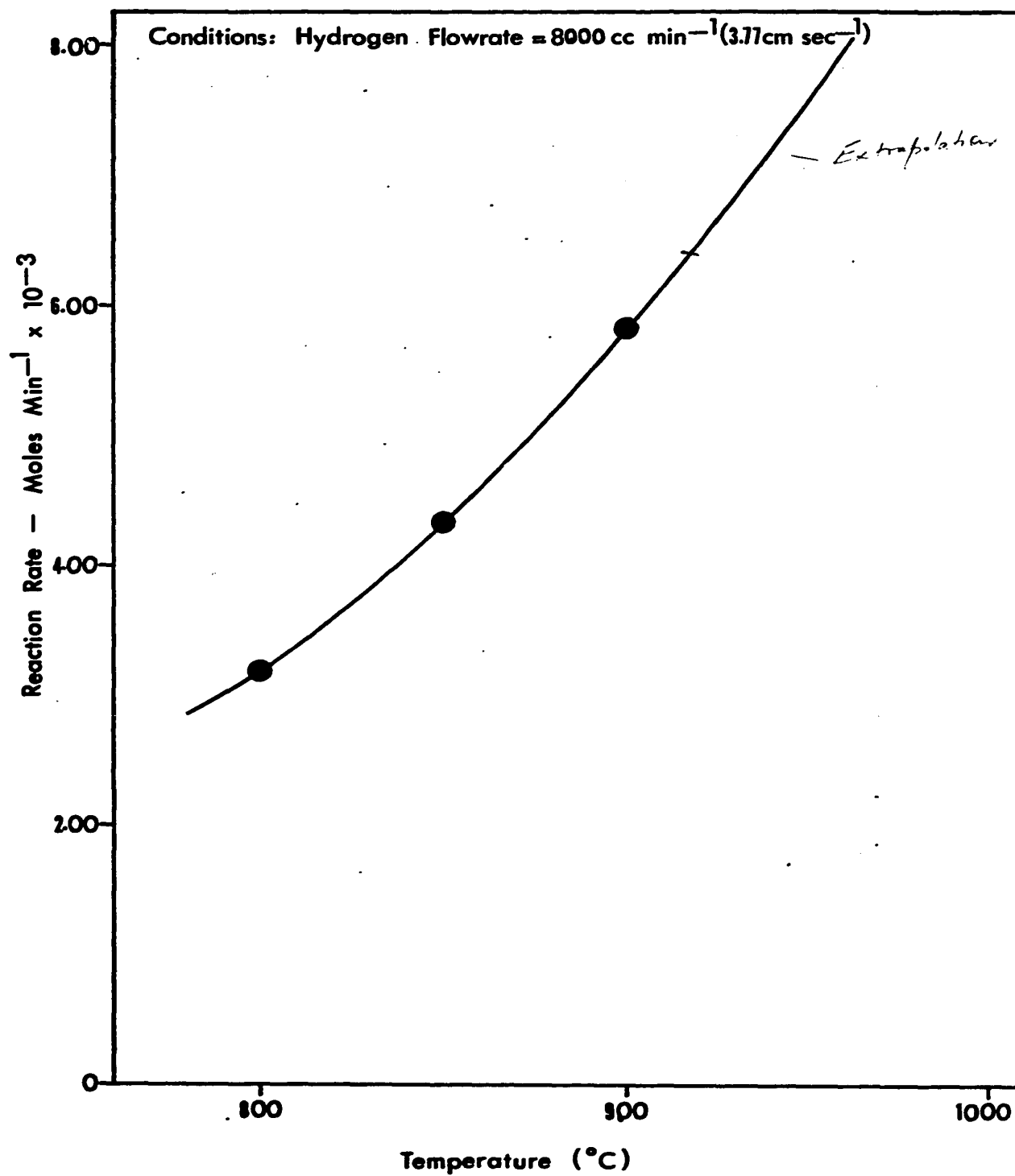


TABLE 9.2-3

Experimental Conditions for the Study of the Effect of Hydrogen
Flowrate on the Rate of Zinc Elimination From the Fluidized Bed

Space Velocity cm sec ⁻¹	Reaction Temperature °C	Reaction Time mins	Particle Size Frac- tion Mesh	Residue Analysis		Pct. Zinc Elimination
				%Zn	%Fe	
3.77	850	60	-150+200	63.98	13.06	4.29
3.77	850	120	-150+200	64.18	13.54	7.42
3.77	850	180	-150+200	64.11	14.17	11.61
3.77	850	240	-150+200	63.75	14.71	15.35
3.77	850	300	-150+200	61.34	14.91	19.64
3.77	850	360	-150+200	60.06	15.20	22.79
7.54	850	60	-150+200	65.29	13.81	7.66
7.54	850	120	-150+200	63.94	14.22	12.14
7.54	850	180	-150+200	61.80	14.83	18.60
7.54	850	240	-150+200	59.27	15.26	24.14
7.54	850	300	-150+200	59.89	16.51	29.14
7.54	850	360	-150+200	60.43	17.24	31.51
7.54	850	1020	-150+200	22.35	49.33	91.15

Figure 9.2-4 Effect of Hydrogen Flowrate on the % Zinc Elimination

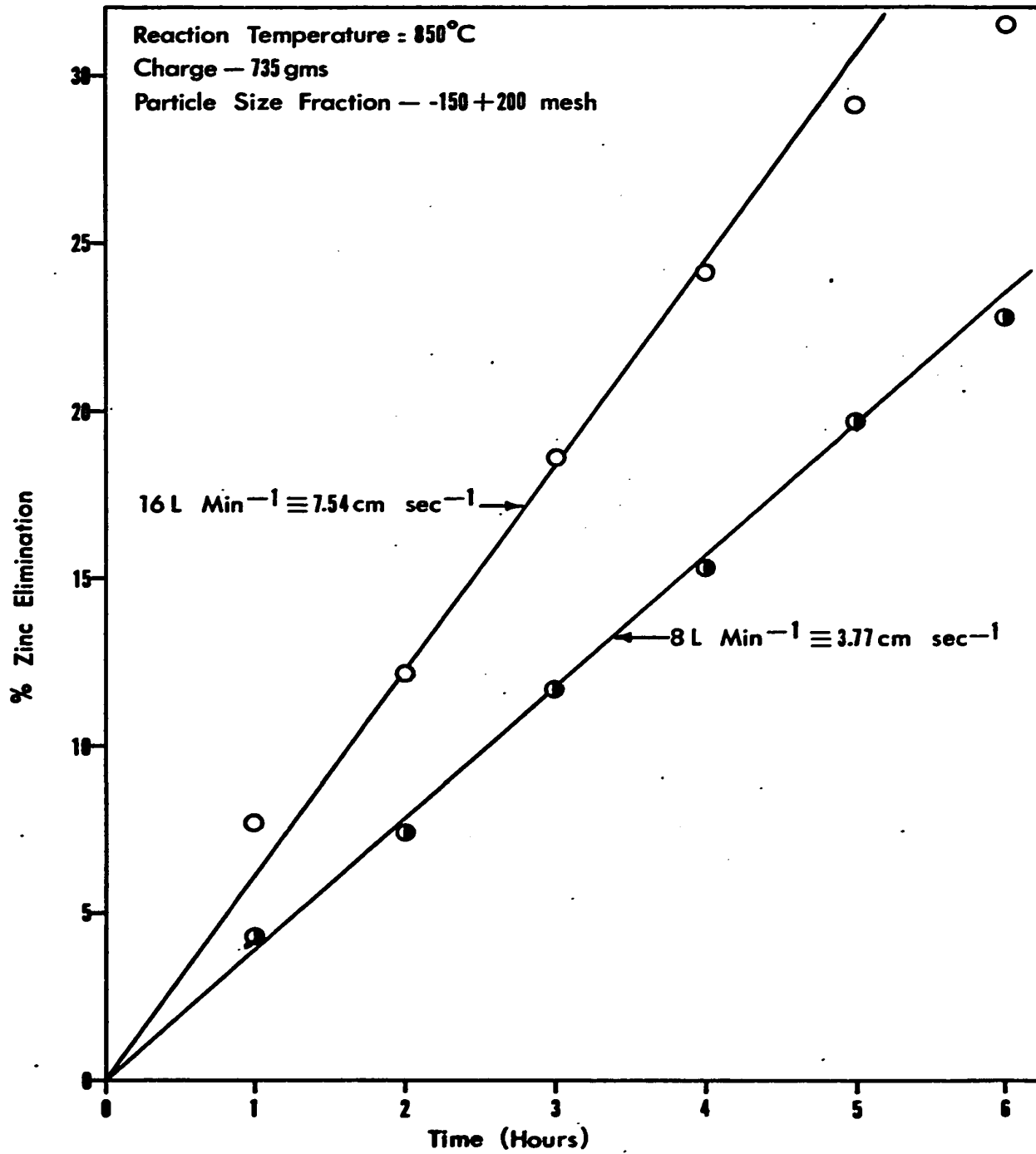
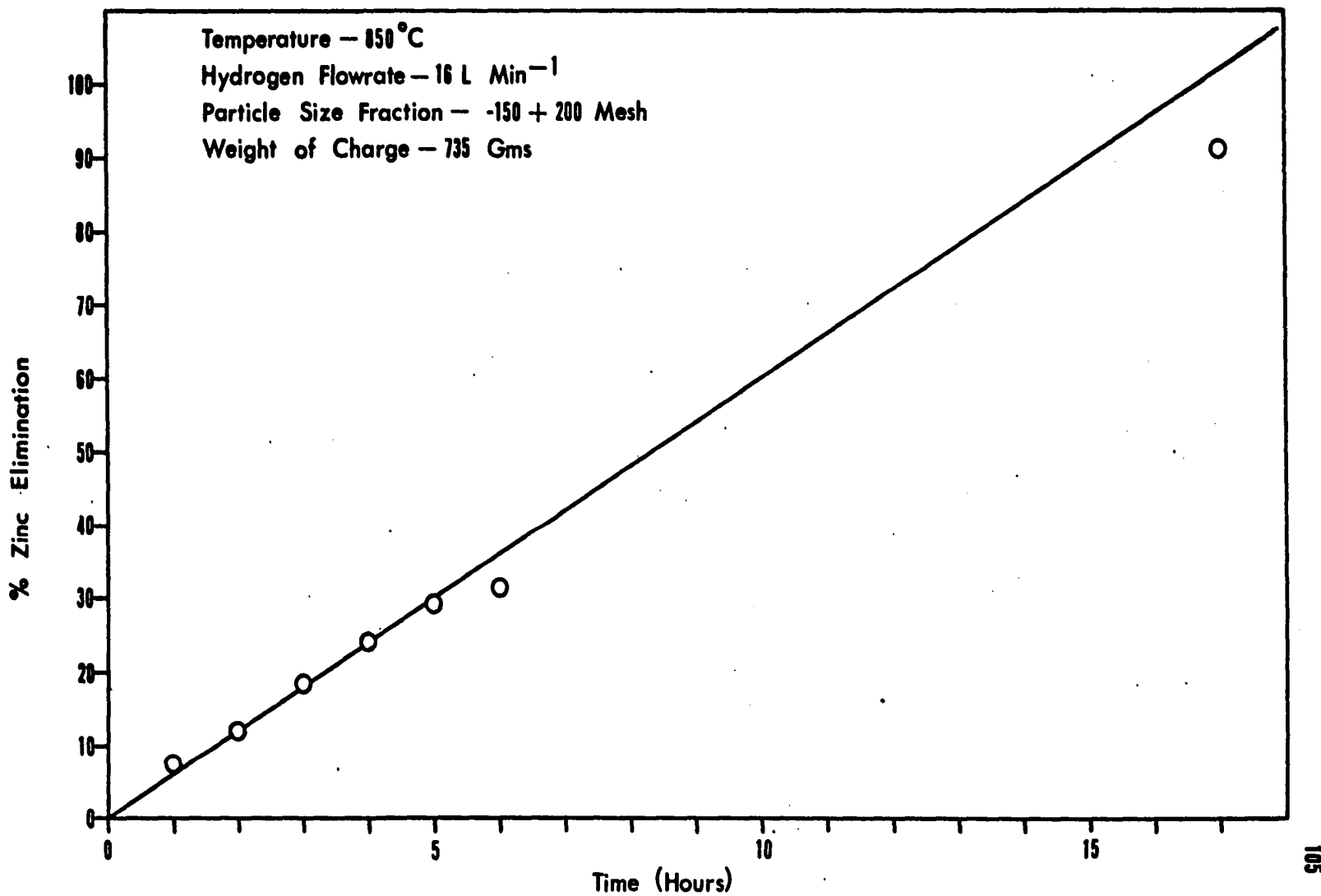


Figure 2-5 Plot of Percentage Zinc Elimination vs Time for an Extended Run



9.3 Hydrogen Efficiency

The hydrogen efficiency in this work has been calculated in two ways. The first determination can be termed a thermodynamic efficiency and it is a measure of the approach to equilibrium conditions in the fluidized bed, i. e., it is a measure of how close the system has come to yielding the maximum zinc attainable under the experimental conditions. In symbols, this thermodynamic efficiency can be expressed as

$$\text{Thermodynamic Efficiency} = \frac{\text{Partial Pressure of Zinc in Effluent Gases}}{\text{Equilibrium partial pressure of zinc}} \times 100$$

$$\text{or Thermodynamic Efficiency} = P_{Zn} / P_{Zn}^{Eq} \times 100 \quad (9.3-1)$$

In the calculation of thermodynamic efficiencies, the equilibrium zinc partial pressures have been taken from Figure 7.0-1, p. 69.

The second type of hydrogen efficiency (the most important from an economic viewpoint) is defined as

$$\text{Economic Hydrogen Efficiency} = \frac{\text{Number of moles of zinc produced}}{\text{Number of moles of hydrogen fed}} \quad (9.3-2)$$

Table 9.3-1 shows the experimental conditions and the calculated hydrogen efficiencies obtained in this study. The results are plotted in Figures 9.3-1 (thermodynamic efficiency) and 9.3-2 (economic efficiency) at a constant gas space velocity of 3.77 cm sec⁻¹.

TABLE 9.3-1

**Experimental Conditions and Calculated Values of the Hydrogen
Efficiencies Obtained in This Study**

Temp. °C	Space Velocity cm sec ⁻¹	Reaction Rate moles min ⁻¹	Equil. P _{Zn} Atmos.	Observed P _{Zn} Atmos.	Thermodynamic Eff. %	Econ. Eff. %
800	3.77	3.199x10 ⁻³	.050	.034	68.00	3.51
850	3.77	4.343x10 ⁻³	.065	.048	73.23	5.00
900	3.77	5.836x10 ⁻³	.087	.066	75.84	7.00
850	7.54	6.954x10 ⁻³	.065	.039	59.23	4.55

Each point on Figures 9.3-1 and 9.3-2 is the average of a minimum of five experimental runs.

The results clearly indicate that there is a noticeable decrease in the thermodynamic hydrogen efficiency with increasing temperature. Table 9.3-1 also indicates that increasing the hydrogen flowrate results in a further decrease in the thermodynamic efficiency.

The economic efficiency, on the other hand, shows a tendency to increase with temperature due to the overbalancing effect of increased P_{Zn} equilibrium with increasing temperature. Increasing the flowrate results in a decrease in the economic efficiency.

Figure 9.3-1 Effect of Temperature on the Thermodynamic Efficiency

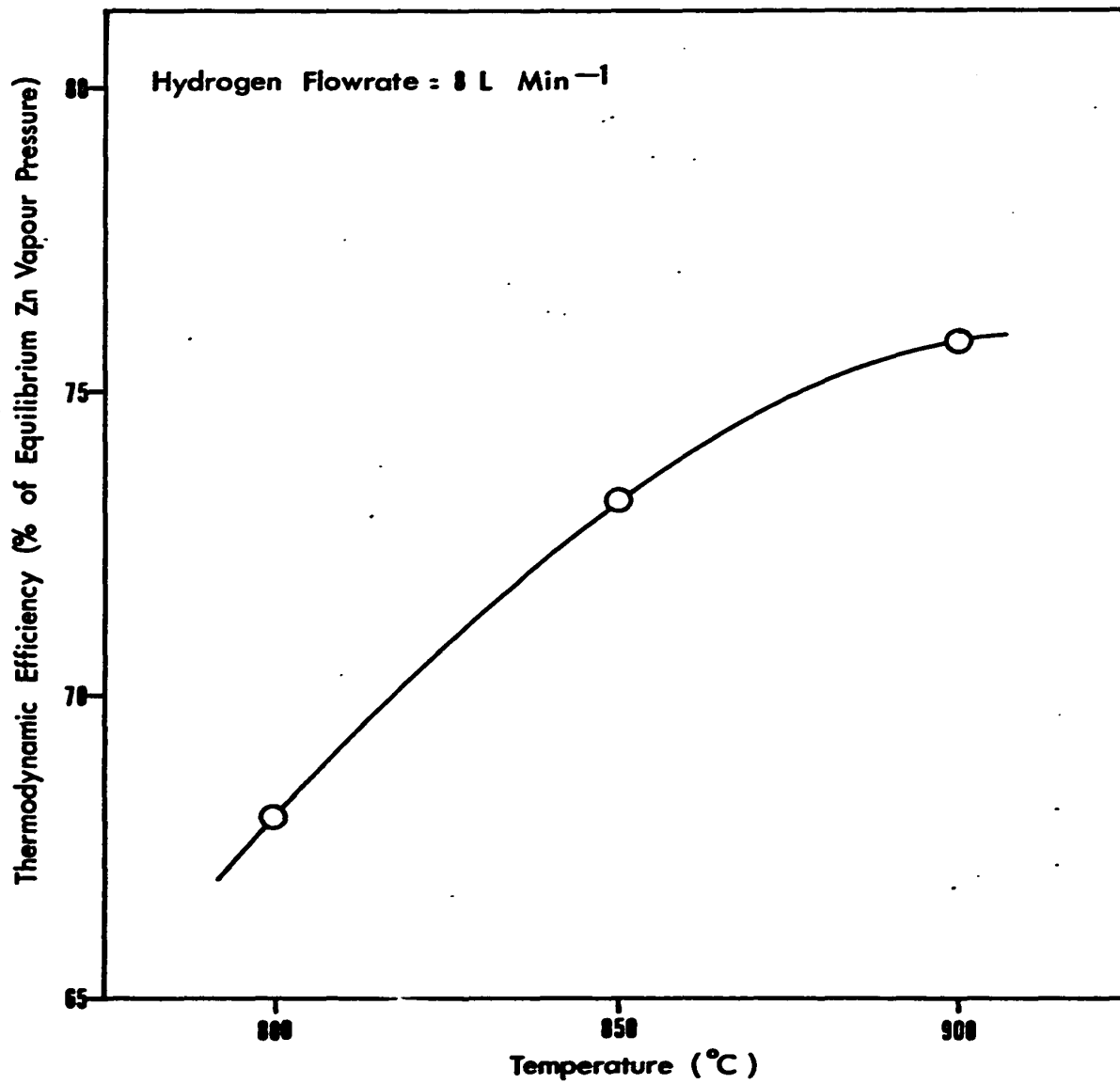
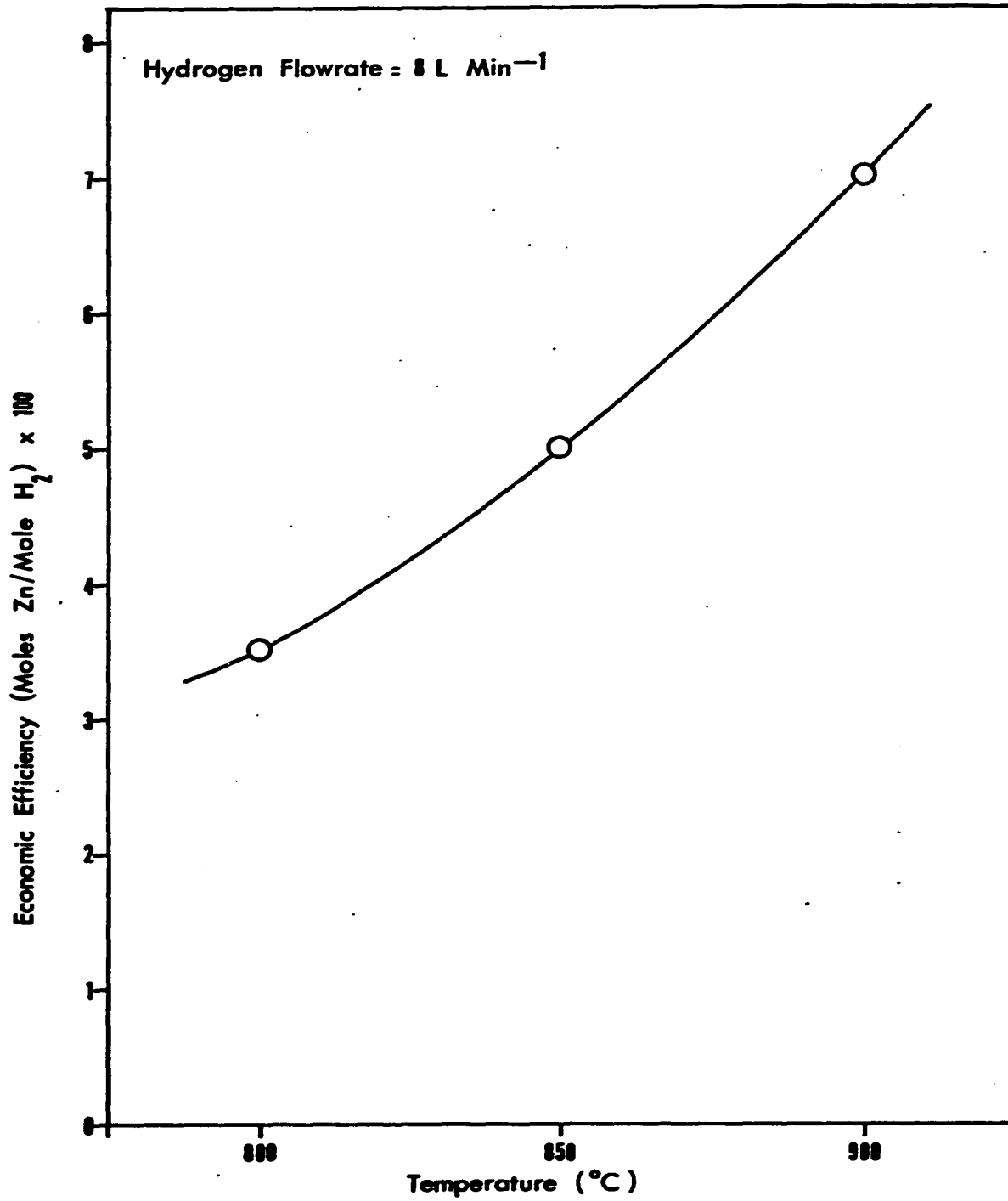


Figure 9.3-2 Effect of Temperature on the Economic Efficiency



In both cases the results tend to indicate that better efficiencies would have been obtained had the experiments been carried out at somewhat lower flowrates, i.e., the system would come closer to equilibrium conditions. Thus the same amount of zinc could be produced by a lesser amount of hydrogen.

In a problem of this nature, however, one is torn between three opposing forces, namely,

- 1) maintaining a minimum hydrogen flowrate to sustain good fluidizing conditions at the possible expense of poor hydrogen efficiencies;
- 2) striving to attain maximum hydrogen efficiencies for reducing purposes;
- 3) obtaining a maximum rate of zinc production even if poor hydrogen efficiencies are obtained.

CHAPTER TEN

DISCUSSION

10.0 Feasibility Considerations — Clinkering and Particle Agglomerations

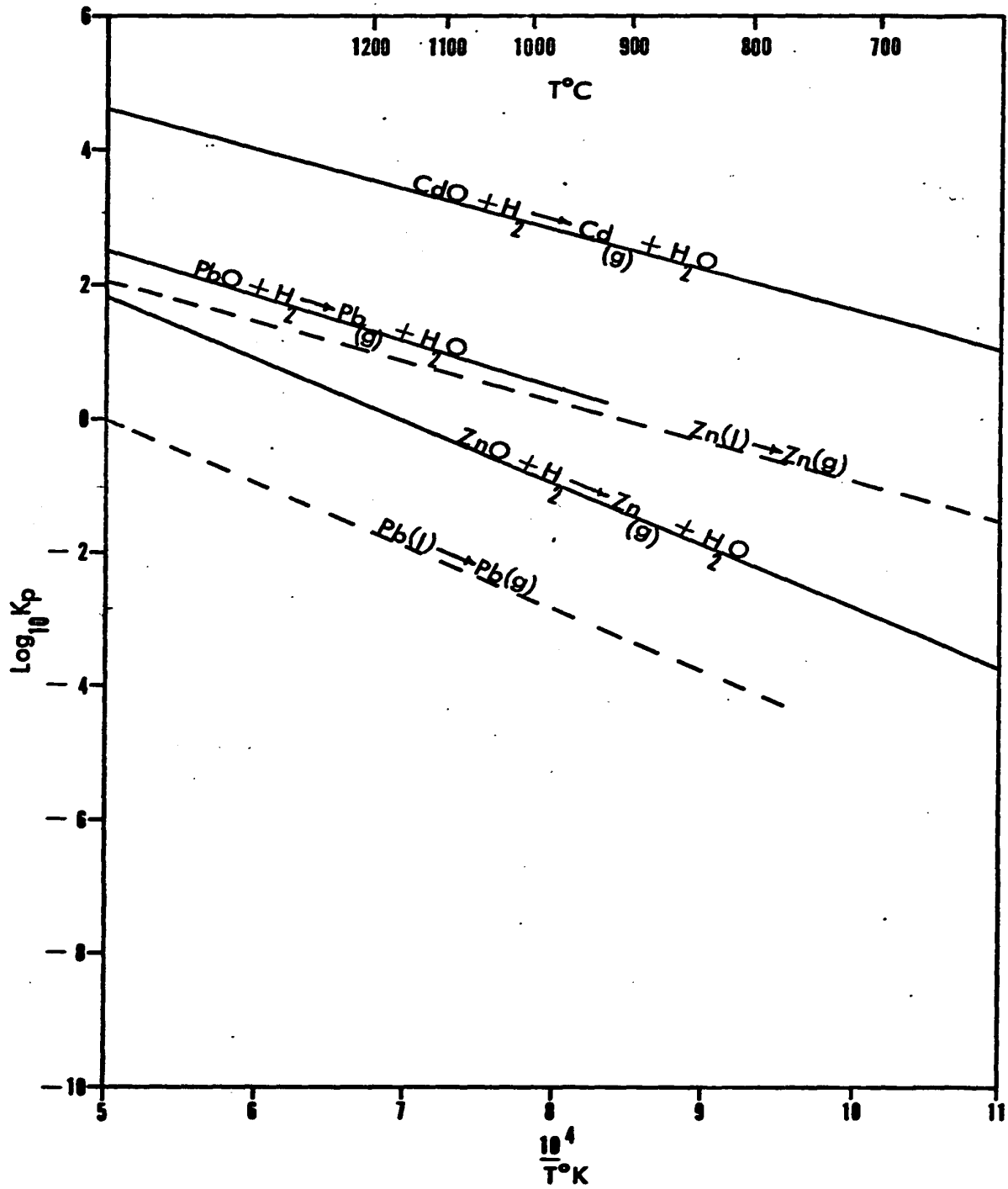
When chemical reactions are carried out in fluidized beds, normally good fluidizing conditions may be disrupted by the agglomeration or clinkering of fine particles into larger masses. This tendency towards defluidization of an otherwise well fluidized bed is almost exclusively restricted to fluidization with a reducing gas. (50)

The most frequent references to this phenomenon have been reported by researchers working on the fluidized bed reduction of iron oxides and ores of iron oxides. Although this characteristic has not been studied in great detail, it is credited to the formation of a sticky surface on the particles by the reduction of a low melting point compound or element which subsequently coats the particle surface and promotes agglomeration by frequent collisions with adjacent particles.

No detailed study of the problem was attempted in this investigation. It seems likely, however, that the clinkering experienced was caused by the reduction of a compound whose product is liquid at the reduction temperatures used.

The analysis of the calcine shows traces of lead (0.13%). Thermodynamic considerations (Fig. 10.0-1) show that the reduction of lead oxide is favourable at these temperatures and that the vapour pressure of lead is low. Figure 10.0-1 also shows that lead oxide is more easily reduced than zinc oxide in a mixture of the two. Hence it can be expected that in the system studied, lead oxide would be reduced simultaneously with the production of zinc vapour and that the product would be substantially liquid lead.

Figure 100-1 Equilibria in the Gaseous Reduction of Metal Oxides



The zinc blast furnace gives some indication of the behaviour of lead and zinc oxides under reducing conditions. While zinc is readily volatilized and passes out of the furnace with the effluent gas stream, most of the lead is collected in the hearth. This behaviour indicates that the lead vaporization rate is slow even at 1200-1300°C and hence it can be expected to be even slower at the lower temperatures used in the present investigation.

Because the vapour pressure of lead over liquid lead is very low in the range 800-900°C (Fig. 10.0-1) it would not be reasonable to expect the problem to be alleviated with time as would be expected if the vapour pressure or the vaporization rate were greater. Although this was borne out in tests of up to 17 hours duration, the tendency towards a less stable clinker was definitely noticeable with increased reaction time.

The belief that the presence of liquid lead in the system is responsible for the observed tendency to clinker is substantiated by the fact that the dimensions of the clinkers remained relatively constant both with reaction time and temperature. If another component, present in greater quantities, were to blame for the clinkering, more serious clinkering problems would be expected with increased production of the component.

Unfortunately, lead was only a trace element in the calcine and hence was indistinguishable on X-ray patterns. It would be of great interest to perform similar reduction tests on pure zinc oxide to determine if clinkering still persists.

Clinker formation in the fluidized bed reduction of other metal oxides, particularly of iron and nickel oxides, has been avoided by carrying out the reduction at well below the melting point of either the metal or the metal oxide. Table 10.0-1 draws a comparison between the temperatures at which different fluidized bed reduction processes were carried out and the melting points of the reaction products.

TABLE 10.0-1

Comparison of the Reduction Temperatures and Melting Points of the Reaction Products for the Reduction of Metal Oxides in Fluidized Beds

Investigators	System	Reduction Temperature	Melting Point of Reaction Products
Brant & Marshall ⁽⁵⁰⁾	Fe-H ₂	750-770°C	FeO - 1377°C Fe - 1530°C
Okura & Lu ⁽⁵²⁾	Fe-H ₂	500-700°C	same
Vavilov et al ⁽⁶³⁾	Fe-H ₂	900-1000°C	same
Masonov et al ⁽⁵¹⁾	Fe-H ₂	490-650°C	same
Kivnick & Hixson ⁽⁶⁴⁾	Ni-H ₂	180-400°C	Ni - 1000°C
Lewis et al ⁽⁶⁵⁾	Cu-CH ₄	650°C	Cu - 1083°C

The universal use of low reduction temperatures points to the seriousness of the problem.

Unfortunately the reduction of zinc oxide at below the melting point of zinc is made impractical for the following reasons:

- 1) The melting point of zinc is relatively low, 419°C.

2) Reduction carried out at such low temperatures could not hope to compete with conventional processes with respect to production rates. Both the reduction kinetics and the zinc vapour pressure are too low to make reduction at these temperatures practical. Figure 10.0-2 is a plot of $\text{Log}_{10} K_E$ vs $1/T$ for the reaction $\text{ZnO} + \text{H}_2 \rightarrow \text{Zn}_{(g)} + \text{H}_2\text{O}$ for temperatures between 0°C and 727°C . This plot indicates that the equilibrium pressures of the zinc and water products are exceedingly low in this temperature range.

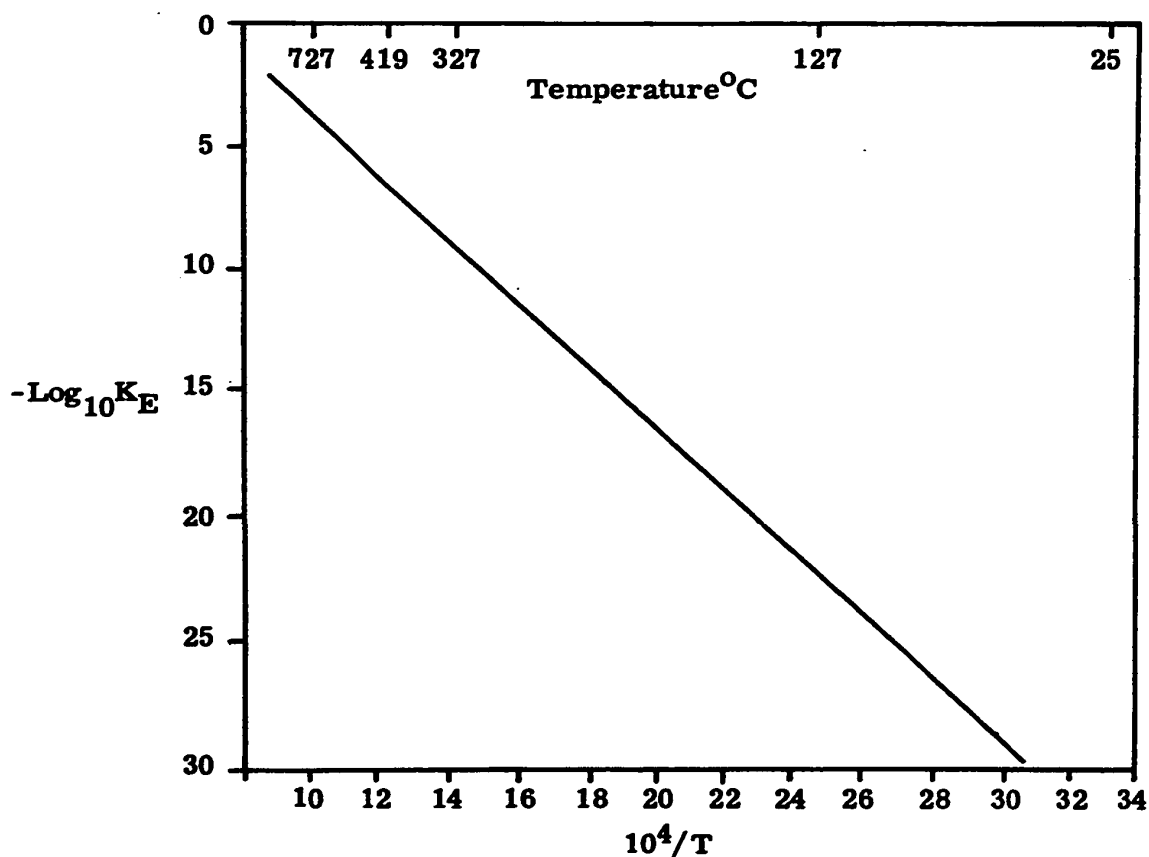


Figure 10.0-2 Equilibria in the ZnO-H₂ System at Low Temperatures (Near the Melting Point of Zinc).

Another interesting result which sheds light on the clinkering problem was obtained from additional experimentation to explain the rate studies. In these tests the calcines were screened on Tyler Standard Sieve Screens at various stages of reduction.

The results (Table 10.4-1, p.130, Figure 10.4-2, p.131) show that there is an early build-up of the largest size particles (-100+150 mesh) at the expense of the smallest particles as a result of agglomeration. After this initial build-up the particle sizes maintain constant fractions with time even though reduction is taking place and the particles might be expected to become smaller.

A more detailed explanation of the significance of this work is given in Section 10.4.

The relative constancy in the fraction of -100+150 mesh material with time (Fig. 10.4-1) indicates that clinkering or agglomeration must have been caused by the reduction of a component of the calcine which does not accumulate with time. If this were not the case, it would be expected that the tendency to clinker would increase with time. Since lead is present only in small quantities, it would seem that the initially reduced lead is sufficient to cause agglomeration but that subsequent lead formation does not increase the tendency to agglomerate. Lead reduced later in the reduction run may in fact coat the more porous structure of the particles.

It will be noted that the amount of clinkered material (-100+150 mesh) decreases slightly during the course of the run. Although lead

has a low vapour pressure at the reaction temperatures, there will be some lead evaporation and this may reduce the amount of clinkering as observed.

10.1 Feasibility Considerations — Hydrogen Efficiency

The hydrogen efficiency has been calculated in two ways; one, the thermodynamic efficiency, was defined as the ratio of the observed partial pressure of zinc in the effluent gas stream to the equilibrium zinc partial pressure at the operating temperature. Thus the thermodynamic efficiency represents how close the system approached to equilibrium which, in turn, represents the best possible situation attainable. The second efficiency calculation which was called an economic efficiency was defined as the ratio of the number of moles of zinc produced to the number of moles of hydrogen fed in during the same time interval.

Figure 9.3-1 shows that there is a definite increase in thermodynamic efficiency with increasing temperature but that the rate of efficiency increase falls off at the higher temperatures (all other variables constant).

Figure 7.0-1 yields a possible explanation. For the reaction between pure zinc oxide and hydrogen at these temperatures, the equilibrium zinc partial pressure rises exponentially with increasing temperature. Although the overall reaction rate for the process shows an increase with rising temperatures, it is likely that the increase in reaction rate is insufficient to keep pace with the rate of rise of the equilibrium zinc vapour pressure at these elevated temperatures. This

aspect is discussed in detail in Section 10.4, "Reduction Mechanisms."

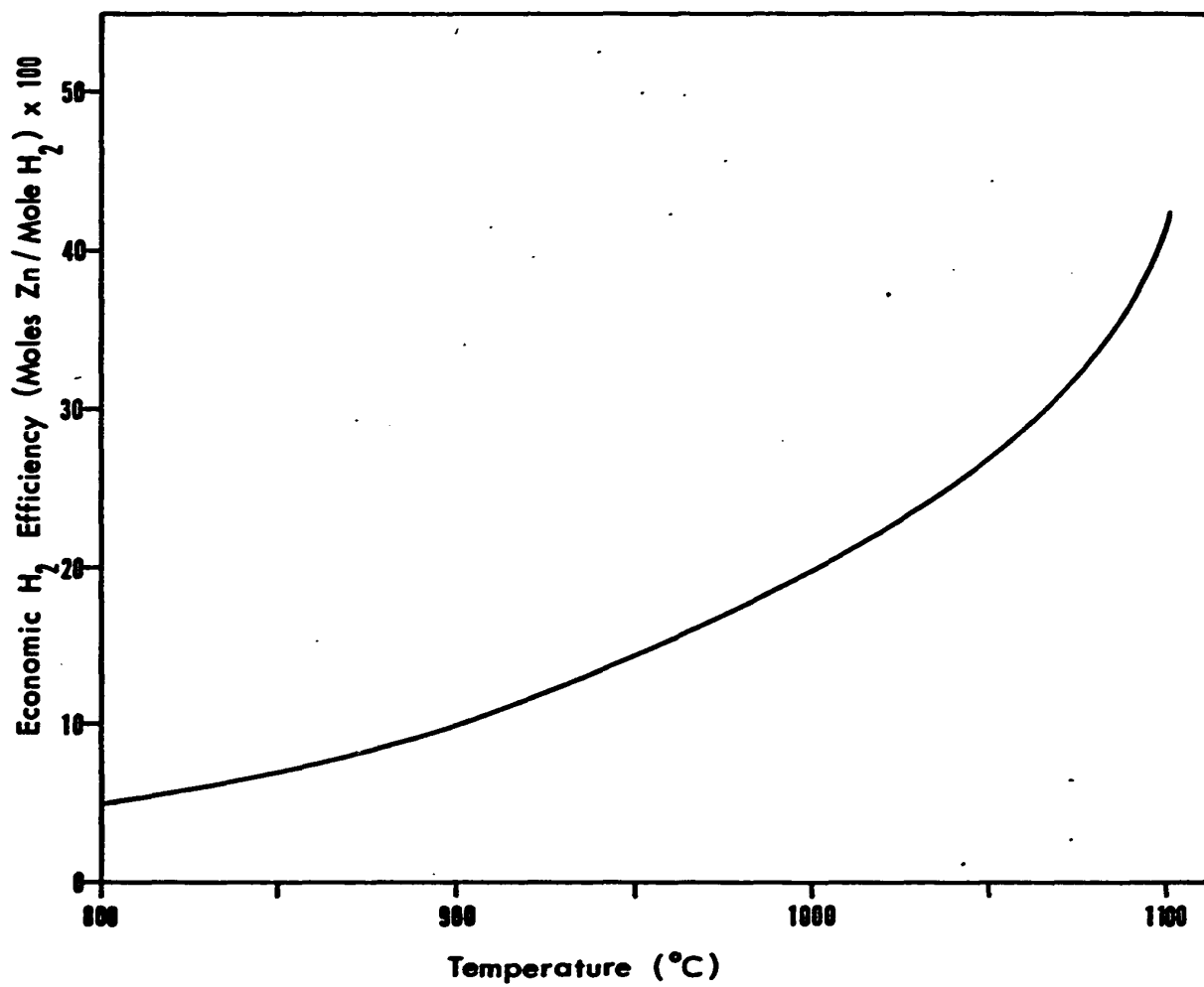
The results also show that by increasing the hydrogen flowrate a significant increase in the zinc elimination rate can be obtained at the expense of a decrease in the thermodynamic and economic efficiencies. Again, for kinetic reasons, the result is to move the system farther from equilibrium.

Figure 9.3-2 shows that the "economic efficiency" rises with temperature aided by both an increase in the reaction rate and an increase in P_{Zn}^{Eq} with increasing temperature. Consequently, if the molar influx of hydrogen into the bed is held constant, the effectiveness of the hydrogen will increase with increasing temperature.

It must be noted that even under equilibrium conditions the economic efficiency of hydrogen utilization is low (Fig. 10.1-1) even at the attainment of equilibrium conditions. Even at 1000°C the potential maximum economic efficiency is 20% (1 mole of zinc produced per 5 moles of hydrogen introduced).

It is clear, therefore, that any commercial operation will have to remove the product H_2O from the gases by condensation and that the H_2 will have to be recycled.

Figure 10.1-1 Effect of Temperature on the Maximum "Economic" Hydrogen Efficiency Attainable at Equilibrium



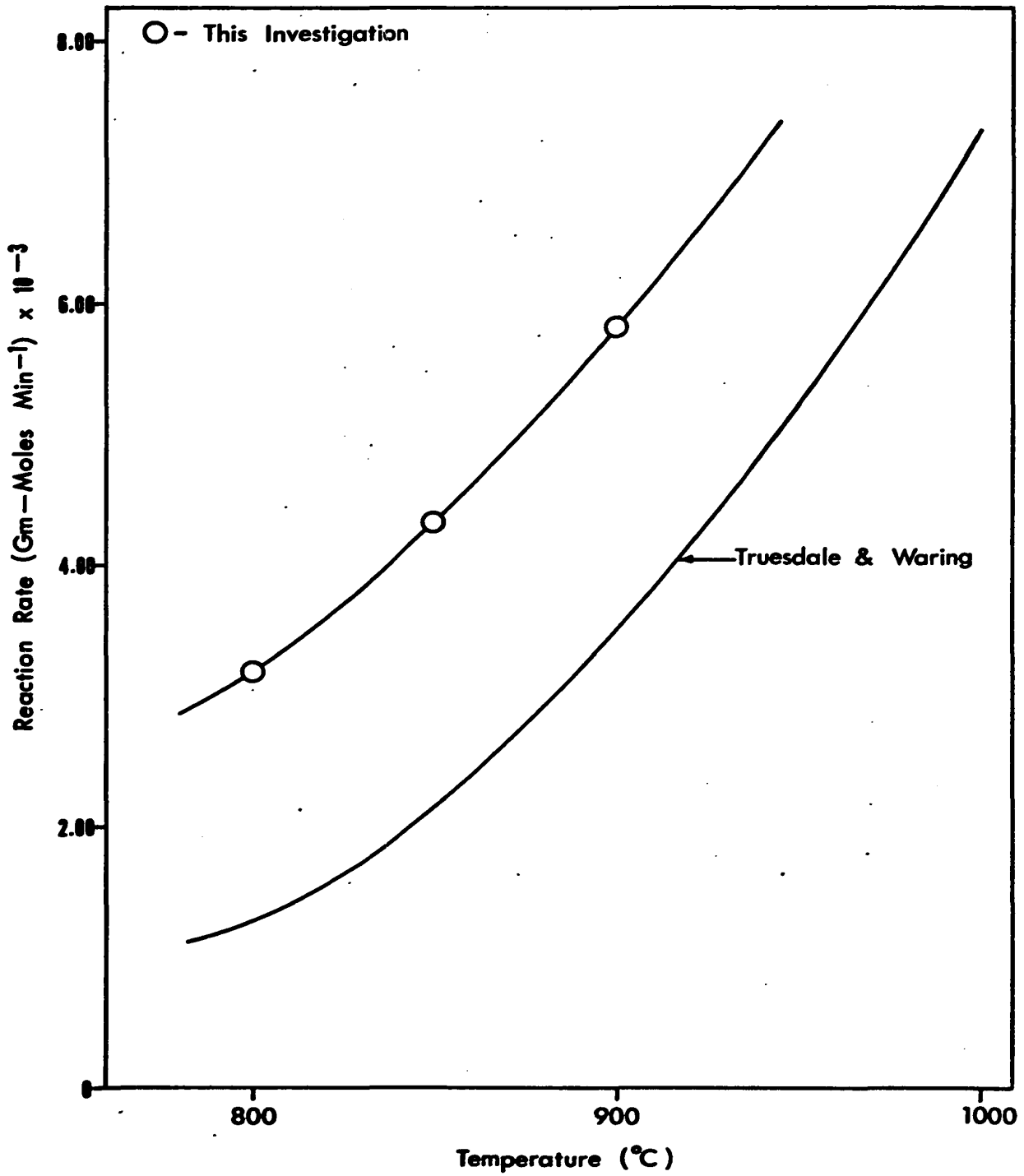
10.2 Reaction Kinetics

10.2-1 Variation of the Reaction Rate with Temperature

The variation of the overall reaction rate, calculated from the percentage zinc elimination curves, with reaction temperature was shown in Figure 9.2-2. For comparison, Figure 10.2-1 includes the same plot obtained by Truesdale and Waring⁽⁴⁴⁾ for the reduction of briquets of zinc oxide with hydrogen.

The Truesdale and Waring single particle studies are more typical of the type of results expected for the reduction of zinc oxide in a fixed bed since the hydrogen velocity used (1.50-1.95 cm sec⁻¹) would be insufficient to fluidize a bed of particles of this size (0.25-1.00 inches diameter). This comparison thus confirms that substantial increases in the reaction rate can be realized by conducting the reduction with smaller particles. A further discussion of the effect of temperature on the reaction rate appears in Section 10.4 "Postulation of Reaction Mechanisms."

Figure 10.2—1 Variation of the Apparent Reaction Rate with Temperature



10.2-2 Variation of the Reaction Rate with Gas Flowrate

The effect of hydrogen flowrate on the reduction of zinc calcines has been illustrated in Figure 9.2-4 in which it was shown that the rate of zinc elimination increases markedly with increased flowrate. No quantitative correlation between the overall reaction rate and the gas flowrate has been attempted because of an insufficient number of data points.

The dynamic behaviour of fluidized beds have been commented on previously (Chapter Five) and it was noted that at gas velocities above minimum fluidization excess gas passed through the bed in the form of bubbles. In such cases a fluidized bed consists of two regions: one, the region of smooth fluidization in which the gas flowing through the solid was in viscous flow and the solid particles were close to each other, the second consisting of gas bubbles moving erratically up through the otherwise smooth bed. This general type of behaviour was witnessed in a low temperature model in this work.

Toomey and Johnstone⁽⁶⁶⁾ attributed the violent mixing present in fluidized beds to the action of bubbles and noted that the region adjacent to the rising bubbles was in a state of high turbulence. They also indicated that by far the greater portion of the solid in the bed is present in the region of smooth fluidization.

If this is an accurate representation, it is likely that the bulk of the mass transfer and hence the bulk of the reaction takes place in the highly turbulent region adjacent to the bubbles passing up through

the smoothly fluidized part of the bed. Therefore the effect of increased hydrogen flowrate might stem from three causes. Firstly, a greater flowrate of hydrogen more rapidly supplies hydrogen to the neighbourhood of the ZnO surface and more rapidly draws off the H_2O and $\text{Zn}_{(g)}$ products. Secondly, the increase in flowrate is accompanied by an increase in turbulence and therefore an increase in the area for mass transfer, i.e., there are more bubbles and hence a greater amount of turbulent region. Thirdly, the increase in turbulence would be expected to increase the mass transfer coefficient in the turbulent region adjacent to the rising bubbles since the mass transfer coefficient increases with increasing particle Reynolds Number⁽¹⁰⁾.

10.3 Variation of the Reaction Rate with Time

Calculations based on Figures 9.2-1 and 9.2-4 show that for runs of six hours duration, the reaction rate is constant with time for any set of constant operating conditions (see Fig. 10.4-1). Figure 9.2-5 indicates that this linearity continues until approximately 85% of the zinc has been expelled from the bed. Calculations based on the chemical analysis of the "as received" zinc calcine and the considerations of Chapter Six show that initially the bed contains about 63%ZnO, 25%ZnFe₂O₄, and 3%ZnO·2ZnSO₄. X-ray diffraction patterns of the calcine and partially reduced calcine (Figs. 10.3-1, 2, 3) substantiate the view that initially there are no lines present to denote the existence of free iron oxides.

The apparent decrease in the zinc elimination rate at about 85% zinc elimination (Fig. 9.2-5) may be due, in part, to the virtual disappearance of free ZnO at this elimination level.

It should be noted that in this particular calcine (composition: 11.7% Fe, 59.9% Zn) the iron will tie up 12% of the available zinc as zinc ferrite. After 88% zinc elimination, therefore, there should be no zinc oxide present in the reduced calcine.

It would be expected that the zinc elimination rate would fall off under these conditions due to the much lower activity of ZnO in the ferrite and the consequently much lower equilibrium concentration of zinc in the effluent gases.

Figure 10.3-1

Debye-Scherrer X-ray pattern of "As Received" zinc calcine. Diffracted lines denote the presence of the following compounds: ZnO , ZnFe_2O_4 , and $\text{ZnO} \cdot 2\text{ZnSO}_4$. Lines for other compounds are not present. Radiation used: $\text{FeK}\alpha$ ($\lambda = 1.9375 \text{ \AA}$).

Figure 10.3-2

Debye-Scherrer X-ray pattern of partially reduced calcine after reduction for 6 hrs at 900°C and a hydrogen flowrate of $8 \text{ litres min}^{-1}$ (3.77 cm sec^{-1}). Lines for ZnO , ZnFe_2O_4 , and $\text{ZnO} \cdot 2\text{ZnSO}_4$ are still present and there are no new lines denoting the formation of additional compounds through reduction. Radiation used: $\text{FeK}\alpha$ ($\lambda = 1.9375 \text{ \AA}$).

Figure 10.3-3

Debye-Scherrer X-ray pattern of partially reduced calcine after reduction for 17 hours at 850°C and a hydrogen flowrate of $16 \text{ litres min}^{-1}$ (7.54 cm sec^{-1}). The diffraction lines indicate the presence, still, of ZnO , ZnFe_2O_4 , and $\text{ZnO} \cdot 2\text{ZnSO}_4$ and there are no lines for compounds of iron indicating that zinc ferrite has not been appreciably reduced even though the zinc elimination is 91%. Lines for iron and oxides of iron are probably too weak to be detected at this point. Radiation used: $\text{FeK}\alpha$ ($\lambda = 1.9375 \text{ \AA}$).

Figure 10.3-1



Figure 10.3-2



Figure 10.3-3



Figure 10.3-1



Figure 10.3-2



Figure 10.3-3



10.4 Postulation of Reaction Mechanisms

10.4-1 Reaction Rate as a Function of Reaction Time

The reaction rate, calculated from Figure 9.2-1 has been plotted as a function of the reaction time and is shown in Figure 10.4-1.

The constancy of the reaction rate with time, at least until the latter stages of reduction, suggests that the reduction of zinc oxide is not controlled by diffusion through a growing solid layer as in the case for iron and nickel reduction. (66-70, 64)

10.4-2 Interpretation of the Reaction Rate

The invariance of the reaction rate with time has lead to the interpretation of the process as one controlled by a mass transfer step. The reduction rate has been represented by

$$\dot{N} = -KA (C_{Zn}^B/2 - C_{Zn}^{Eq}) \quad (10.4-1)$$

where \dot{N} is the number of moles of Zn vaporized min^{-1}

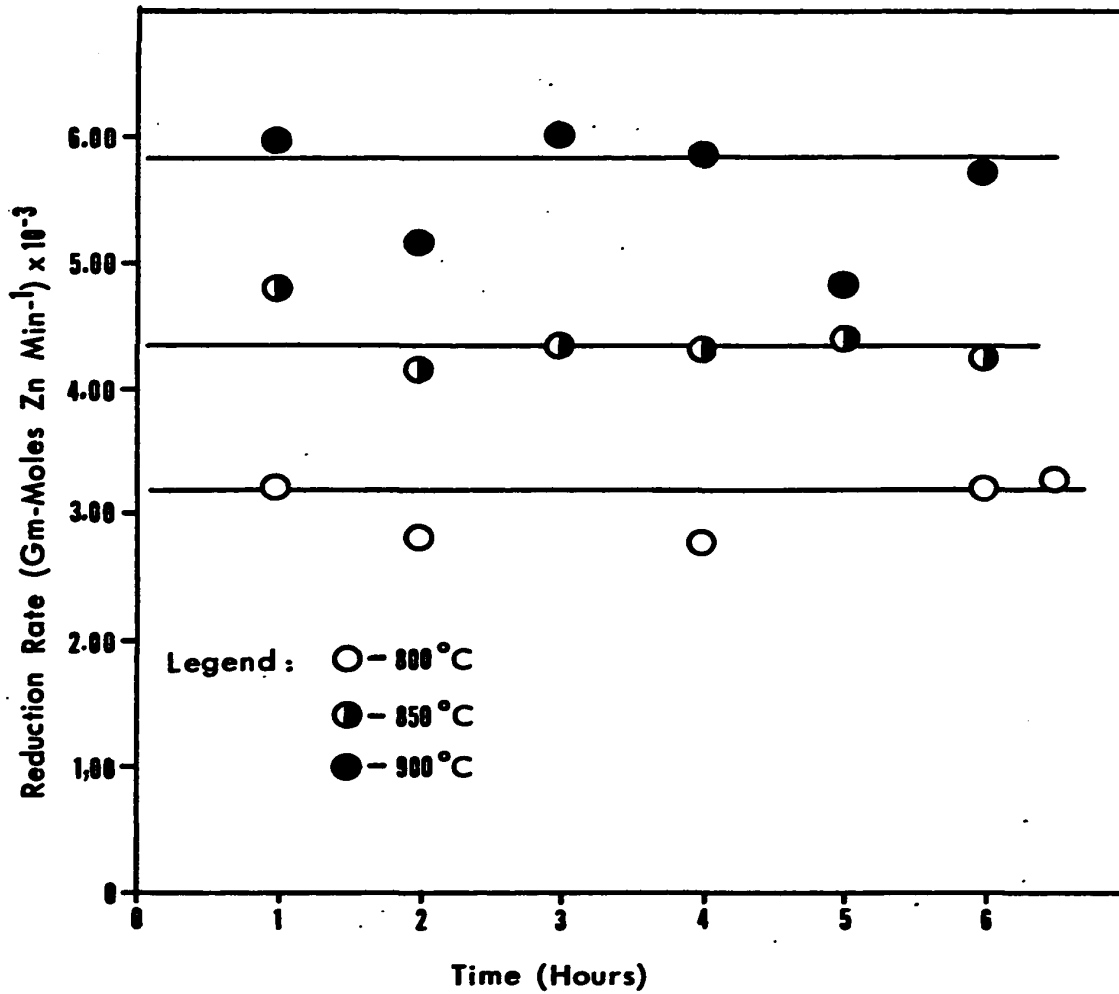
K is the reaction rate constant, cm min^{-1}

A is the total exposed interfacial area

C_{Zn}^B is the calculated off gas zinc content in the bulk of the gas, moles cm^{-3}

C_{Zn}^{Eq} is the equilibrium zinc content of the gas for any given temperature, moles $\text{cm}^{-3} = P_{Zn}^{Eq}/RT$

Figure 10.4-1 Variation of Reduction Rate With Time



The factor $C_{Zn}^B/2$ is employed in the bracketed term of equation 10.4-1 because, while initially the hydrogen entering the bed contains no zinc, the gas leaving the bed contains C_{Zn}^B moles cm^{-3} of zinc. The average zinc content of the gases in the bed is, therefore, $C_{Zn}^B/2$ moles cm^{-3} . This assumption leads to an average rate of zinc elimination from the bed. An incoming "packet" of hydrogen will, of course, react very quickly with the first ZnO particles it meets as C_{Zn}^B will initially be zero. Gas leaving the bed will have more nearly the equilibrium concentration of $Zn(g)$ and H_2O , hence the final rate will be low.

Equation 10.4-1 can only give a constant reaction rate with time if the mass transfer coefficient is constant, if P_{Zn}^{Eq} is constant, and if the total area available for mass transfer remains constant. P_{Zn}^{Eq} can be considered to remain constant while pure zinc oxide continues to be present in the particle.

P_{Zn}^{Eq} being constant, it can be seen that a constant \dot{N} with time requires a constant value of KA with time, i. e.:

$$KA = \frac{\dot{N}}{(C_{Zn}^{Eq} - C_{Zn}^B/2)} \quad (10.4-2)$$

Any proposal for a reaction mechanism must, therefore, take this factor into account.

10.4-3A Particle Size and Interfacial Area

Table 10.4-1 shows the screen analysis of the partially reduced calcine from the experimental reduction runs. Figure 10.4-2 shows a plot of the weight fraction of calcine appearing in the size ranges as a function of reduction time. Each point represents the average for all experiments.

TABLE 10.4-1
Weight Percent of Calcine Appearing in Mesh
Size Ranges Against Reaction Time

Temp.	Hydrogen Flowrate cc/min	Time Hours	-100+150	-150+200	-200+270	-270+325	-325
800	8000	1	25.53	43.80	20.54	2.41	3.63
800	8000	2	24.27	44.58	18.71	3.46	4.89
800	8000	4	21.73	45.06	24.63	4.38	2.57
800	8000	6	17.41	48.16	23.37	6.89	3.72
850	8000	1	26.07	43.86	23.26	.09	6.56
850	8000	2	23.89	45.01	24.30	4.44	2.37
850	8000	3	21.89	44.21	19.88	6.45	5.85
850	8000	4	25.22	46.84	21.73	5.12	1.01
850	8000	5	24.49	44.73	25.55	1.11	3.39
850	8000	6	21.33	43.99	22.81	4.97	4.89
850	16000	1	21.77	44.43	22.50	0.59	7.25
850	16000	2	18.09	44.46	23.56	9.51	4.37
850	16000	3	21.12	42.81	24.61	3.56	8.20
850	16000	4	15.75	44.10	27.87	7.64	4.94
850	16000	5	17.03	45.24	26.46	5.89	5.04
850	16000	6	31.19	44.06	19.97	2.31	2.48
850	16000	17	19.44	28.33	36.11	11.11	5.00
900	8000	1	11.94	44.10	27.87	10.83	4.94
900	8000	2	23.04	41.98	24.62	5.47	4.33
900	8000	3	21.76	43.67	23.98	7.93	2.01
900	8000	4	24.32	44.21	22.44	6.56	2.25
900	8000	5	22.17	44.86	24.19	5.21	3.66
900	8000	6	28.50	46.00	19.33	4.67	1.50
As Received Calcine Sized to -150+200			3.10	44.12	34.37	9.31	8.43

Figure 10.4-2 Particle Size Variation With Reduction Time

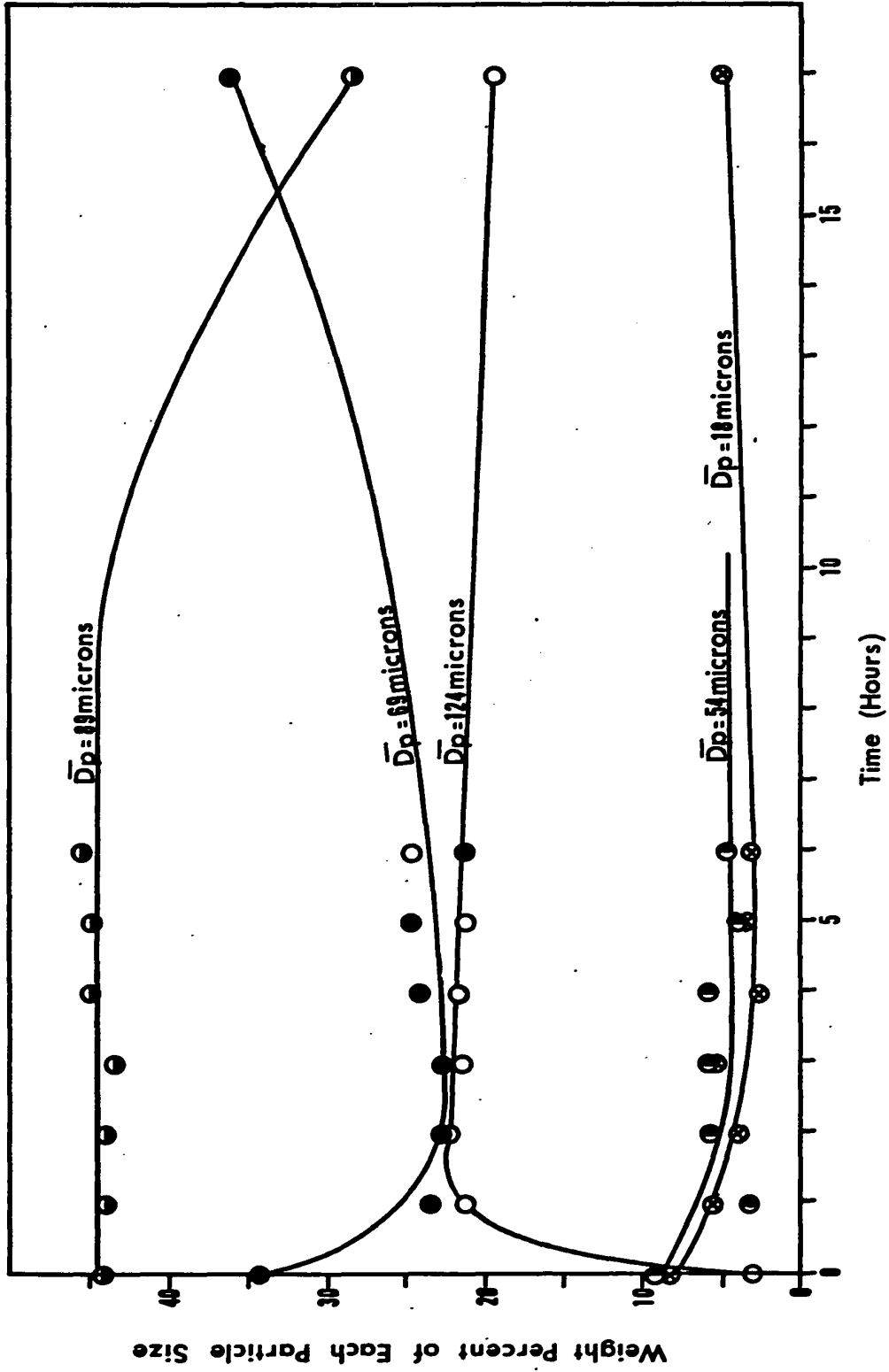


Figure 10.4-2 shows that the amount of calcine appearing within each size range remains essentially constant with time until all or nearly all of the free zinc oxide has been depleted. Hence it appears that the initial dimensions of the particles are preserved as a particle skeleton as the reduction time progresses.

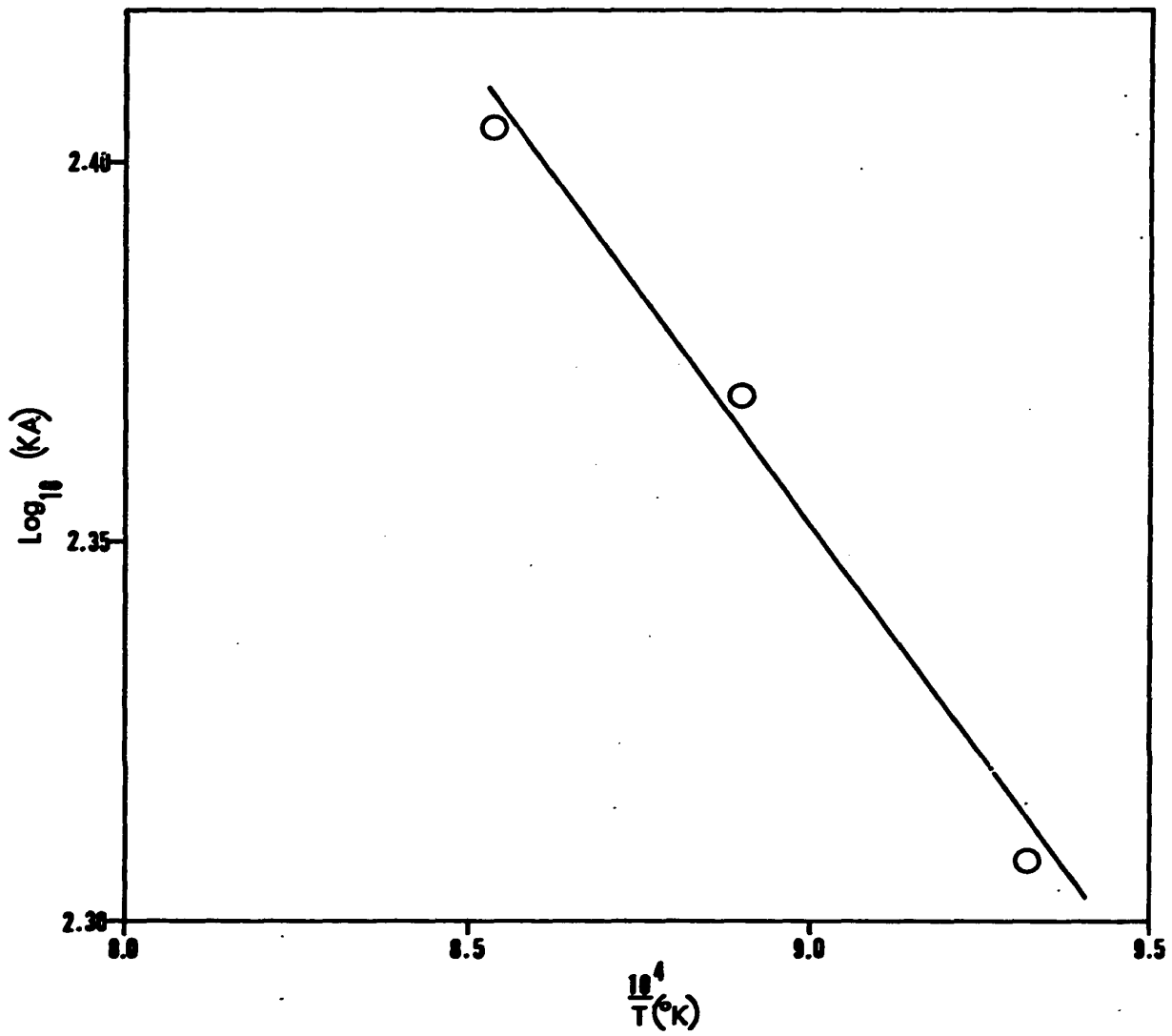
This situation can be explained in terms of the composition of the initial feed material. Since, as stated in Chapter 6, all of the iron reports in the roasted product as zinc ferrite, approximately 25% of the original calcine, is zinc ferrite. This zinc ferrite is not reduced by hydrogen until the latter stages of reduction and so it seems likely that the zinc ferrite forms a shell or matrix which binds the free zinc oxide within the particle. Thus, as the reduction proceeds and zinc is volatilized, a skeleton of the original particle remains which retains the original dimensions of the particles.

10.4-3B The Product KA as a Function of Temperature and Flowrate

Table 10.4-2 shows the calculated values of the product KA for the three temperatures studied in the investigation. Figure 10.4-3 shows an Arrhenius plot of $\text{Log}_{10}(\text{KA})$ against $1/T$. The activation energy calculated from the plot is 12 ± 2 Kcal/mole which is representative of gas diffusion processes rather than chemically controlled reactions.

TABLE 10.4-2
Calculated KA Products for the Reduction Temperatures Studied

Temperature °C	Space Velocity of Gas Through Bed cm sec ⁻¹	KA cm ² sec ⁻¹
800	3.77	208
850	3.77	234
900	3.77	254

Figure 10.4-3 Arrhenius Plot of $\text{Log}_{10} KA$ vs $1/T$ 

The mass transfer coefficient, K , is a function of the diffusion coefficient, D . Support for a gas phase diffusion controlled process would require a temperature dependency of the mass transfer coefficient comparable to the temperature dependency of the diffusion coefficient.

The temperature dependence of the gas diffusion coefficient can be approximated by

$$D_1/D_2 = (T_1/T_2)^n \quad (44) \quad (10.4-3)$$

where T is the absolute temperature, $^{\circ}\text{K}$

n varies between 1.5 and 2.0

Taking $n = 2.0$, the ratios of the diffusion coefficients have been calculated for the three temperatures studied and are compared with the corresponding ratios of the product KA in Table 10.4-3.

TABLE 10.4-3

Comparison of D_{T_1}/D_{T_2} and $(KA)_{T_1}/(KA)_{T_2}$ (Temperatures in $^{\circ}\text{C}$)

D_{800}/D_{800}	$(KA)_{800}/(KA)_{800}$	D_{850}/D_{800}	$(KA)_{850}/(KA)_{800}$	D_{900}/D_{800}	$(KA)_{900}/(KA)_{800}$
1.00	1.00	1.10	1.12	1.20	1.22

The excellent agreement between the activation energy considerations and the results shown in Table 10.4-3 supports the view of a process controlled by a gas phase transport mechanism.

10.4-4 Variation of KA with Gas Flowrate

Kettenring et al⁽¹⁰⁾ have shown that for mass transfer controlled processes in fluidized beds, the mass transfer coefficient, K , increases by approximately 20% for a doubling of the particle Reynolds number in

the range corresponding to this work. Table 10.4-4 shows the variation of KA with space velocity obtained in the present work.

TABLE 10.4-4
Velocity Dependence of KA

Temperature °C	Space Velocity, cm sec ⁻¹	KA, cm ² sec ⁻¹
850	3.77	234
850	3.77	278

The observed increase in the value of KA for a doubling of the space velocity is 19% which shows good agreement with the Kettenring et al suggestion.

10.4-5 Reaction Mechanism

While Sections 10.4-1, 2, 3, and 4 present evidence to indicate that the rate controlling step for the fluidized bed reduction of zinc calcine by hydrogen is gas phase diffusion, the postulation of a mechanism requires an explanation for the observation of a constant product KA with time. As a first step a mechanism which explains a constant area for mass transfer must be suggested.

Figures 10.4-4, 5, and 6 show photomicrographs of the calcine particles at various stages of reduction.

Figure 10.4-4 shows the calcine as received. The photograph shows that the outer surface of the particles are mainly zinc oxide and that there are pockets of zinc oxide within the structure. The particles appear to be supported on a skeleton of zinc ferrite (ZnFe₂O₄).

Figure 10.4-5 shows that as reduction proceeds the outer layer of zinc oxide has been reduced and a honeycomb structure of zinc oxide within the ferrite skeleton remains.

The final photomicrograph (Fig. 10.4-6) shows that at 91% elimination of zinc there are still discrete pockets of zinc oxide within the honeycomb structure. The existence of these pockets of free zinc oxide at this level of elimination (theoretical depletion of free zinc oxide occurs at 88% elimination) indicates that hydrogen attack of the outer zinc ferrite skeleton must have occurred. The X-ray diffraction patterns (Figs. 10.3-1, 2, and 3), however, do not conclusively substantiate this claim.

Figure 10.4-5 corresponds to particles that have undergone 6 hrs. reduction at 900°C and a hydrogen space velocity of 3.77 cm sec⁻¹. At this point approximately 30% of the zinc has been reduced.

Calculations based on perfect spheres indicate that a 30% reduction in volume has associated with it a 23% reduction in surface area.

The photomicrographs indicate, however, that the reduced calcine is porous in nature and it is likely that new surfaces of zinc oxide are being exposed as reduction proceeds. It is likely, therefore, that the area of exposed zinc oxide does not decrease significantly at least during the first 30% of reduction. It is notable, however, that even at 85% reduction (Fig. 9.2-5), the zinc elimination rate has not fallen off significantly.

The photographic evidence also indicates that the pores are large enough to allow free access of hydrogen to the reaction sites and to allow diffusion of the reaction products away from the reaction sites to the bulk gases.

It would seem, therefore, that the constant zinc elimination rate can be tentatively explained by the creation of new zinc oxide surface area and the opening of pores in the particle structure.

Figure 10.4-4

Photomicrograph of "As Received" zinc calcine. Light coloured areas are concentrations of zinc oxide. Dark grey area is zinc ferrite. As the photograph indicates, zinc oxide concentrates as a layer around the particle with local concentrations within the particles themselves. The entire particle appears to be bound together by a network of predominantly zinc ferrite. (Magn. 600 X.)

Figure 10.4-5

Photomicrograph of a zinc calcine particle after six hours reduction at 900°C and a hydrogen flowrate of $8 \text{ litres min}^{-1}$ (3.77 cm sec^{-1}). The approximate degree of reduction is 30%. This photograph indicates that the outer layer of zinc oxide has been reduced, leaving localized "pockets" of zinc oxide within the particle. (Magn. 500 X.)

Figure 10.4-6

Photomicrograph of zinc calcine particles after seventeen hours reduction at 850°C and a hydrogen flowrate of $16 \text{ litres min}^{-1}$. The approximate degree of reduction is 91%. This photograph indicates that most of the zinc oxide has been reduced leaving a skeleton of the original particle composed entirely of zinc ferrite. (Magn. 200 X.)

Figure 10.4-4



Figure 10.4-5

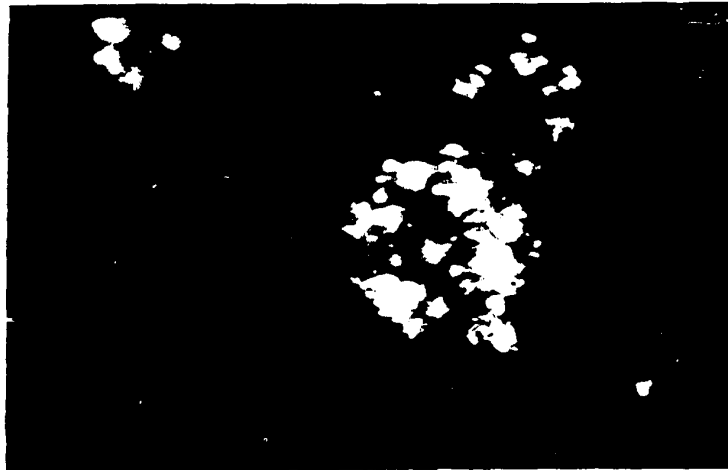


Figure 10.4-6



Figure 10.4-4

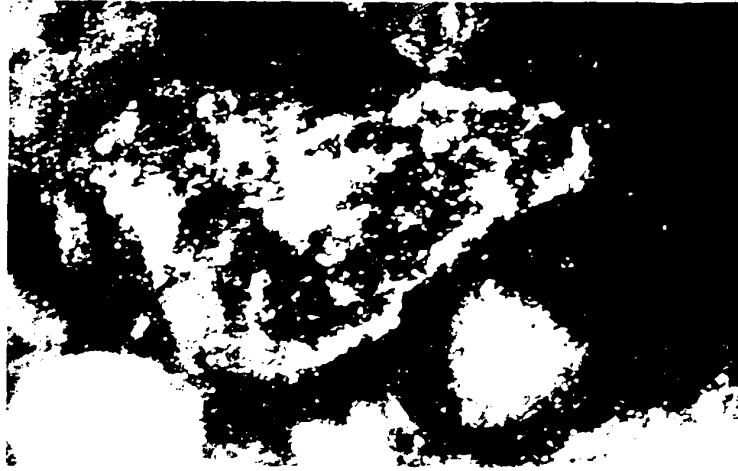


Figure 10.4-5

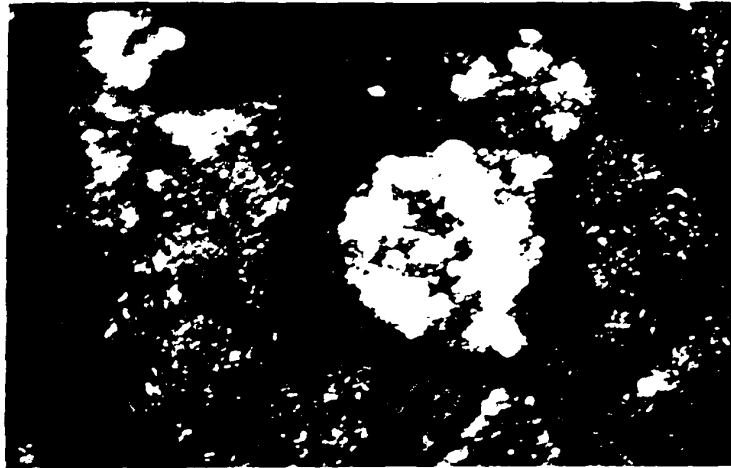
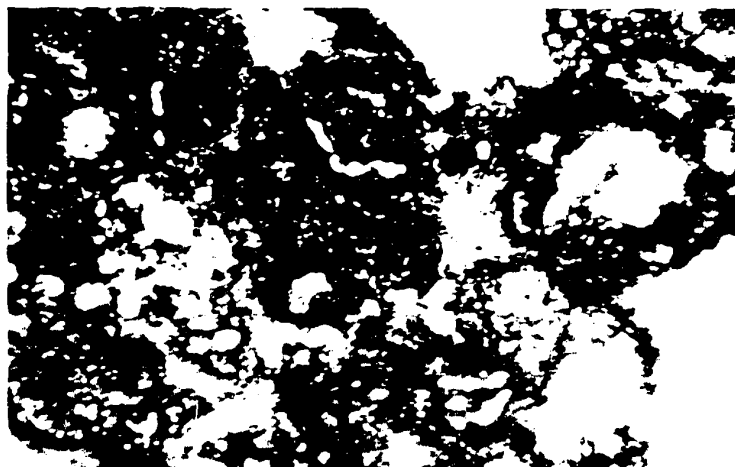


Figure 10.4-6



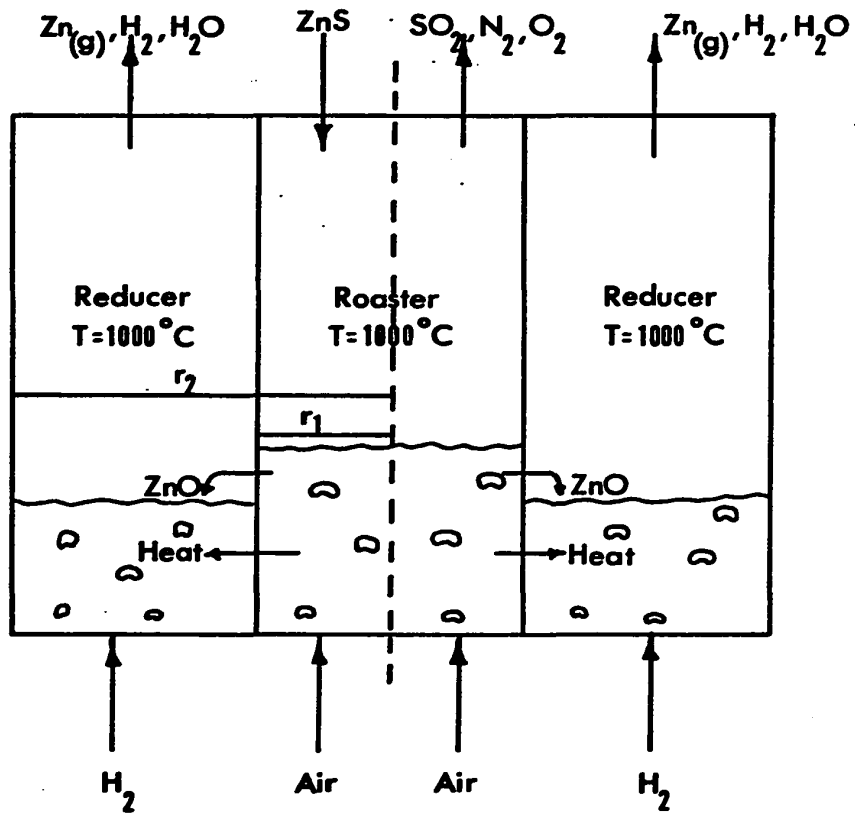
10.5 Predictions for Full Scale Reactors

Figure 10.5-1 shows, schematically, the general flow pattern of materials and the equipment requirements for the zinc production scheme outlined briefly in Chapter One, Section 1.0.

The potential technical and economic advantages of such a process are outlined briefly as follows:

- 1) Fluidized beds have very few moving parts and hence, maintenance costs should be low.
- 2) Through continuous operation and a high degree of automation, labour requirements should be reduced appreciably.
- 3) Fuel requirements should be lowered since the exothermic heat of the roasting reactions can be recovered by:
 - a) hot charging the roasted calcine to the reduction fluidized bed;
 - b) preheating the reducing gases with the hot effluent gases from the roasters;
 - c) combining the roasting fluidized beds and the reducing fluidized beds within a single container to make use of the roasting heat of reaction for the endothermic reduction reaction.
- 4) Alternative reducing gases, e.g., methane, propane, natural gas, may be used to provide heat by combustion. The combustion products of these gases would be used for the reduction of the zinc calcine.

Figure 10.5-1 Proposed Integrated Fluidized Roaster Bed—
Reduction Bed Zinc Production Furnace



This section of the thesis will deal with the calculation of two important parameters for an industrial scale plant based on the diagram in Figure 10.5-1. These two calculations have been:

- a) prediction of the requirements for total reduction vessel area, i. e., the plan area required for the reduction beds;
- b) prediction of the potential fuel savings to be gained from the hot feeding of calcine, of preheating the reducing gas fed to the reduction fluidized bed, and of combining the roasting and reduction beds in one container.

The calculations have been made for a) reduction with hydrogen and for b) reduction with methane. The data for the roasting step has been taken from the current practice at Canadian Electrolytic Zinc Ltd., while the data for the reduction step has been taken from the present experimental data.

In the calculations, the assumption has been made that the roaster feed material is pure sphalerite (ZnS).

Table 10.5-1 shows the pertinent operating data from the Canadian Electrolytic Zinc Lurgi turbulent layer fluidized bed roasters.

TABLE 10.5-1

**Operating Data for the Lurgi Turbulent Layer Fluidized Bed
Roasters at Canadian Electrolytic Zinc Limited**

Feed Rate	10 tph (wet) = 9.5 tph (dry)
Air Blowing Rate	15,700-17,300 Nm ³ hr ⁻¹ (10,000-12,000 SCFM)
Bed Grate Area	34 m ² (366 ft ²)
Bed Temperature	950°C
Average Space Velocity	146 ft. min ⁻¹
Boiler Inlet Temperature	970°C
Boiler Outlet Temperature	350°C
Solid Product Distribution	12.5% to Roaster Overflow 87.5% to Waste Heat Boilers
Average Zinc Content in Concentrate	52% (dry basis)
Roaster Off-Gas Composition	10-11% SO ₂ 5-6 % O ₂ 9-11% H ₂ O 73-76% N ₂

10.5-1 Basis of the Design Calculations

The plan area of the reactor for the reduction of zinc oxide has been based on a plant capable of producing 50 tons of zinc per day. To achieve this, the operating data of the C.E.Z. roasters (Table 10.5-1)

were scaled down while preserving similarity in space velocity and air to concentrate ratio. The scaled down parameters are shown in Table 10.5-2.

TABLE 10.5-2
**Scaled Down Parameters for a Fluidized Bed Roaster Capable
of Producing 50 tpd of Zinc Oxide**

Concentrate Feedrate	4.0 tph
Zinc Production Rate	3.28 gm moles ft. ⁻² min. ⁻¹
Air Blowing Rate	4,000 SCFM
Roaster Grate Area	146.5 ft. ⁻²
(calculated to give a space velocity of 146 ft. min. ⁻¹ as in the C.E.Z. beds (Table 10.6-1))	

The reduction rates estimated for ZnO reduction with a) hydrogen and b) methane at 1000°C were based on operation with a 40" deep bed (10 times the bed height used in the experimental study) and the higher experimental gas space velocity of 7.54 cm. sec.⁻¹. Operating under these conditions, it was assumed that the equilibrium zinc content was established in the effluent gases. The equilibrium assumption seems justified as the residence time in the full scale bed will be 10 times that in the present experimental bed.

To facilitate subsequent heat balance calculations, all calculations have been based on the production of 1 gm. mole of zinc.

10.5-2 Calculation of the Plan Area Requirements for ZnO Reduction

Table 10.5-3 shows the data for the estimation of the plan area required for ZnO reduction in a fluidized bed.

TABLE 10.5-3

Estimation Data of the Plan Area Required
for ZnO Reduction in a Fluidized Bed

	Hydrogen Reduction	Methane Reduction
Depth of bed	40 inches	40 inches
Gas Space Velocity	7.54 cm. sec. ⁻¹	7.54 cm. sec. ⁻¹
Gas Residence Time in the bed (calculated)	13.5 secs.	13.5 secs.
Equilibrium P_{Zn} (1000°C)	0.166 atmos.	0.315 atmos.
Moles of Zinc produced per mole of gas fed in	0.2	1.37
Plan area Expt'l bed	0.0378 ft. ²	0.0378 ft. ²
Zinc Production Rate (calculated)	0.82 gm. moles ft. ⁻² min. ⁻¹	5.55 gm. moles ft. ⁻² min. ⁻¹

For Hydrogen Reduction

The plan area of the reduction fluidized bed can now be calculated based on a designed zinc production rate of 3.28 gm. moles Zn ft. ⁻² min. ⁻¹ and a roaster grate area of 146.5 ft. ⁺² (Table 10.5-1).

It can readily be seen that the reduction bed grate area required is

$$\frac{3.28 \text{ gm. moles ft. }^{-2} \text{ min. }^{-1}}{0.82 \text{ gm. moles ft. }^{-2} \text{ min. }^{-1}} \times 146.5 \text{ ft. }^2 = 590 \text{ ft. }^2$$

Using the annulus design of Figure 10.5-1, the radius of the reduction fluidized bed is $15.3(r_2)$ feet as compared with the radius of the internal roaster of $6.8(r_1)$ feet. The dimensions of the device are shown in Figure 10.5-1.

For Methane Reduction

For methane reduction of ZnO, on the other hand, the required plan area is

$$\frac{3.28 \text{ gm. moles ft.}^{-2} \text{ min.}^{-1}}{5 \text{ 55 gm. moles ft.}^{-2} \text{ min.}^{-1}} \times 146.5 = 87 \text{ ft.}^2$$

and the radius of the reduction bed will be 8.6 feet around the central roaster of 6.8 feet radius (Fig. 10.5-1).

10.5-3 Heat Calculations Based on a Roast-Reduction Integrated Process

For the Production of Zinc

Chapter One, Section 1.0, and Chapter Ten, Section 10.5 have projected an idea for a novel method of smelting zinc ores and have commented on the potential advantages to be derived from an integrated zinc production scheme.

Energy requirements, in particular the conservation and efficient utilization of energy, are extremely important items in determining the economic feasibility of a new process, particularly where a process demands high temperatures for operation.

The pyrometallurgical production of zinc requires high temperatures to yield zinc at perceptible rates by conventional reduction methods. Large heat requirements are needed because a) the reduction is highly endo-

thermic and b) the reduction temperature must be maintained to prevent reoxidation of zinc vapour.

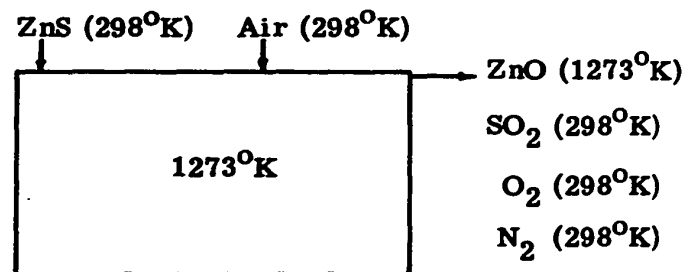
By using the large heat evolved from the exothermic roasting reactions to offset the heat requirements for reduction, it will be shown that the integrated process can result in substantial fuel savings.

The heat balance has been calculated for hydrogen and for methane reduction. It has been assumed that pure ZnS is roasted to pure ZnO. The reduction process has been assumed to reach equilibrium and it has been assumed that there is no heat transferred to the surroundings. These assumptions represent, therefore, an ideal case. Figure 10.5-1 shows one method which is thought to approach this ideality.

Usable Heat Evolved During Roasting

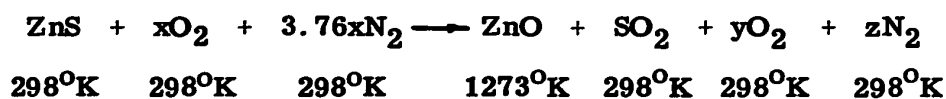
The only usable heat which can be salvaged from the roasting of ZnS is the sensible heat of the ZnO and the roaster off gases. Figure 10.5-2 shows the material flow pattern and temperatures considered in the roaster heat balance.

Figure 10.5-2 Schematic Heat Balance for the Roasting of ZnS at 1000°C



This flow pattern assumes that a) all the sensible heat of the effluent roaster gases can be recovered and b) the hot ZnO (1273°K) is charged

directly to the reduction fluidized bed. The heat balance has been calculated on the basis of 1 gm. mole ZnS. The roasting reaction is



The values of x, y, and z have been calculated from the roaster off gas analysis given in Table 10.5-1. The values are:

$$x = 2.00 \text{ moles O}_2$$

$$y = 0.50 \text{ gm. moles O}_2$$

$$z = 3.76x = 7.60 \text{ gm. moles N}_2$$

Data (62, 71) for the heat balance are given in Table 10.5-4.

TABLE 10.5-4

Heat Data for ZnS Roasting at 1000°C

Material	N Gm. Moles	$H_f^o, 298$ cal/mole	$H_T^o - H_{298}$ cal/mole	Temp. °K	$H_T = H_f^o, 298 + (H_T^o - H_{298})$ cal/mole	Total Enthalpy $H_T \times N$ cal.
ZnS	1.00	-48200	0	298	-48200	-48200
O ₂	2.00	0	0	298	0	0
O ₂	0.50	0	0	298	0	0
N ₂	7.60	0	0	298	0	0
ZnO	1.00	-83200	11700	1273	-71500	-71500
SO ₂	1.00	-71000	0	298	-71000	-71000

The enthalpy change for the reaction = Enthalpy of Products - Enthalpy of Reactants

$$= (H_{\text{ZnO}} + H_{\text{SO}_2} + H_{\text{O}_2} + H_{\text{N}_2}) - (H_{\text{ZnS}} + H_{\text{O}_2} + H_{\text{N}_2})$$

$$= (-71500 - 71000 + 0 + 0) - (-48200 + 0 + 0)$$

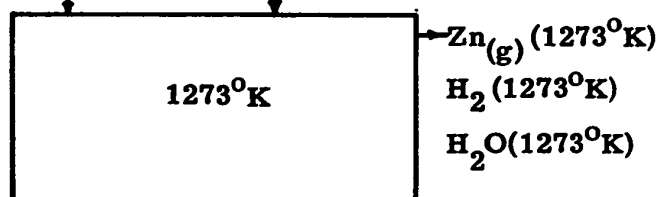
$$= -94300 \text{ cal (gm. mole)}^{-1} \text{ZnO}$$

That is, the roasting process can ideally deliver 94300 cal (gm. mole)⁻¹ of ZnO to the reduction bed.

Heat Required for the Reduction of Zinc Oxide by Hydrogen

Figure 10.5-3 shows a schematic representation of the heat balance for the reduction of zinc oxide by hydrogen.

Figure 10.5-3 Schematic Heat Balance for the Reduction of Zinc Oxide by Hydrogen at 1000°C
ZnO(1273°K) H₂(298°K)



Assuming that the effluent gas stream contains the equilibrium amount of zinc vapour ($P_{\text{Zn}}^{\text{Eq}} = 0.166$ atmos., 1000°C), it can be shown that

$$\frac{N_{\text{Zn}}}{N_{\text{Zn}} + N_{\text{H}_2} + N_{\text{H}_2\text{O}}} = 0.166 \quad (10.5-1)$$

where N is the number of moles of each gaseous component.

From the stoichiometric equation, $\text{ZnO} + \text{H}_2 \rightarrow \text{Zn}_{(\text{g})} + \text{H}_2\text{O}$, it can be seen that $N_{\text{Zn}} = N_{\text{H}_2\text{O}}$. Therefore, solving equation 10.5-1 for the production of one gm. mole of Zn, it can be seen that there will be 4.0 gm. moles of H₂ per gm. mole of Zn produced in the effluent gases. The required amount of input hydrogen is, then, 5.0 gm. moles H₂ per gm.

mole of Zn produced. The defining reduction equation is, therefore,

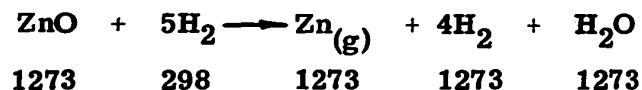


Table 10.5-5 contains the enthalpy data (28, 62) for the solution of the reduction heat balance.

TABLE 10.5-5
Heat Data for ZnO Reduction by Hydrogen at 1000°C

Material	N Gm. Moles	$H_{1273}^{\circ} - H_{298}^{\circ}$ cal/mole	$H_f^{\circ}, 298$ cal/mole	$H_T = H_f^{\circ}, 298 + (H_T^{\circ} - H_{298}^{\circ})$ cal/mole	Total Enthalpy $H_T \times N$ cals.
Input H_2	5.0	—	0	0	0
Output H_2	4.0	6900	0	6900	27600
$\text{Zn}_{(g)}$	1.0	36000	0	36000	36000
ZnO	1.0	11700	-83300	-71500	-71500
H_2O	1.0	19500	-68300	-48800	-48800

$$\begin{aligned} \text{The enthalpy change} &= (H_{\text{H}_2\text{O}} + H_{\text{H}_2} + H_{\text{Zn}}) - (H_{\text{ZnO}} + H_{\text{H}_2}) \\ &\quad 1273 \quad 1273 \quad 1273 \quad 1273 \quad 298 \\ &= (-48800 + 27600 + 36000) - (-71500 + 0) \\ &= 86300 \text{ cal. (gm. mole ZnO)}^{-1} \end{aligned}$$

Unrecoverable Roaster Heat

Comparison of the total usable roaster heat (94300 cal per mole ZnO) evolved during the roasting of ZnO with the heat required to reduce 1 mole ZnO (86600 cal per mole ZnO) shows that the integrated process is autogenous provided that all the roaster heat can be utilized. However, since the roaster gases are at 1000°C and the reduction occurs at the same temperature, the sensible heat of the roaster gases can only be

used to a) preheat ZnS and b) preheat H₂ which both enter at 298°K.

It is useful, therefore, in calculating the final heat balance of the process, to estimate how much of the roaster gas sensible heat can be used and how much is waste heat.

The sensible heat required to raise the temperature of ZnS from 25°C to 1000°C is

$$\begin{aligned} & \int_{298}^{1273} C_{pZnS} dT \\ &= \int_{298}^{1273} (12.16 + 1.24 \times 10^{-3}T - 1.36 \times 10^{-5}T^{-2}) dT \\ &= 12.16(1273 - 298) + 0.62 \times 10^{-3}(1273^2 - 298^2) + 1.36 \times 10^5 \\ & \quad (1/1273 - 1/298) \\ &= 12500 \text{ cal (gm. mole)}^{-1} \end{aligned}$$

The sensible heat required to raise the temperature of 5.0 gm. moles of H₂ from 25°C to 1000°C is

$$\begin{aligned} & 5.0 \int_{298}^{1273} (6.52 + 0.78 \times 10^{-3}T + 0.12 \times 10^{-5}T^{-2}) dT \\ &= 34900 \text{ cal} \end{aligned}$$

The total sensible preheat required = 34900 + 12500 = 47400 cal.

The extractable heat from the roaster products for preheating purposes comes from cooling the roaster off gases. The heat evolved on cooling to room temperature is:

For SO₂ = -11700 cal.

O₂ = 0.5 x (-7600) = -3800 cal.

N₂ = 7.60 x (-7300) = -55500 cal.

The total heat available in the roaster gases = 70000 cal.

Therefore it can be seen that not all of this available heat can be used. In fact, the total unusable heat

$$\begin{aligned} \text{Total Unusable Heat} &= \text{Heat Available by Cooling Roaster Gases} - \text{Heat} \\ &\quad \text{to Raise Temperature of Feed Materials.} \\ &= 70000 - 47400 = 22600 \text{ cal.} \end{aligned}$$

This is equivalent to saying that the roaster gases will leave the system at a temperature higher than room temperature.

$$\begin{aligned} \text{Thus, the net thermal deficiency for the overall process} &= \text{the} \\ \text{reduction heat required} &- (\text{oxidation heat} - \text{unusable roaster off gas heat}). \\ &= 86300 - (94300 - 22600) \\ &= 14600 \text{ cal.} \end{aligned}$$

Even under ideal conditions, therefore, the process using air is not completely autogenous with the result that heat will have to be added to the system.

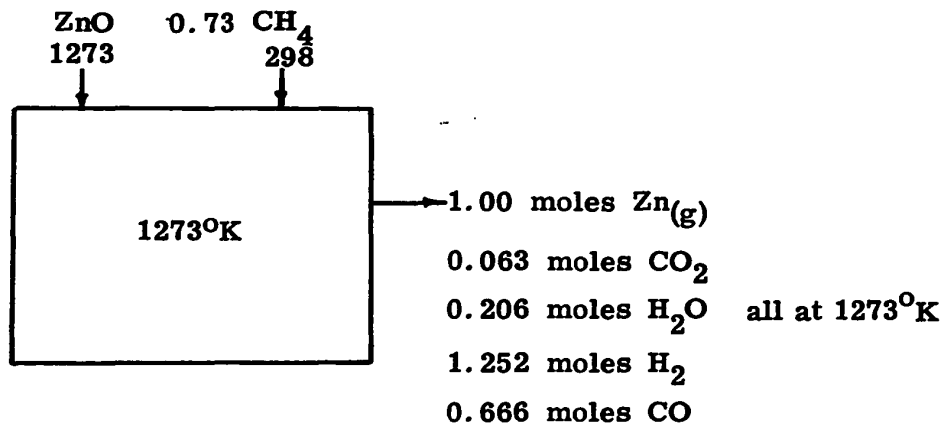
It can be shown, however, that by using air enriched to 37% O₂, the process can be made to run autogenously under ideal conditions.

Heat Required for the Reduction of Zinc Oxide by Methane

Assuming that conditions in the fluidized bed reduction vessel are such that equilibrium is achieved in the effluent gases, the composition of the off gases at 1000°C can be shown to be 31.5% Zn, 2.0% CO₂, 6.5% H₂O, 39.5% H₂, and 21.0% CO. ⁽²⁸⁾ By performing a mass balance on carbon or hydrogen it can be shown that 0.73 gm moles of CH₄ are required to produce 1 gm mole of zinc vapour.

Figure 10.5-4 shows schematically the heat balance for the reduction of zinc oxide by methane.

Figure 10.5-4 Schematic Heat Balance for the Reduction of Zinc Oxide by Methane at 1000°C



The quantity of reaction products was calculated from the equilibrium effluent gas composition and is based on the production of 1 gm. mole of zinc vapour.

Table 10.5-6 gives the enthalpy data for the system shown in Figure 10.5-4.

TABLE 10.5-6

Enthalpy Data for the Reduction of ZnO by Methane

Material	N Gm. Moles	$H_{f,298}^{\circ}$ cal/mole	$H_T^{\circ} - H_{298}^{\circ}$ cal/mole	Temp. °K	$H_T = H_{f,298}^{\circ} + (H_T^{\circ} - H_{298}^{\circ})$ cal/mole	Total Enthalpy N x H cals.
ZnO	1.00	-83300	11700	1273	-71500	-71500
CH ₄	0.73	-17900	0	298	-17900	-13000
Zn(g)	1.00	0	36000	1273	36000	36000
CO	0.67	-26400	7300	1273	-19100	-12800
H ₂	1.25	0	6900	1273	6900	8600
H ₂ O	0.21	-68300	19500	1273	-48800	-10200
CO ₂	0.06	-94000	11600	1273	-82400	-4900

The enthalpy change for the reaction depicted in Figure 10.5-4 is

$$\begin{aligned}
 & \text{(Enthalpy of Products - Enthalpy of Reactants)} \\
 & = (H_{\text{Zn(g)}} + H_{\text{CO}} + H_{\text{H}_2} + H_{\text{H}_2\text{O}} + H_{\text{CO}_2}) - (H_{\text{ZnO}} + H_{\text{CH}_4}) \\
 & \quad 1273 \quad 1273 \quad 1273 \quad 1273 \quad 1273 \quad 1273 \quad 298 \\
 & = (36000 \quad -12800 \quad +8600 \quad -10800 \quad -4900) - (-71500 \quad -13000) \\
 & = 100,600 \text{ calories}
 \end{aligned}$$

Unusable Heat, Methane Case

As for the case of hydrogen reduction, the enthalpy of the roaster gases can only be used to preheat the incoming ZnS and methane. The sensible heat required to raise the temperature of 1 gm mole of ZnS from 298°K to 1273°K is 12500 cal., as calculated previously. Likewise, the sensible heat required to raise the temperature of methane from 298°K to 1273°K is

$$\begin{aligned}
 & 0.73 \int_{298}^{1273} (5.65 + 11.44 \times 10^{-3}T - 0.46 \times 10^5 T^{-2}) dT \\
 & = 0.73 \left[5.65(1273-298) + 5.72 \times 10^{-3}(1273^2 - 298^2) + 0.46 \times 10^5 (1/1273 - 1/298) \right] \\
 & = 10300 \text{ cal.}
 \end{aligned}$$

The total sensible heat required to raise the feed materials to the reacting temperature is, therefore, 22,800 cal. The total waste or unusable heat is

$$70,000 - 22,800 = 47,200 \text{ cal.}$$

Calculating as before, the net overall thermal deficiency for methane reduction is

$$100,600 - (94,300 - 47,200) = 53,500 \text{ cal.}$$

Thus, this process is very endothermic even under ideal reactor conditions.

Comments

The calculations for the heat requirements of an integrated roast-reduction process for the production of zinc have been made for a) hydrogen reduction and b) methane reduction. The calculations presented apply for a process operated under the best possible conditions, i.e., no heat losses and the attainment of thermodynamic equilibrium during reduction.

The comparative merits of the two reduction systems show that from a thermal viewpoint, reduction by hydrogen is a better process (thermal deficit 15 Kcal vs 54 Kcal per gm mole of zinc produced). In fact the roasting-hydrogen reduction process can be made largely auto-genous by enriching the roaster air to approximately 37% O₂.

Although the kinetics of methane reduction have not been studied in the present work, Mathewson⁽²⁸⁾ indicates that methane reduction is rapid at 1000°C. Therefore, it seems likely that methane reduction of zinc oxide is a more attractive process in terms of the absolute reduction rates obtained. Thus the size of reduction fluidized beds required per unit of zinc produced will be much more favourable using methane as a reductant.

10.6 Summary and Critique of the Present Work

In Chapter Three of this work a review of the current pyrometallurgical solutions to the problem of zinc smelting has been presented with due consideration given to both the advantages and disadvantages of each process. In addition, a fairly comprehensive review of previous attempts to seek alternatives to the conventional processes has been given.

The main purpose of this work has been, therefore, to give the reader another alternative for consideration, i.e., the production of zinc by an integrated fluidized roaster bed-reduction bed technique. A number of experiments and calculations, constituting the initial development stages of the process, have been conducted with certain goals in mind. These included:

- 1) proof of the technical feasibility of the envisioned process;
- 2) attempts to optimize some of the important operating parameters of the process, i.e., operating temperature and reducing gas flowrate;
- 3) elucidation of some, if not all, of the most important potential problem areas which could prove troublesome to a commercial installation of the process.

The constructed experimental apparatus and technique has proved successful in showing that zinc metal can be produced by the gaseous reduction of zinc oxide based calcines in a fluidized bed. However, the lack of a suitable sampling technique and power limitations of the heating

furnace greatly limited the scope and range of the variables studied. An effort was made to develop a sampling technique that would have made possible the completion of a reduction curve in a single run. However, practical problems arose and it was decided that time spent on perfecting this technique might have been counter-productive. A less sophisticated technique which provided only one data point per run was therefore used. In retrospect, while this decision appeared to be the correct one at the time, taking all the factors then apparent into consideration, it may not in fact have been the wisest decision from the point of view of the overall results obtained. It is felt, however, that the consistency of the results that were obtained supported the use of the sampling technique and experimental procedure to confirm the reproducibility of the results.

The use of a heating furnace with a higher output power rating or a more suitable method of preheating the incoming reducing gas to the fluidized bed would have permitted reduction runs to be carried out at temperatures above 900°C. Ideally the temperature dependence of the reduction rate should have been evaluated up to approximately 1100°C.

Although the experimental apparatus included a condenser to recover the zinc vapour from the effluent gases, zinc condensation studies were not undertaken in this investigation.

It can be said without a doubt that the experimental observations indicate that clinkering and particle agglomerations could pose serious problems to an industrial process of this type. Since no detailed experimental tests were undertaken to investigate this problem more fully,

assumptions that the reported observations will apply to large scale reactors must be made with caution.

As an integral part of the development of this process, two theoretical calculations (one an overall heat balance for the process; the other a calculation of the plan area of the equipment) have been made based on the best possible operating conditions, i. e., the attainment of chemical equilibrium during reduction and the assumption that there are negligible heat losses from the process. Using hydrogen as a gaseous reducing agent and air enriched to 37% O₂, it has been shown that the process can be run autogenously. Although the experimental results do not show conclusively what conditions of temperature and hydrogen flowrate will lead to chemical equilibrium in the bed, it was felt that by using a deep bed (i. e., increasing the gas residence time in the bed) and a moderate gas flowrate, equilibrium could be achieved at say 1000°C.

Operation under non-ideal conditions will, of course, result in diminished reduction rates and the need for a larger reduction bed grate area. Consequently, there will be higher heat losses due to the larger physical size of the reactor. In such cases, additional fuel would have to be burned to compensate for the additional heat losses.

No attempt has been made during the course of this work to suggest or speculate on construction details or materials which would be suitable for a commercial installation of the process. This aspect still must be evaluated and given much thought. Most certainly, materials

Leaf 158 omitted
in page numbering.

capable of withstanding high temperatures (up to 1100°C) during continuous operation and attack by gaseous zinc must be used. While the outer walls of the integrated reactor must be well insulated to reduce heat losses to the outside, the wall of the internal roaster fluidized bed, on the other hand, must be as thin as expedience will allow to provide maximum transfer of roasting heat to the reduction fluidized bed.

Notwithstanding the limited scope of the results obtained in this experimental investigation, it can be stated conclusively that the primary objective has been successfully met, i. e., that zinc can be produced by gaseous reduction in a fluidized bed. It is hoped that the success of this work will spur others to continue and that ultimately the process will achieve commercial realization.

10.7 Suggestions for Future Work

The present work has led to the proposal of a novel and previously unexplored technique for the production of zinc.

Some suggestions for future work to further exploit the results presented in this thesis and to widen the scope of this technique include:

- 1) Further exploration into the effect of temperature on the zinc production rate. The fluidized bed reduction technique should be investigated at temperatures above the boiling point of zinc, say up to 1100°C . Condensation of the vapours should be included.
- 2) A further study of the effect of the hydrogen flowrate on zinc production rates. The present work suggests that the gas flowrate has a marked effect on zinc production rates and, therefore, this variable should be investigated further, both for a wider range of hydrogen flowrates and for different temperatures. Other workers, particularly Kivnick and Hixson⁽⁶⁴⁾, have suggested that, for nickel oxide reduction with hydrogen, increases in the gas flowrate have a greater beneficial effect on nickel production with increasing temperature.
- 3) A study of the effect of particle size on zinc production rates.
- 4) A study of the effect of the bed depth or length to diameter ratio of the bed on zinc production rates and hydrogen efficiencies.

- 5) The use of other reducing agents. Suggested reducing agents include methane or natural gas and a mixed bed of coke and zinc calcine fluidized with air or oxygen enriched air. Both these techniques have the advantage that heat can be supplied internally by combustion. By selecting the proper air rate, both methane or natural gas and coke can be burned under reducing conditions to produce 1) heat and 2) sufficient unburned fuel to carry out the reduction process.
- 6) A pilot scale roaster-reduction bed device should be built to determine the most suitable method to optimize heat recovery.

10.8 Conclusions

- 1) The results of the present work have shown that it is technically feasible to produce zinc metal by the reduction of oxidized zinc sulphide concentrate by hydrogen in a fluidized bed.
- 2) The rate of zinc production increases with increasing temperature in the range 800°C to 900°C.
- 3) The rate of zinc production increases with increasing hydrogen flowrate in the range of space velocities 3.77 cm sec⁻¹ to 7.54 cm sec⁻¹.
- 4) Particle agglomeration due to the presence of lead in the charge was observed. Agglomeration might be a problem in an industrial scale plant.
- 5) It has been shown that the rate of zinc elimination is almost constant up to 88% zinc elimination. The rate controlling step appears to be gas phase mass transport.
- 6) The maximum attainable "economic efficiency" of hydrogen utilization (1000°C) is 1 mole of zinc produced per 5 moles of hydrogen introduced. The unused hydrogen will have to be dehydrated and recycled to the reduction process.
- 7) Calculations have shown that under ideal conditions a combined roaster bed-hydrogen reduction bed is not quite auto-genous employing air as the roaster gas feed. Enrichment of the roaster feed gas to 37% O₂ makes the ideal roaster-

reducer bed combination autogenous. Fuel must be combusted in the reduction bed to compensate for non-ideal heat losses.

- 8) Preliminary calculations suggest that the reducing bed grate area will be 3 to 4 times that required for the roasting bed.
- 9) The use of methane or natural gas as a reductant greatly favours reduction rates but will require a greater heat of combustion in the reducing bed.

APPENDICES

APPENDIX I

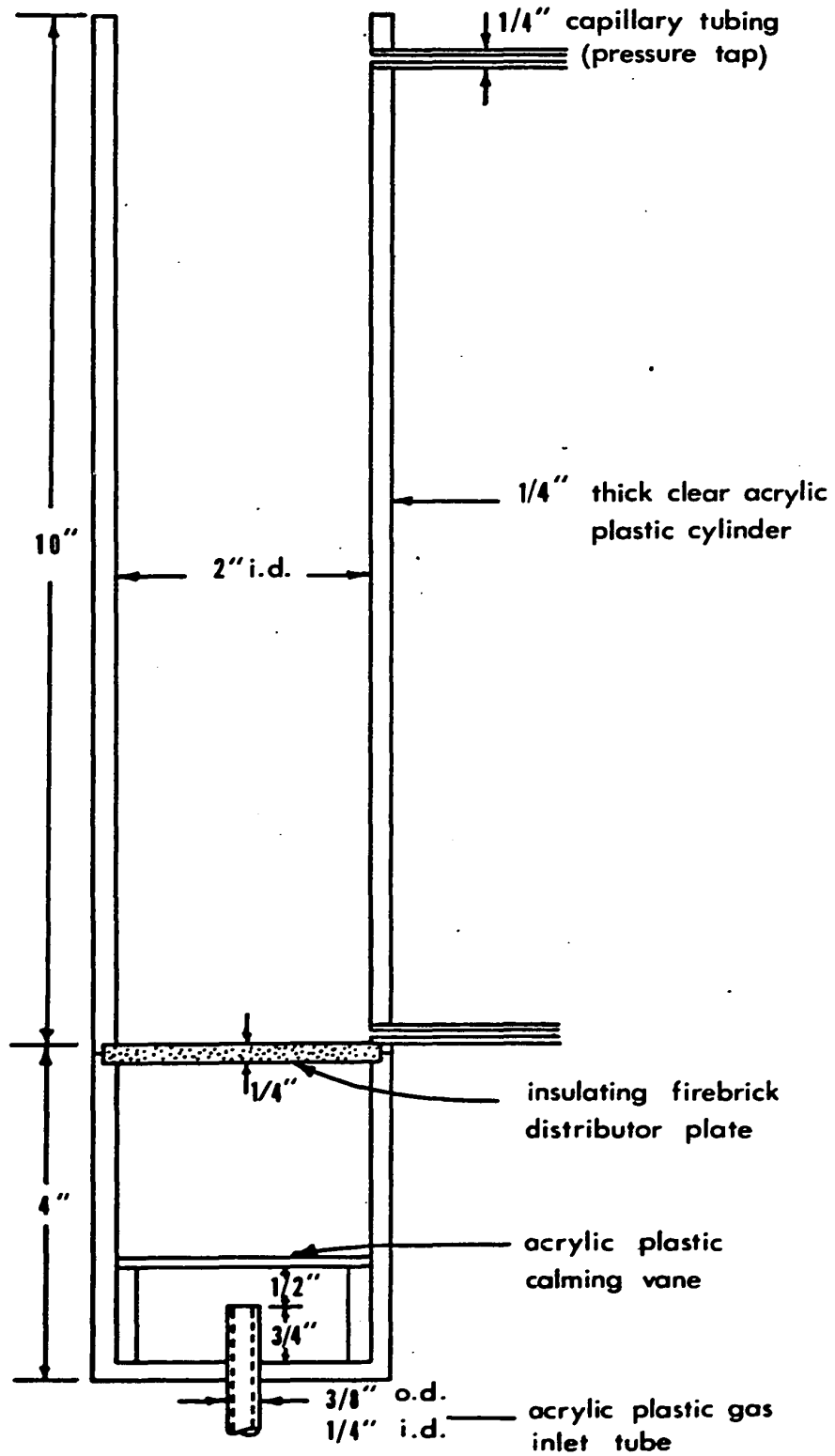
LOW TEMPERATURE FLUIDIZED BED INVESTIGATION

Prior to the initiation of the high temperature investigation, a room temperature model of the fluidized bed was constructed to find and test a suitable distributor plate for the high temperature work.

The suitability of the distributor plate was judged by its ability to withstand high temperatures and its ability to give an evenly distributed gas flow through the bed, i. e., an avoidance of slugging and channelling. Wire gauze (200 mesh), perforated stainless steel plate, and insulating firebrick were the materials tested with the firebrick giving the best results. Thus insulating firebrick discs were used in the high temperature study.

The low temperature fluidized bed was constructed entirely of clear acrylic plastic and it conformed exactly to the design of the high temperature fluidized bed reactor. The only differences were that the reactor diameter was 2 inches i. d. vs 2.635 inches for the high temperature reactor and two pressure taps for observing the pressure drop across the bed were inserted through the reactor wall. The lower tap was situated directly above the distributor plate and the upper was located above the bed. Both were flush with the reactor wall. Figure A 1 shows a detailed drawing of the low temperature fluidized bed.

Figure A1 Diagram of the Low Temperature Fluidized Bed



The fluidization quality was judged from the pressure drop against mass flowrate or gas velocity curve. This curve is presented in Figure 5.1-1, p. 39 for the insulating firebrick distributor. Any tendency towards channelling or slugging in the bed is usually quite evident from these plots.

Channelling is characterized by the pressure drop across the bed never quite recovering after the minimum fluidization flowrate to the theoretical flowrate defined by the bed weight per unit cross sectional area.

Slugging, on the other hand, is generally not observed until very high flowrates are reached, at which time slugging is observed by either a) violent fluctuations in the pressure drop or b) a greater than theoretical pressure drop.

ACKNOWLEDGEMENTS

Sincere appreciation is extended to Professor W.G. Davenport for supervision and assistance given during the course of this work.

Thanks are due to Professor W.M. Williams, Chairman, Department of Metallurgical Engineering, McGill University, and to Professors R.I.L. Guthrie and W.T. Thompson for their interest and encouragement.

The author wishes to extend his thanks to Mr. M. Knoepfel for his invaluable technical assistance.

The author is indebted to the National Research Council of Canada for providing generous financial assistance.

LIST OF SYMBOLS

<u>Symbol</u>		<u>Units</u>
U_{mf}	Minimum fluidizing velocity	cm sec ⁻¹
U_t	Terminal velocity	cm sec ⁻¹
G_{mf}	Minimum fluidizing mass velocity	gm cm ⁻² sec ⁻¹
ϕ_s	Particle sphericity	Dimensionless
D_p	Particle diameter	cm
\bar{D}_p	Average particle diameter for a mixture of particles of different sizes	cm
D_{pi}	Average particle diameter for particles lying between two designated particle diameters	cm
ρ_f	Fluid density	gm cm ⁻³
ρ_s	Solid density	gm cm ⁻³
ρ_b	Bulk bed density	gm cm ⁻³
ρ_i	Density of the i th gas in a mixture of gases	gm cm ⁻³
ϵ_{mf}	Minimum fluidization bed voidage fraction	Dimensionless
ϵ	Fixed bed voidage	Dimensionless
μ	Gas viscosity	gm cm ⁻¹ sec ⁻¹
μ_i	Gas viscosity of the i th gas in a mixture of gases	gm cm ⁻¹ sec ⁻¹
g	Acceleration due to gravity	cm sec ⁻²
X_i	Weight fraction of a group of particles lying between two designated particle diameters	Dimensionless
y_i	Weight fraction of the i th gas in a mixture of gases	Dimensionless

<u>Symbol</u>		<u>Units</u>
V_i	Volume fraction of the i^{th} gas in a mixture of gases	Dimensionless
V	Volume	cm^3
w	Solids weight	gms
K_E	Thermodynamic equilibrium constant	Suitable units
P_a^{Eq}	Equilibrium partial pressure of a gas (subscript denotes the gas to which partial pressure applies)	Atmospheres
P_a	Partial pressure of a gas in the bulk gas (subscript denotes the gas to which partial pressure applies)	Atmospheres
\dot{N}	Reaction rate	gm-moles min^{-1}
K	Mass transfer coefficient	cm min^{-1}
A	Total particle area	cm^2
C_a^B	Bulk concentration of a gas (subscript denotes gas to which concentration applies)	gm-moles cm^{-3}
C_a^{Eq}	Equilibrium concentration of a gas (subscript denotes gas to which concentration term applies)	gm-moles cm^{-3}
D	Gaseous diffusion coefficient	$\text{cm}^2 \text{sec}^{-1}$
T	Absolute temperature	$^{\circ}\text{K}$
N_a	Number of moles of a substance (subscript denotes substance)	gm-moles
$H_{f,298}^{\circ}$	Standard enthalpy of formation of a substance	$\text{cal (gm-mole)}^{-1}$
H_T°	Enthalpy of a substance at some temperature other than 298°K	$\text{cal (gm-mole)}^{-1}$

<u>Symbol</u>		<u>Units</u>
ΔG_T°	The standard free energy of reaction at temperature T°K	cal (gm-mole) ⁻¹
D_t	Fluidized bed diameter	cm
B	Particle shape factor	Dimensionless

LIST OF TABLES

<u>Table</u>		<u>Page</u>
2.0-1	Comparison of Types of Contacting for Reacting Gas-Solid Systems, Illustrated by Metallurgical Examples .	6
2.2-1	Survey of Metal Sulphide Roasting	8
2.2-2	Survey of Direct Reduction Processes and INCO Nickel Oxide Reduction Process	10
3.0-1	Current Zinc Production Figures	12
4.0-1	Chemical Analysis of the Ores Treated by Brant and Marshall.	32
4.0-2	Effect of the Iron Ore on the Time Required to Achieve 80% Metallization as Observed by Brant and Marshall.	32
4.0-3	Effect of Hydrogen Pressure on Iron Oxide Reduction. .	33
5.1-2	Some Empirical and Theoretical Expressions Used to Predict the Minimum Fluidization Gas Velocity. . . .	43
6.0-1	Equilibrium Constants for Reactions in the Zn-S-O System Reaction	52
6.1-1	Equilibrium Constants for Reactions in the Fe-S-O System.	57
8.1-1	Identification of the Components of Figure 8.1-1	73
8.1-2	Identification of Parts of the Fluidized Bed Reactor. . .	75
8.1-4	Identification of the Parts of the Control Circuit	82
8.2-1	Chemical Analysis of Canadian Electrolytic Zinc Calcine	84
9.2-1	Experimental Conditions for the Study of the Effect of Reaction Temperature on the Rate of Zinc Elimination From the Fluidized Bed.	99
9.2-2	Calculated Apparent Reaction Rates for the Reduction of Zinc Calcines by Hydrogen in a Fluidized Bed	100

<u>Table</u>	<u>Page</u>
9.2-3 Experimental Conditions for the Study of the Effect of Hydrogen Flowrate on the Rate of Zinc Elimination From the Fluidized Bed.	103
9.3-1 Experimental Conditions and Calculated Values of the Hydrogen Efficiencies Obtained in This Study . . .	107
10.0-1 Comparison of the Reduction Temperatures and Melting Points of the Reaction Products for the Reduction of Metal Oxides in Fluidized Beds	114
10.4-1 Weight Percent of Calcine Appearing in Mesh Size Ranges Against Reaction Time	130
10.4-2 Calculated KA Products for the Reduction Temperatures Studied	132
10.4-3 Comparison of D_{T_1}/D_{T_2} and $(KA)_{T_1}/(KA)_{T_2}$ (Temperatures in °C)	134
10.4-4 Velocity Dependence of KA.	135
10.5-1 Operating Data for the Lurgi Turbulent Layer Fluidized Bed Roasters at Canadian Electrolytic Zinc Limited	142
10.5-2 Scaled Down Parameters for a Fluidized Bed Roaster Capable of Producing 50 tpd of Zinc Oxide	143
10.5-3 Estimation Data of the Plan Area Required for ZnO Reduction in a Fluidized Bed.	144
10.5-4 Heat Data for ZnS Roasting at 1000°C	147
10.5-5 Heat Data for ZnO Reduction by Hydrogen at 1000°C	149
10.5-6 Enthalpy Data for the Reduction of ZnO by Methane .	152

LIST OF FIGURES

<u>Figure</u>		<u>Page</u>
3.2-2	Zinc Distillation Furnace	15
3.2-3	St. Joseph Electrothermic Furnace	19
3.2-4	Electrothermic Zinc Metal Furnace	20
3.3-1	Imperial Smelting Furnace	22
3.3-2	Lead-Zinc Phase Diagram	24
5.1-1	Typical Pressure Drop — Mass Flowrate Plot for a Fluidized Bed	39
5.1-2	Plot of Minimum Velocity vs Particle Diameter . .	42
5.1-3	Minimum Fluidizing Voidage vs Particle Diameter .	45
5.1-4	Plot of Minimum Fluidizing Gas Velocity vs Particle Size.	47
6.0-1	The Zn-S-O System	53
6.0-2	Stable Equilibria in the Zn-S-O System	56
6.1-1	The Fe-S-O System	59
6.1-2	Stable Equilibria in the Fe-S-O System	60
6.2-1	The Zn-Fe-S-O System	62
6.2-2	Stable Equilibria in the Zn-Fe-S-O System	63
7.0-1	Effect of Temperature on the Hydrogen Reduction of Zinc Oxide.	69
8.1-1	The Experimental Apparatus	74
8.1-2	Diagram of the Fluidized Bed Reactor.	76
8.1-3	Photographs of the Experimental Apparatus	78
8.1-4	Schematic Drawing of the Control Circuit	83
8.3-1	Particle Size Distribution of the "As Received" Zinc Calcine	86

<u>Figure</u>		<u>Page</u>
9.1-1	Photographs of Some of the Clinkers Obtained During the Reduction of Zinc Calcine	93 to 96
9.2-1	Effect of Temperature on the % Zinc Elimination	101
9.2-2	Variation of the Apparent Reaction Rate with Temperature	102
9.2-4	Effect of Hydrogen Flowrate on the % Zinc Elimination.	104
9.2-5	Plot of Percentage Zinc Elimination vs Time for an Extended Run	105
9.3-1	Effect of Temperature on the Thermodynamic Efficiency	108
9.3-2	Effect of Temperature on the Economic Efficiency	109
10.0-1	Equilibria in the Gaseous Reduction of Metal Oxides	112
10.0-2	Equilibria in the ZnO-H ₂ System at Low Tempera- tures (near the Melting Point of Zinc)	115
10.1-1	Effect of Temperature on the Maximum "Economic" Hydrogen Efficiency Attainable at Equilibrium .	119
10.2-1	Variation of the Apparent Rate with Temperature.	121
10.3-1	Debye-Scherrer X-Ray Pattern of "As Received" Zinc Calcine	126
10.3-2	Debye-Scherrer X-Ray Pattern of Partially Reduced Zinc Calcine.	126
10.3-3	Debye-Scherrer X-Ray Pattern of Partially Reduced Zinc Calcine.	126
10.4-1	Variation of Reduction Rate with Time	128
10.4-2	Particle Size Variation with Time	131
10.4-3	Arrhenius Plot of Log ₁₀ (KA) vs 1/T.	133
10.4-4	Photomicrograph of a particle of the "As Received" Zinc Calcine	138

<u>Figure</u>		<u>Page</u>
10.4-5	Photomicrograph of Zinc Calcine Particle after Six Hours' Reduction at 900°C	138
10.4-6	Photomicrograph of Zinc Calcine Particles after Seventeen Hours' reduction at 850°C	138
10.5-1	Proposed Integrated Fluidized Roaster Bed — Reduction Bed Zinc Production Furnace.	140
10.5-2	Schematic Heat Balance for the Roasting of ZnS at 1000°C	146
10.5-3	Schematic Heat Balance for the Reduction of Zinc Oxide by Hydrogen at 1000°C	148
10.5-4	Schematic Heat Balance for the Reduction of Zinc Oxide by Methane at 1000°C	152
A 1	Diagram of the Low Temperature Fluidized Bed. .	165

REFERENCES

1. Leva, M.: "Fluidization," McGraw-Hill Book Company, Inc., New York, 1959.
2. Kunii, D., and Levenspiel, O.: "Fluidization Engineering," John Wiley & Sons, New York, 1969.
3. Heino, K.H., McAndrew, R.T., Ghatas, N.E., and Morrison, B.H.: paper presented to the A.I.M.E. World Lead-Zinc Symposium, St. Louis, Mo., October 1970.
4. Roggero, C.E.: Trans. A.I.M.E., 227, pp. 105-11, 1963.
5. Newman, R.I., LaVine, A.J.: paper presented at the First Operating Metallurgy Conference of the Metallurgical Society of the A.I.M.E., Pittsburgh, Pa., November 29 - December 3, 1965.
6. Coolbaugh, W.E., and Neider, R.F.: paper presented at the First Operating Metallurgy Conference of the Metallurgical Society of the A.I.M.E., Pittsburgh, Pa., November 29 - December 3, 1965.
7. Natesan, K., and Philbrook, W.O.: Trans. A.I.M.E., Vol. 1, pp. 1353-1360, May 1970.
8. Mickley, H.S., and Trilling, C.A.: Ind. Eng. Chem., 41(6), pp. 1135-47, 1949.
9. Leva, M., Weintraub, M., and Grummer, M.: Chem. Eng. Prog., 45(9), pp. 563-72, 1949.
10. Kettenring, K.N., Manderfield, E.L., and Smith, J.M.: Chem. Eng. Prog., 46(3), pp. 139-45, 1950.
11. Mickley, H.S., and Fairbanks, D.F.: A.I. Ch.E. J., 1, 374, 1955.
12. Wamsley, W.W., and Johanson, L.N.: Chem. Eng. Prog., 50(7), pp. 347-55, 1954.
13. Wen, C., and Leva, M.: A.I.Ch.E. J., 2(4), 482, 1956.
14. Wender, L., and Cooper, G.T.: A.I.Ch.E. J., 4(1), 15, 1958.
15. Frantz, J.F.: Chem. Eng. Prog., 57(7), pp. 35-42, 1961.

16. Lewis, W.K., Gilliland, E.R., and Girouard, H.: Chem. Eng. Prog. Symposium Series on Fluidization, Vol. 58, No. 38, pp. 87-97, 1962.
17. Resnick, W., and White, R.R.: Chem. Eng. Prog., 45(6), pp. 377-90, 1949.
18. McCune, L.K., and Wilhelm, R.H.: Ind. Eng. Chem., 41(6), pp. 1124-34, 1949.
19. Gilliland, E.R., and Mason, E.A.: Ind. Eng. Chem., 41(6), pp. 1191-96, 1949.
20. Curlook, W., and Roorda, H.J.: Trans. A.I.M.E., 64, pp. 122-26, 1961.
21. Blair, J.C.: paper presented to the First Operating Metallurgy Conference of the Metallurgical Society of the A.I.M.E., Pittsburgh, Pa., November 29 - December 3, 1965.
22. Stephens, F.M.: Chem. Eng. Prog., 49(9), pp. 455-58, 1953.
23. McGannon, H.E., Ed.: "Making, Shaping, and Treating of Steel," 8th edition, 1964, publication of the United States Steel Corporation.
24. Cronan, C.S.: Chem. Engrg., Vol. 67, pp. 64-5, April 1960.
25. Labine, R.A.: Chem. Engrg., Vol. 67, p. 96, February 1960.
26. Tomasicchio, G.: Proc. Intern. Symp. on Fluidization, Netherlands University Press, Amsterdam, 1967.
27. The International Nickel Company of Canada, Ltd.: private communication.
28. Mathewson, C.H.: "Zinc, the Science and Technology of the Metal, its Alloys and Compounds," Reinhold Publishing Corporation, New York.
29. Bray, J.L.: "Non-Ferrous Production Metallurgy," second edition, p. 486, John Wiley & Sons, Inc., New York, 1947.
30. Newton, J.: "Extractive Metallurgy," John Wiley & Sons, Inc., New York, 1963.
31. Bunce, E.H., and Handwerk, E.C.: Trans. A.I.M.E., 121, pp. 427-40, 1936.

32. Weaton, G.F., Najarian, H.K., and Long, C.C.: *Trans. A.I.M.E.*, Vol. 159, p. 141, 1944.
33. Anon.: publication of the St. Joseph Lead Company, Ltd., no date.
34. Morgan, S.W.K., and Temple, D.A.: *J. of Metals*, pp. 23-29, August 1967.
35. Morgan, S.W.K.: *Trans. I.M.M.*, Vol. 66, pp. 553-65, 1956-57.
36. Anon.: "Imperial Smelting Process Throughout the World," publication of the Imperial Smelting Corporation, Westerham Press, Great Britain, copyright 1963.
37. Smithells, C.J.: "Metals Reference Book," Vol. 1, 3rd edition, p. 438, Butterworths, London, 1962.
38. Maier, C.G.: "Zinc Smelting from a Chemical and Thermodynamic Viewpoint," U.S. Bureau of Mines, Bull. 324, 1930.
39. Doerner, H.A.: *Trans. A.I.M.E.*, Vol. 121, p. 636, 1936.
40. Imbert, A.H.: U.S. Patents 807,271; 894,383, 1905 and 1906.
41. Peterson, P.E.: *Trans. Am. Electrochem. Soc.*, Vol. 24, p. 215, 1913.
42. Gross, P., and Warrington, M.: *Discussions Faraday Soc.*, Vol. 4, pp. 215-17, 1948.
43. McCabe, C.L.: *J. of Metals*, September 1954.
44. Truesdale, E.C., and Waring, R.K.: *Trans. A.I.M.E.*, Vol. 159, p. 97, 1944.
45. Imoto, T., Harano, Y., and Nishi, Y.: Municipal University, Osaka, Japan, *Nippon Kagaku Zasshi*, Vol. 84, pp. 115-19, 1963.
46. Bodenstein, M.: *Trans. Am. Electrochem. Soc.*, Vol. 51, p. 449, 1927.
47. Shkuridin, I.S.: *Tsvet. Metally*, 10(2), pp. 41-5, 1967.
48. Jones, T.S., and Davis, H.M.: *Trans. A.I.M.E.*, Vol. 239, pp. 244-48, 1967.
49. Langenberg, F.C.: U.S. Patent, 2,979,396, 1961.

50. Brant, H.H., and Marshall, W.E.: "Physical Chemistry of Process Metallurgy," Part 2. An International Symposium held at Pittsburgh, Pa., April 27 - May 1, 1959. Interscience Publishers, New York.
51. Masonov, P. Ya., Vasil'ev, E.N., Lur'ye, I.L., and Knyazev, V.F.: Russian Mining and Metallurgy, September - October 1962.
52. Okura, A., and Lu, W-K.: Can. Metall. Quarterly, Vol. 8, p. 325, October - December 1969.
53. Frantz, J.F.: Chem. Eng. Prog. Symposium Series on Fluidization, Vol. 58, No. 38, 1962.
54. Miller, C.O., and Logwinuk, A.K.: Ind. Eng. Chem., Vol. 43, pp. 1220-1226, 1951.
55. van Heerden, G., Nobel, P., and van Krevelen, D.W.: Chem. Eng. Sci., 1(1), pp. 37-49, 1951.
56. Johnson, E.: Inst. Gas Engrs., (London) Repts., publication No. 378/179, 1949-50.
57. Benner, R.L., and Kenworthy, H.: U.S. Bureau of Mines, Report of Investigations 6769, part 2, August 1965.
58. Ingraham, T.R. and Kellogg, H.H.: Trans. A.I.M.E., 227, pp. 1419-25, 1963.
59. Hopkins, D.W.: Trans. Am. Electrochem. Soc., Vol. 96, No. 3, 1949.
60. Kato, Y. and Takei, T.: J. Electrochem. Soc., 17, p. 297, 1930.
61. Snurnikov, A.P., Larin, V.F., Margulis, E.V., and Krasavina, S.M.: Tsvet. Metally, 10(3), pp. 25-8, 1966.
62. Wicks, C.E. and Block, F.E.: U.S. Bureau of Mines Bulletin 605, 1963.
63. Vavilov, N.S., Tsylev, L.M., and Ch'ung-Chih, C.: Russian Mining & Metallurgy, pp. 23-32, Jan.-Feb. 1962.
64. Kivnick, A., and Hixson, A.N.: Chem. Eng. Prog., Vol. 48, No. 8, pp. 394-400, 1952.
65. Lewis, W.K., Gilliland, E.R., and Reed, W.A.: Ind. Engrg. Chem., 41(6), pp. 1227-37, 1949.

66. Wetherill, W.H. , and Furnas, C.C.: Ind. Engrg. Chem. , 26(4), pp. 983-991, 1934.
67. Strangway, P.K., and Ross, H.U.: Can. Metall. Quarterly, 5(3), 1966.
68. Seth, B.B.L. , and Ross, H.U.: Can. Metall. Quarterly, 5(4), 1966.
69. Lu, W-K. , and Bitsianes, G.: Can. Metall. Quarterly, 7(1), 1968.
70. Strangway, P.K., Lien, H.O. , and Ross, H.U.: Can. Metall. Quarterly, 8(2), 1969.
71. Kubaschewski, O. , and Evans, E. Ll.: "Metallurgical Thermodynamics," 3rd ed. , Pergamon Press, London, 1958.